A Parylene Real Time PCR Microdevice

Thesis by

Quoc (Brandon) Quach

In Partial Fulfillment of the Requirements

For the Degree of

Doctor of Philosophy

California Institute of Technology

Pasadena, California

2010

(Defended December 4th, 2009)

To Cuong Quach and Nga Huynh

It never ceases to amuse me that I was once a 7 year old weekend factory worker, a 10 year old dry cleaner, and now a Caltech PhD graduate all within a 10 mile radius.

Cheers to the American Dream!

Acknowledgements

I would like to acknowledge my parents whose courageous journey as (Chinese) refugees from war-torn Vietnam to the United States serves as an inspiration for everything I do in life. Their dangerous flight in small boats off the coast of Vietnam under the cover of darkness followed by years of hard work raising a family in uncertain conditions as immigrants to the United States was all done to provide a better life for their family and especially their children. It is from my desire to show my deep appreciation and endless gratitude that I have been able to produce and present this thesis and earn my PhD from Caltech. To my parents: such is the level of accomplishment I have been able to achieve from the sacrifices you made on my behalf.

Right next to the turtle pond, Guggenheim Laboratory is a special place on campus for me. Armed with only a dream and a desire to achieve it, I knocked on the door of the chairman of the bioengineering department, Professor Morteza Gharib, during Spring Break of 2003 without an appointment nor any advanced warning. After 5 knocks and 2 minutes waiting, I figured he was out of town and took 6 steps towards the exit when his door cracked open, he stuck out his head, and he welcomed me into his office. Already with two back-to-back letters of rejection from Caltech, I pleaded my case to him in 5 of the most life-changing and legendary minutes of my professional life. Thank you, Professor Gharib for seeing in me the talent and desire to purse this highest level degree and personally accepting me into the highest quality institute of technology.

The most enjoyment, amusement, and awe I have experienced during my time at Caltech has come from my interaction with the campus community. I would like to thank my advisor, Professor Yu-Chong Tai, for his advice, guidance, and enlightening and entertaining answers to my technical questions. I would also like to thank him for demonstrating how to be a leader and pursue excellence. To this day, he remains the only person in the world with whom I can explain all my technical worries and questions and in return I receive an out of this world solution or explanation that is based on fundamental physics but points to amusing directions that tickle your brain. Nowhere else can I get the experience of being in his office and saying "hmmm…maybe you're right," and with a chuckle hesitantly acknowledge "that might work."

I would like to thank my colleagues from the Caltech Micromachining Lab: Justin Boland for introducing me to machines and the stock market, Matt Liger for that night we tried to use the CMP machine (it has yet to be touched again to this day), Damien Rodger for being very "niche" and introducing me to the lab, Scott Miserendino for being a cool officemate, Victor Shih for helping to improve my processes, Siyang Zheng for being my student mentor when I first joined the lab, Qing He for helping me with fluidic couplings, Nick Lo for being my contact person for any EE theory, Wen Li for our discussions about everybody else while in the cleanroom and for helping me keep the Ebeam running, PJ Chen for lending me the pressure regulators, Jason Shih for being the master of fluidics, Mike Liu for being from Berkeley too, Luca Giacchino for taking over for Matt Liger as the representative of all of Europe, Ray Huang for continuing the consulting club, Jeffrey Lin for the late night dinners (which you still owe me one for helping you with the SEM),

Monty Nandra for being the master of EE and optics, Justin Young-Hyun Kim for always saying hi, Bo Lu for putting my name on that paper, Yu Zhao for being a fun officemate, Penvipha Satsanarukkit for being a hard-working mentee, Bo Lu for inspiring me with enthusiasm for your lab results, Wendian Shi for all your answers to my photography questions, and Charles DeBoer for keeping me company during lunch. The friendly administrative staff of Tanya Owen, Christine Garske, and Agnes Tong were highly efficient while the lab engineer Trevor Roper kept the lab and machines running smoothly. Finally, I would like to thank the Caltech Glee Club and Caltech Consulting Club for making my last years at Caltech memorable and music-filled.

Abstract

The polymerase chain reaction (PCR) is a powerful biochemical assay that is used in virtually all biochemical labs. By specifically amplifying a small sample of DNA, this technique is useful in the fields of paternity testing, forensics, and virus detection, just to name a few. A useful advancement of PCR involves monitoring the fluorescence generated by an increase in DNA during the amplification. This so called real time (RT) PCR allows quantification of the initial sample amount and allows for shorter assay times by stopping the reaction when enough fluorescence has been detected.

Technology in the field of micro-electro-mechanical systems (MEMS) has advanced from the academic laboratory level to a handful of commercially successful devices. Work on adapting MEMS to biochemical applications, however, is still at the laboratory research stage. Recent breakthroughs in the use of more biocompatible materials in MEMS devices have helped to advance bio-MEMS. In particular, the polymer Parylene has superior properties that present a promising new platform for this field.

This work presents the design, fabrication, and testing of a parylene-based MEMS RTPCR device. By combining advancements in both biology and MEMS engineering, this work demonstrates the feasibility of such a device along with quantitative analysis and data that serve as a guide for its future development.

Table of Contents

List of Figures

List of Tables

1 PCR and Real Time PCR

1.1 Introduction to the Polymerase Chain Reaction

The polymerase chain reaction (PCR) is an *in vitro* molecular biology technique used to amplify deoxyribosenucleic acids (DNA). Developed primarily by Kary Mullis (Nobel Prize, Chemistry 1993) while at Cetus Corporation in the 1980s, PCR is now a standard technique used in nearly all biology labs in the world. Using the reaction, scientists can amplify a target region of DNA located within the template DNA (Figure 1-1). The product is called the amplicon. This technique greatly simplifies DNA amplification which before the development of PCR required DNA to be reproduced *in vivo* in bacteria using cloning techniques. The amplification of a specific target region makes PCR an exceptional tool for a wide variety of applications including paternity tests, genotyping, and pathogen detection.

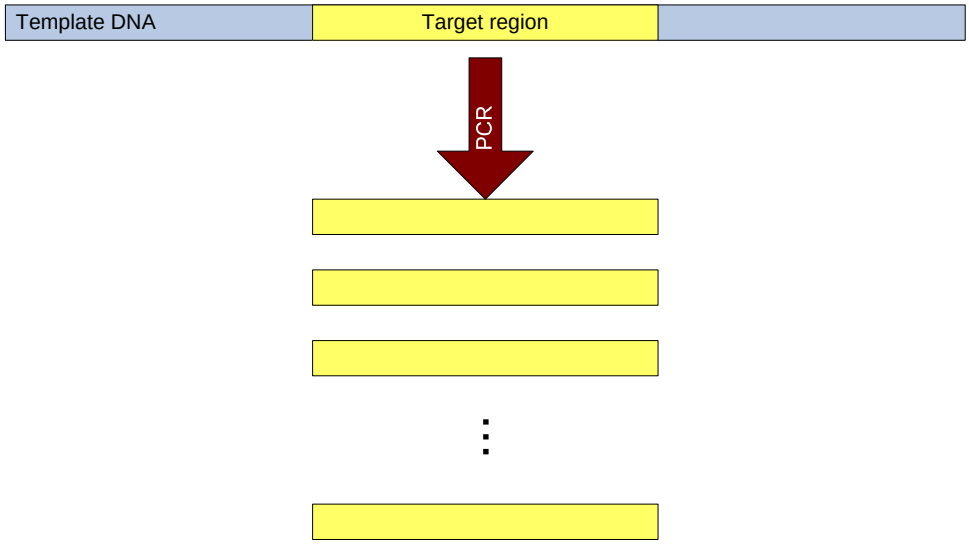

Figure 1-1: Basic concept of PCR amplification

To explain PCR in detail, a list of components will be provided, followed by the procedure, equipment, and applications.

1.1.1 Components

To prepare the reaction, the components of PCR are mixed together in a thin walled (for improved heat transfer) test tube. Oftentimes this tube will be certified as DNAse free to prevent degradation of the template and products by the DNAase enzymes. The components are commonly placed inside a bucket of crushed ice to minimize reactions while mixing. Below is a list of components. The order of the list does not reflect the order in which reactants are added.

- The *DNA template* is the original source DNA that contains the target region. This can be as simple as a synthesized strand of single stranded DNA or the entire genome of an organism. In reverse transcriptase PCR, the template is a strand of RNA which, before the reaction starts, is reverse transcribed by the reverse transcriptase enzyme into the corresponding complimentary DNA (cDNA). Depending on the assay, some sample preparation may be required to obtain a suitable template material. For example, tissues have to be treated to access cells, which then are lysed into a suspension that undergoes DNA extraction using a glass solid phase chromatography. Care must also be taken to ensure contaminants from the sample preparation steps do not inhibit the PCR reaction.
- *Deoxynucleoside triphosphates* (dNTPs) are the monomeric building blocks of DNA. The standard set of dNTPs used consists of: deoxyadenosine triphoshate (dATP), deoxyguanosine triphosphate (dGTP), deoxythymidine triphosphate (dTTP), and

deoxycytidine triphosphate (dCTP). They are composed of a ribose sugar, three phosphate groups, and a base (Figure 1-2). The base component determines the type of nucleotide it is. RNA has an OH group at the 2' of the ribose sugar while DNA has only a hydrogen atom there. For normal PCR operation, equal ratios of the four standard dNTPs are added to the reaction mix. Deviation from the standard recipe can be useful for special applications. For example, to study random mutations to the target region, one of the dNTPs can be added in excess to increase the chance of erroneously incorporating that nucleotide into the amplicons. For other applications, slight variants of the standard nucleotides can be used. Deoxyuridine triphosphate (dUTP) can be substituted along with biotin or fluorescently labeled variants of dUTP. These modified nucleotides provide useful functions such as binding to streptavidin and detection by fluorescence, two properties that are heavily exploited in biochemistry and biotechnology.

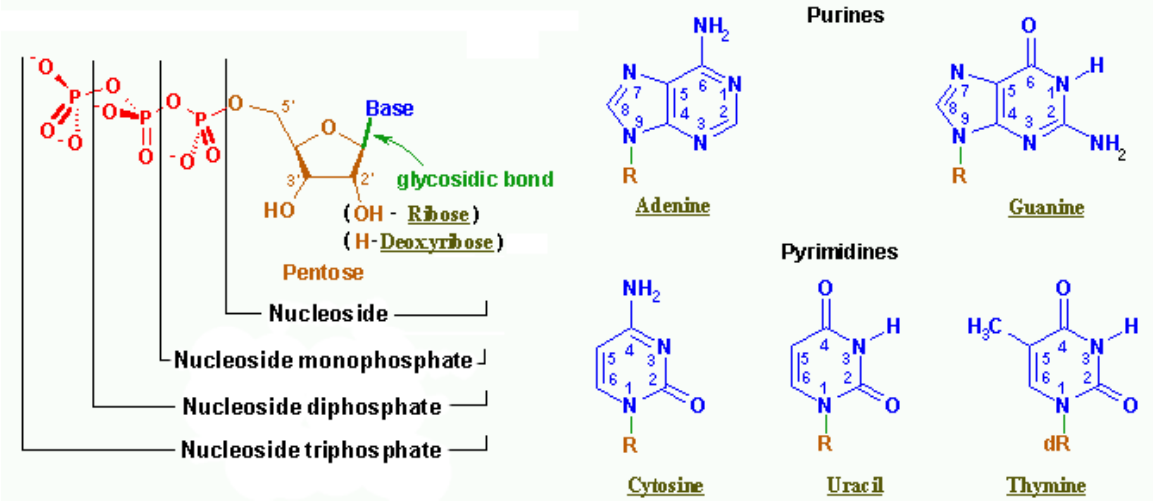

Figure 1-2: Chemical structure of nucleoside triphosphates[1]

- The two DNA *primers* are short (20–100 bases) single stranded pieces of DNA that flank the target region within the DNA template. See Figure 1-3 and Figure 1-4, for an illustration as to why the primer pair defines the target region. When they bind to the template, they define the starting point of amplification. The starting point of one strand is the ending point of its complimentary strand. Thus, after a few cycles all the products start and end at the DNA primers. These primers can be synthesized in-house or easily obtained from a vendor such as Integrated DNA Technologies[2]. Design of these sequences can be complicated, but software such as MIT's Prime3 exists to facilitate the primer design process[3]. Some guidelines are given below:
    - The sequences should be designed such that the target DNA is contained between the primers and is about 100–1000 base pairs (bp) in length.
    - Sequence length should be about 15–30 bases long. Sequences that are too short lack specificity. To illustrate this point, consider that the complementary sequence of a primer of length 1 can be found in ¼ of the sequences of length 1. For length 2, about 1/16 of the length 2 sequences are complimentary. For length 16, only one in set of 4.3×10^9 (4^{16}, about the length of the human genome) random 16-mers will match. Thus, sequences should be larger than about 16 bases. The upper limit is driven by specificity as well. An extremely long primer will base pair despite a single-base mismatch because the other correct pairings provide enough thermodynamic driving force to sustain one mismatch. The most common primer lengths used are about 20 bases long. Within these 20 bases, the 3' end of the primer is most important since Taq DNA Polymerase will

extend this end when assembling the new strand even if the 5' end is slightly mismatched and not binding efficiently. In fact, the 5' end can be modified to carry additional sequences such as restriction sites that are not complementary to the template.

- The melting temperature (T_m) of primers should be about 52–58^oC. This is the temperature above which the DNA separates from its compliment to become two single strands of DNA. T_m that is too low will require a low annealing temperature that allows nonspecific primer binding while temperatures should not be higher than the elongation temperature as DNA synthesis will prematurely start. The annealing temperature is often set at 5^oC lower than the lower T_m of the two primers to start then further optimized using trial and error. A simplified correlation for estimating the melting temperature for primers is:

$$T_m(^oC) = 4(G+C) + 2(A+T) \quad \text{Equation 1-1}$$

Where G,C,A,T represent the number of instances of the respective bases.

- Primers should not contain sequences that result in secondary structure. This structure occurs when two regions of the primer compliment each other, causing the DNA strand to curve and bind to itself much like tape sticking to itself. This shields the primer DNA from accessing the template DNA. Furthermore, primers should not be complementary to each other to avoid primer-dimer formation. Partial dimer formation will result in amplification of the primers themselves.

- In some cases, mispriming is specifically designed into the primers. Point mutations (a difference of one nucleotide between the mutant and original DNA strand) can be introduced into DNA sequences by first introducing them into primers. Larger sets of nucleotides such as a restriction endonuclease recognition site can be added to the 5' ends of primers to allow the amplicons to be inserted into a cloning vector and expressed in bacterial cells. These techniques are part of the field of molecular biology enabled by PCR: molecular cloning.

- *DNA Polymerase* is an enzyme that continues synthesis of a complementary strand of DNA. In the early implementations of PCR, E.Coli DNA polymerase (in particular, the Klenow fragment) was destroyed at the melting DNA temperatures (~95^{o}C) and thus replaced after every cycle. Furthermore, the ideal temperature for synthesis using this polymerase was 37°C; however, this allowed primers to bind to noncomplementary regions thus reducing specificity. Biologists eventually moved to Taq Polymerase I because it is thermally stable at 95^{o}C. This move is considered by many as the most important development towards the wide usage of PCR[4]. Taq polymerase was originally isolated from *Thermus aquaticus* bacteria that live in hot springs and thus have polymerase that can withstand high temperatures. The enzyme has optimal activity around 70–80^{o}C, and a half life of about 10 minutes at 97^{o}C.[5] Not only did this lead to survivability at the denaturization step, it allowed higher annealing temperatures which lead to increased primer binding specificity and reduction in secondary structures in the template and target strands. At the optimal temperature, Taq polymerase has an estimated extension speed of about 60

nucleotides per second. For the ~120 bp target region in this study, this would mean a minimum of 2 seconds is required for the DNA synthesis step; however, the processivity (average number of nucleotides incorporated until the polymerase dissociates) of the enzyme is only about 60 nucleotides thus a full 15 seconds is used. The enzyme also features a 5' → 3' exonuclease activity, meaning it can destroy a pre-existing strand of DNA that is in front of it when synthesizing the new strand. This feature is useful for FRET-based real time PCR, discussed in Section 1.2.2.2. Taq polymerase used in modern reactions are recombinant (i.e., have an altered protein sequence) and packaged with molecules that disable activity at room temperature but restore full activity upon heating to 95^{o}C ("hot start" polymerase). Invitrogen's Taq polymerase contains anti-Taq polymerase antibodies that serve this function[6]. One major disadvantage of Taq polymerase is the lack of a "proofreading" ability, resulting from random errors in replication (about 1 per 10^4 nucleotides[4]). Since the errors are random, they are not significant for most applications of PCR since a given site has an overwhelming number of correct nucleotides compared to the erroneous ones. For applications where even slight errors are not tolerable, DNA polymerase from other organisms such as *Pyrococcus furiosus* and *Thermococcus Litoralis* can be used.

- The *buffer solution* maintains the optimal pH and salt concentration values for efficient amplification. This solution is often purchased from a vendor in a pre-mixed form. It is typically a Tris-HCl buffer system around pH 8.4 with KCl and some $MgCl_2$ already added. Of particular importance is the concentration of Mg^{2+} ions that are often supplied separately since each reaction condition requires a different

concentration. The ions function as a cofactor for Taq polymerase and also enhance the ability of primers to bind to the target/template DNA. Excess Mg^{2+}, however, causes Taq DNA polymerase to become more error prone[4]. The buffer solution may also be tested for the absence of DNase and RNase, enzymes that degrade DNA and RNA, respectively.

1.1.2 Procedure

The PCR reaction solution is assembled to a total of 20–100 µL in a plastic thin walled reaction tube and placed in a thermal cycler for 30–40 cycles.

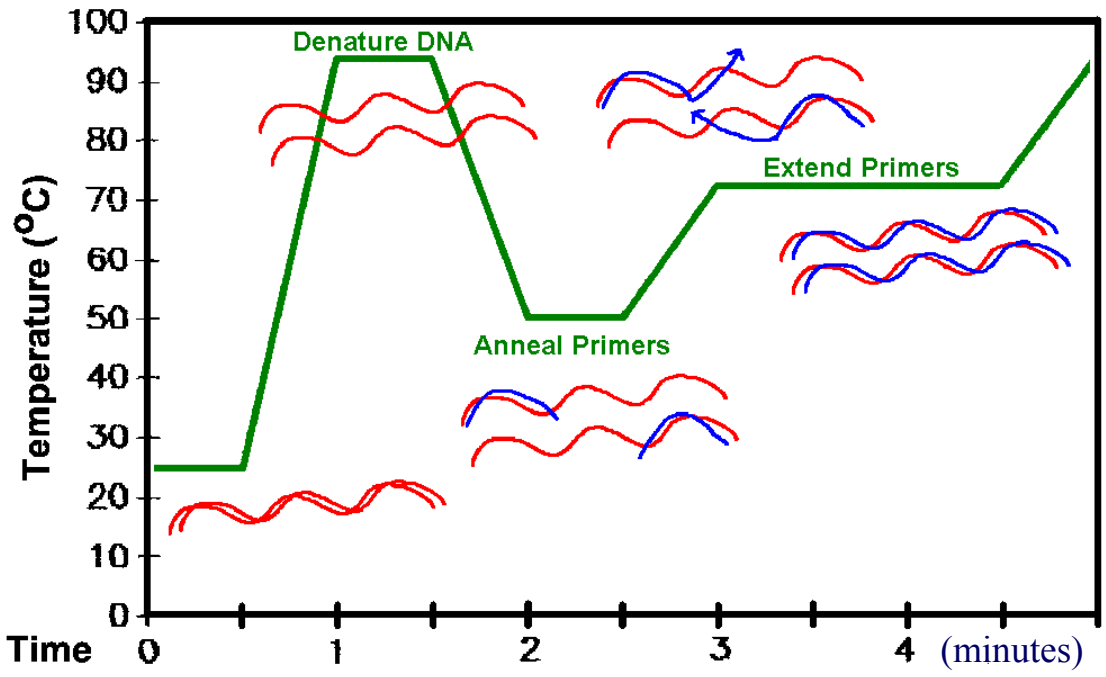

Figure 1-3: Typical thermal recipe for PCR

A typical thermal recipe is:

1. 94^0C for 2 minutes. This *initialization step* activates specially modified Taq polymerases which are designed for minimal activity at room temperature. Also, during this step the template DNA and primers fully dissociated. This step occurs only once in the reaction.
2. 94^0C for 15–30 seconds. This *denaturation step* dissociates the DNA targets (also called amplicons) produced during previous cycles by disrupting the hydrogen bonds between complementary bases. This exposes the bases and allows the primers bind to them in the next step.
3. 55^0C for 15–30 seconds. During this *annealing* step, the primers bind to their complementary sequences in the target DNA.
4. 72^0C for 15–30 seconds. This is the *extension* step when the DNA polymerase extends the DNA strand starting from the primers, assembling from the 5' to 3' end of the new DNA strand by adding the complementary dNTP to the elongating strand.
5. Repeat steps 2–4 for about 30–40 cycles. After each cycle, the number of DNA molecules is theoretically doubled if 100% efficient.
6. *Final Elongation*. This step is often performed at 72^0C for 5 minutes to ensure any remaining single-stranded DNA is fully extended.

The exact temperatures and times used vary from reaction to reaction. For a given reaction, a series of conditions must be tested to find an optimal set. Here are some guidelines for choosing a thermal recipe:

- Denaturation step: Increasing temperature causes faster breakdown of Taq polymerase while lowering the temperature below the melting point of the target DNA would halt replication.
- Annealing step: This temperature varies the most as it has the most effect on PCR. Too high temperature will result in reduced products since a smaller fraction of primers can overcome the thermal energy required to remain bonded. Too low temperature is also detrimental as it allows primers to bind nonspecifically, resulting in multiple products, seen as multiple bands on gel electrophoresis. Low temperatures promote secondary structures on DNA.
- Extension step: Excessively high or low temperatures will result in non-optimal performance by Taq polymerase.

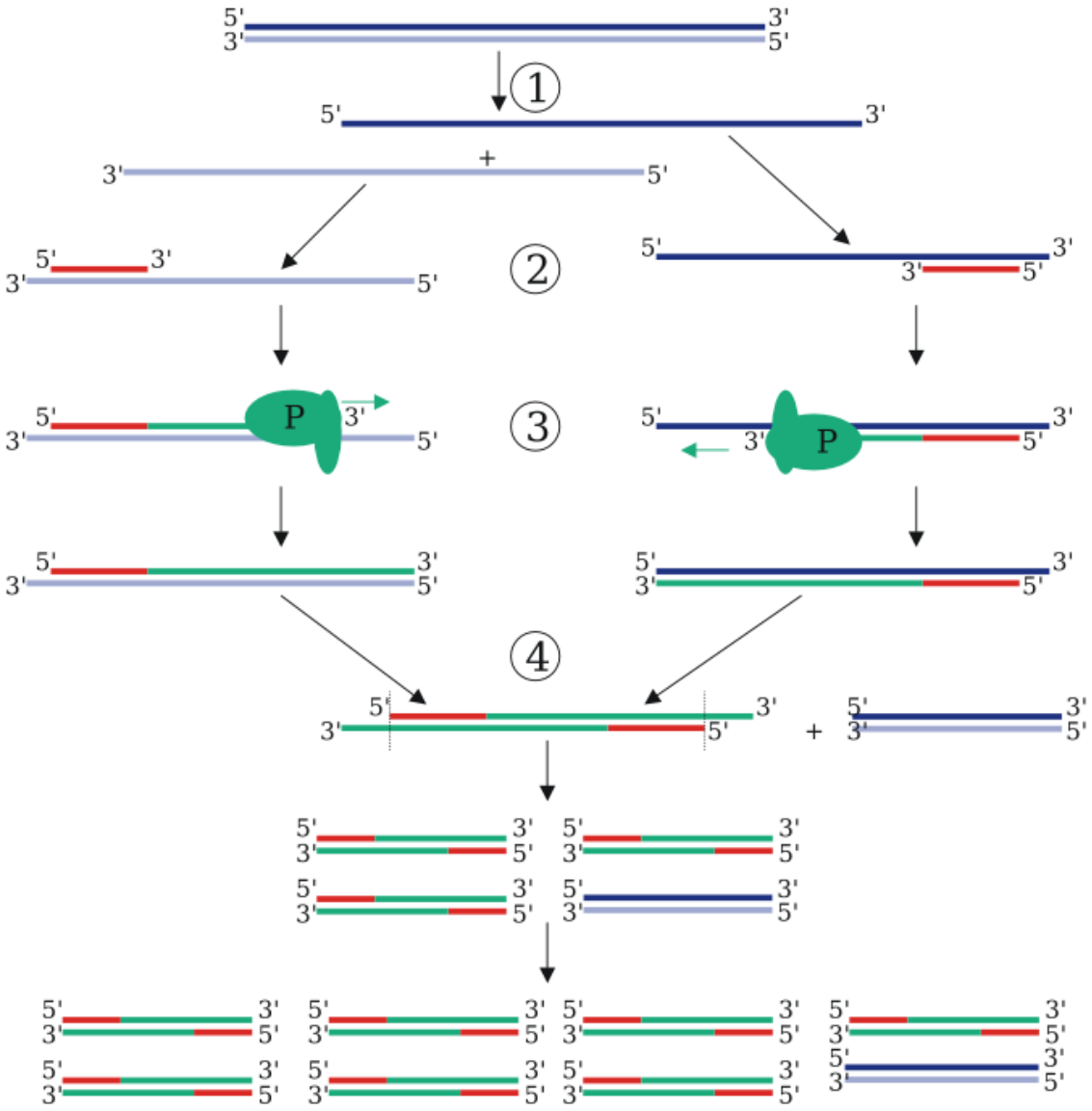

Figure 1-4: PCR schematic illustrating selective amplification of the target region between the primer pairs[7].

1.1.3 Molecular Level Theory

In Figure 1-4, step 1 refers to the denaturalization of the template forming two single stranded pieces of DNA. Step 2 shows the annealing step where the primers bind. Step 3 is the elongation step. Notice that although elongation starts at the primer, it ends when the polymerase (labeled with a P) simply runs out of template to replicate. For the template molecules, this end can be incredibly far from the primer binding region, creating extra-long products. These products, when used in the next cycle, however, produce products whose length is the region between the primers (step 4). It can be seen that after the first few cycles, the majority of products (also called amplicons) will contain only the target region while the original templates and extra-long products become a minority. A more quantitative description will be provided in the next chapter.

1.1.4 Equipment

The main piece of equipment required to perform PCR is a thermal cycler. Such a machine attempts to cycle between the relevant temperatures as quickly as possible. In early implementation of PCR, the scientist would manually transfer the PCR mixture from one water bath to the next. Furthermore, before the Taq DNA polymerase came into usage, PCR required addition of fresh *E. coli* DNA polymerase after each denaturing step. Modern machines have one computer-controlled heating block that cycles through temperatures at programmed times. The machines also have a heated cover that keeps the caps of the reaction tubes at 105^{o}C. This prevents condensation of the water vapor on the cap, which in turn keeps the concentrations and pH of the reaction solution constant.

A typical machine is the Bio-Rad MJ Mini Gradient Thermal Cycler (Figure 1-5**Error! Reference source not found.**). Some specifications are provided in Table 1-1 below[8]:

Table 1-1: Technical specifications for the Bio-Rad MJ Mini PCR Machine

Ramping speed	2.5^0C/s
Input power	400W max
Dimensions (WxDxH)	19 x 32 x 20 cm
Weight	4.1 kg

Figure 1-5: MJ Thermal Cycler from Bio-RAD

Currently PCR machines are relatively large, heavy, slow, and require hundreds of watts power. The use of a bulky thermal block causes slow temperature ramp rates. These issues can be addressed using MEMS technology.

1.1.5 Gel Electrophoresis

Following PCR, gel electrophoresis is used to determine if the anticipated DNA target was amplified. Using this technique, a DNA ladder (mixture of fragments of DNA of known size) is run alongside the PCR sample to obtain an estimate of the size of the product (sometimes referred to as the amplicon). If only one product is formed that is of the anticipated length, one can be reasonably assured that the amplicon is in fact that

identical to the target DNA. If further reassurance is required, one can sequence parts of the amplicon or bind it to a probe strand of known sequence.

1.1.6 Applications

Since PCR is a DNA-based analysis it is versatile due to the fact that all organisms have DNA or RNA which can be converted to DNA. The usage of DNA primers takes advantage of the naturally evolved base pairing phenomenon that provides excellent specificity. The assay is also practical because tests can be performed in about one hour using a few pieces of equipment that are standard in modern biology laboratories and using cheap, easily obtainable reagents.

PCR can supply large amounts of specific DNA for further analysis and can be used "downstream" from other assays. This is particularly useful when only small amounts of the original template DNA is present such as in forensic analysis. It can be used to isolate a specific region of DNA for purposes such as bacterial transformation and is a central part of the Sanger sequencing method for determining the sequence of DNA fragments. Perhaps the most well known application of PCR is DNA fingerprinting used in criminal trials. DNA fingerprinting can also be used in paternity testing and even determine evolutionary relationships between organisms. By designing primers that amplify a DNA sequence that is unique to virus, one can identify its presence in a sample. PCR can also be used to diagnose diseases such as cancer.

1.2 Real Time PCR

The real time polymerase chain reaction (RTPCR) or quantitative polymerase chain reaction (qPCR) is a procedure based on PCR where a piece of target DNA is both amplified and quantified (using fluorescence) simultaneously.

1.2.1 Theory

From the background of PCR, it is seen that the number of DNA target molecules doubles after every cycle. Mathematically, this can be written as:

$$T = T_0 * 2^c \quad \text{Equation 1-2}$$

where
T = current number of target molecules
T_0= initial number of target molecules
c = number of cycles

Furthermore, if one allows for a nonidealistic efficiency, the value "2" can be substituted with (1+E) where E ($0 < E < 1$) is the average efficiency after c cycles. Thus, **Equation 1-2** becomes:

$$T = T_0 (1 + E)^c \quad \text{Equation 1-3}$$

Since we choose a constant value for E here **Equation 1-3** is only valid for the early cycles, before the efficiency becomes unpredictable due to a variety of factors such as degradation of Taq polymerase after repeated thermal cycling. These early cycles are referred to as the "exponential phase" and their termination can be identified by the

deviation in exponential shape of a T versus c curve or deviation of linearity in a log (T) versus c curve.

1.2.2 Fluorescent Indicators

1.2.2.1 SYBR Green

SYBR Green I (SG) is a nucleic acid stain with many uses including double stranded DNA (dsDNA) quantification in real time PCR and gel electrophoresis. For the latter, it is generally considered a safer alternative to ethidium bromide, with 25X better sensitivity. Upon binding to double stranded DNA, its fluorescence intensity becomes 1,000 times that of its unbound state, with a quantum yield of ~0.8.[9] This large gain in fluorescence contributes to a good signal-to-noise ratio as non-bound SG in the solution and walls of the container contribute minimal noise. Its chemical structure is shown in Figure 1-6. At low concentrations, the dye binds to DNA by intercalation; however, at the higher working concentrations for qPCR, surface binding dominates (evidence suggests the surface binding occurs at the minor groove of dsDNA)[10]. The stock stain solution comes dissolved in DMSO (dimethylsulfoxide) and stored frozen (-20^{o}C) until use. After a 10,000X dilution for RTPCR analysis, the working concentration is about 2 μM.

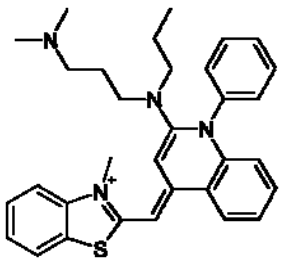

Figure 1-6: Chemical Structure of SYBR Green I

Its double stranded DNA-bound fluorescence spectrum is available in Figure 1-7.

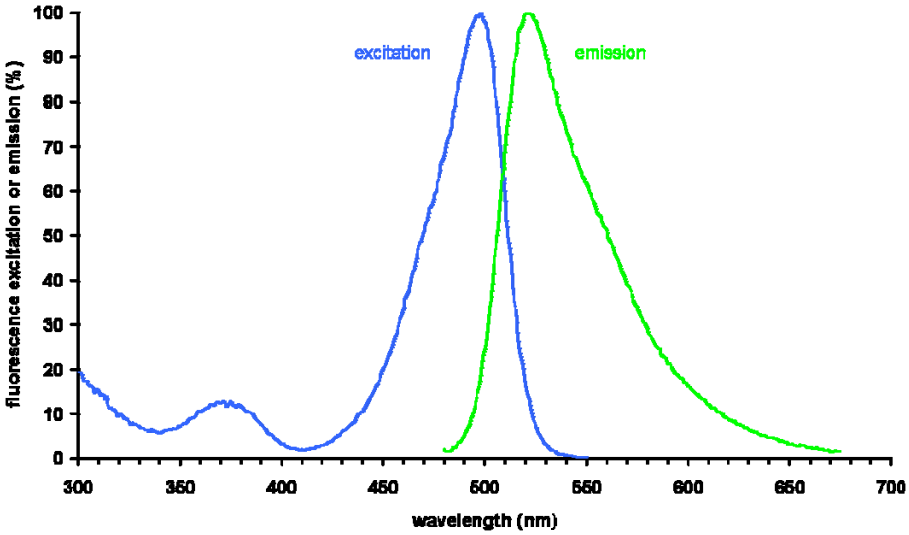

Figure 1-7: Fluorescence spectrum of SYBR Green I[11]

Since SYBR Green I binds to all double stranded DNA (at the working concentrations), it can be used irrespective of target DNA sequence, making it versatile. As the number of double stranded DNA molecules increases, so does the fluorescence. This feature is also its biggest limitation as non-specific (non-target-DNA) sequences that are unintentionally amplified also produce a fluorescence signal. This limitation is partially addressed by the generation of melting curves and gel electrophoresis to check for purity and length of the product. Removal of SYBR Green from DNA can be achieved by ethanol precipitation. Add ethanol to cause the DNA to precipitate, then centrifuge the pellet, wash it again in ethanol, allow to dry, then resuspend in buffer solution.

1.2.2.2 TaqMan

An alternative to SYBR Green I are the family of TaqMan probes. These have the advantage of fluorescing only during the synthesis of the target DNA, thus adding another level of specificity. A schematic of the TaqMan probe system is shown in Figure 1-8.

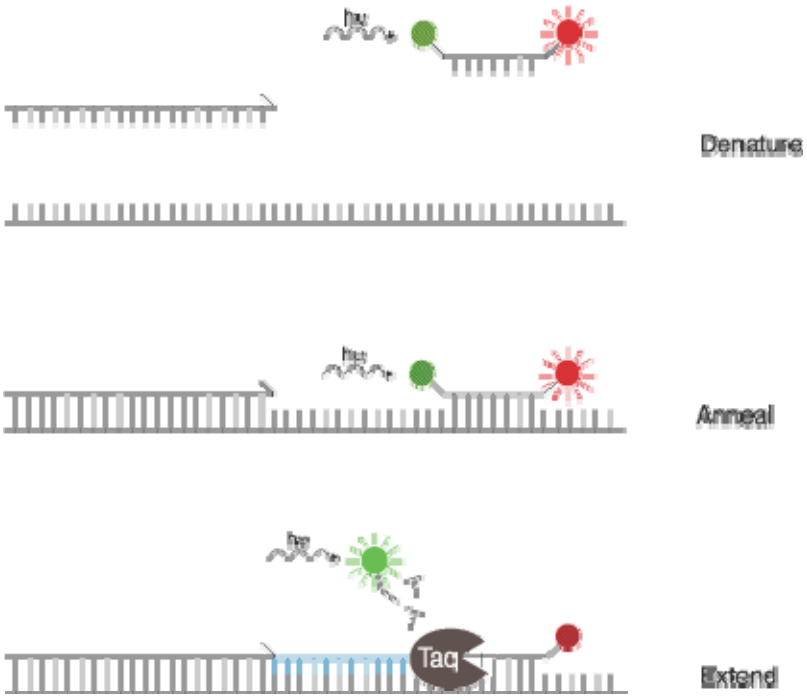

Figure 1-8: Schematic of TaqMan probes

In its free state, the green and red fluorophores are connected via the DNA bases between them. These bases are designed to be complementary to a sequence within the target DNA. The proximity allows Förster resonance energy transfer (FRET) to occur: the energy from the optically excited green fluorophore (donor molecule) transfers to the red fluorophore (acceptor molecule) which accepts and dissipates the energy as heat or

light in a longer wavelength. During the annealing step of RTPCR, the TaqMan probe binds to its complementary sequence on the target DNA (step labeled as “anneal” above). During the extension step, as Taq DNA polymerase extends the target DNA, it destroys the seemingly disruptive Taqman probe as it synthesizes the new strand. This allows the green fluorophore to become spatially separated from the red quenching molecule, thus emitting its green photons instead of participating in FRET. This increase in fluorescence is then measured by the RTPCR machine.

This mechanism is key to the added specificity provided by the Taqman system. If the target DNA does not exist, the probes will not bind and thus not be destroyed by DNA polymerase. Also if the target region is present but the primer pairs fail to function correctly no fluorophore is emitted. The specificity of the Taqman system limits its scope in usage. Custom probes must be synthesized for each target, increasing costs for research.

1.2.3 Calibration Curves

The key that allows real time PCR to be quantitative is the relationship between the starting number of template DNA molecules and the number of cycles required to amplify it to a set amount. If there are more starting molecules, fewer cycles are required. Below is an example of how a calibration curve is obtained followed by an analysis of the process.

- Obtain a sample of known template DNA concentration
- Prepare 10 fold serial dilutions to generate multiple data points for the curve
- Perform RTPCR on these samples

The data from these steps results in a graph such as the one below:

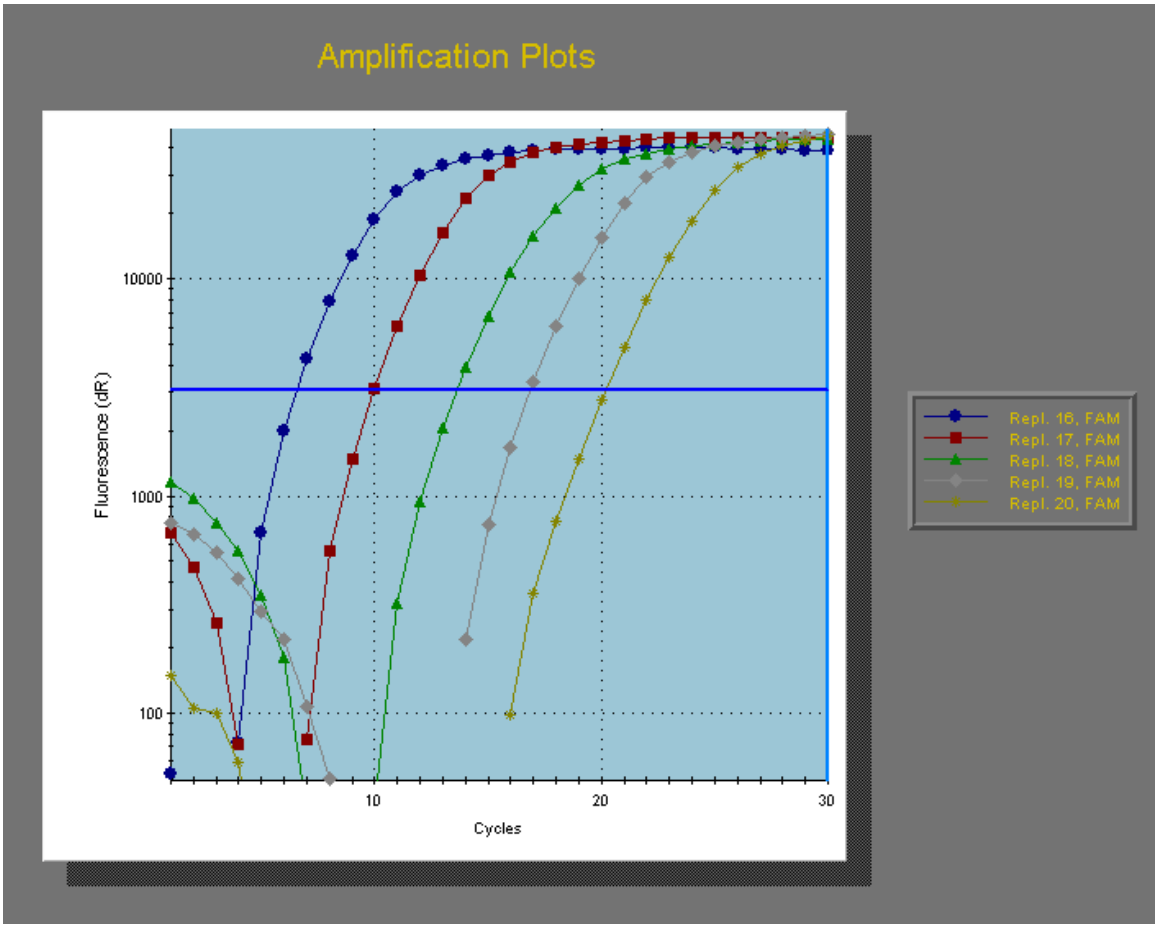

Figure 1-9: Amplification plots for a calibration curve. Replaces 16–20 are 10-fold serial dilutions.

- From the above data, choose a "threshold" fluorescence value (blue solid line) that crosses the sample curve where they are all linear (in a log-fluorescence versus linear cycle number plot)
- Note the number of cycles required by each known concentration to reach the threshold fluorescence, call it c_t and plot it against the concentration

These steps yield a curve such as shown in Figure 1-10:

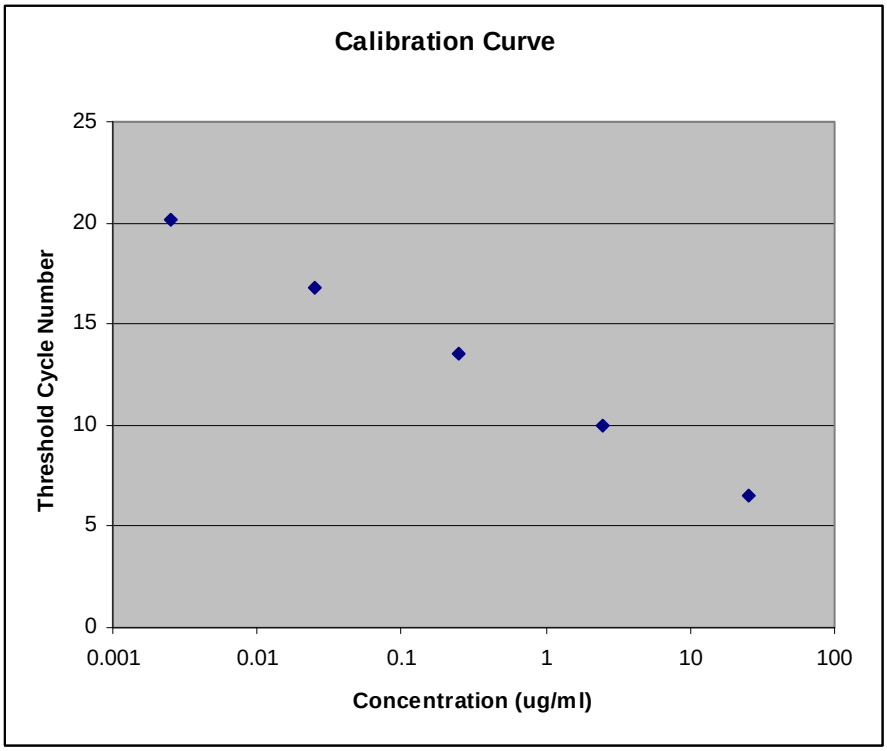

Figure 1-10: Calibration curve for an M13 virus DNA sample

From this plot the concentration of an unknown sample (assuming identical experimental conditions) can be estimated by observing its threshold cycle number. Using linear regression, a relationship for this curve yields:

$$C_t = -3.423 Log(T_0) + 11.33 \quad \text{Equation 1-4}$$
$$E = 95.9\%$$

where

C_t is the number of cycle required to reach the threshold fluorescence

T_0 is the initial concentration of template DNA molecules

E is the efficiency of the reaction

A mathematical derivation of Equation 1-4 is now given. By rearranging **Equation 1-3**, the relationship between starting DNA copy number T_0 and cycle number c can be derived using simple algebra as:

$$c = \frac{-1}{\log(1+E)}\log(T_0) + \frac{\log(T)}{\log(1+E)} \quad \textbf{Equation 1-5}$$

To find a one-to-one correlation, the parameters T and E must be kept constant. For a constant value of target molecules T, we choose a set value for the threshold fluorescence (this assumes a linear relationship between fluorescence reading and number of target molecules which is generally a good assumption) and call it T_t. To obtain a constant efficiency E we narrow the range of threshold fluorescence values to only when the reaction is in the "exponential phase" or the linear phase in a log plot. When T = T_t, the observed c is the threshold cycle number, c_t. Thus,

$$c_t = \frac{-1}{\log(1+E)}\log(T_0) + \frac{\log(T_t)}{\log(1+E)} \quad \text{Equation 1-6}$$

If m is the slope of a c_t versus $\log(T_0)$ plot, the efficiency E can be calculated:

$$m = \frac{-1}{\log(1+E)} \Rightarrow E = 10^{-1/m} - 1 \quad \text{Equation 1-7}$$

1.2.4 Equipment

There are many manufacturers of real time PCR machines including BioRAD, Applied Biosystems, Roche, Cepheid, and Strategene. The "entry level" models from these manufacturers are very similar, most featuring an LED or halogen light source,

peltier-based heating and cooling, CCD or photodiode photodetectors with rotating filter wheels, and a thermal block that fits standard 48 or 96 well plates. These machines typically cost around $30,000, weight 20 kg, use max 10 Amps at 120 VAC, and have a length scale of about 40 cm. Temperature ramping times are typically 10^0C/second and results are obtained in about 1.5 hours.

Some companies seek to differentiate their machines with slight modifications. The Roche Light Cycler 2.0 has a rotating carousel of capillary tubes instead of a 96 well plate thermal block. In this design, temperature distribution is more uniform as a fan blows heated or cooled air past the rotating carousel. The Applied Biosystems StepOne model is a standalone unit that does not require a computer and has its own touch-screen interface. The Strategene MX 3000P and MX 3005P models (shown below) feature a scanning photodetector unit comprised of a fiber optic cable leading to a photomultiplier tube with a 5 color filter wheel. This design eliminates non-uniformity in the fluorescence detection, a problem faced by the CCD image capture approach.

Figure 1-11: Strategene MX3005P benchtop RTPCR system

1.2.5 Applications

Two applications of real time PCR are described below: pathogen detection and mRNA expression profiling.

1.2.5.1 Pathogen Detection

Pathogen detection is a popular application of real time PCR. The versatility of this technique is demonstrated by Zeng et al[12] as they detect the airborne mold *Cladosporium*, an allergen. They determined the presence of 10^4 spores/m^3 in two locations: a countryside house that houses firewood and a paper factory. A higher level at 10^7 spores/m^3 was detected in a cow barn. These levels exceed the medically recommended maximum exposure of 3000 spores/m^3. Prolonged exposure can weaken the immune system and cause severe asthma. In past studies, detection of *Cladosporium* was based on slower methods including cell culture, in which spores were grown in an incubation chamber before microscopic identification by eyes, a time-consuming and labor-intensive approach.

To test the sensitivity of their array, they performed a serial dilution test (Figure 1-12). The most dilute sample detected (labeled #6) corresponded to only 2 spores. This sensitivity of down to 1 genome copy is not uncommon in RTPCR assays.

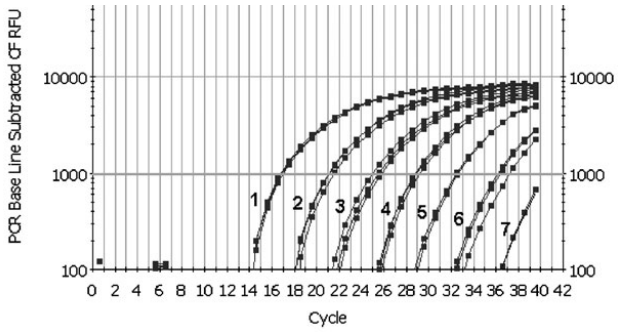

Figure 1-12: Serial dilutions to determine sensitivity of assay[13]

To test for specificity, the authors performed the same assay on different types of fungi (Figure 1-13). The various species of *Cladosporium* gave a typical signal while other types of fungi showed virtually no signal.

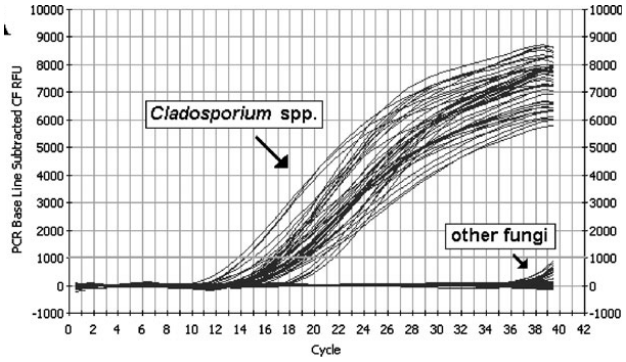

Figure 1-13: Assay specificity

1.2.5.2 mRNA Expression Profiling

As described in the earlier section, real time PCR allows quantification of initial template DNA amount when compared against a calibration curve. An extension of this technique is to quantify the amount of specific messenger ribonucleic acid (mRNA) expressed in a cell or tissue by first reverse transcribing the mRNA into complementary DNA (cDNA). This technique is referred to as reverse transcription quantitative PCR (RTqPCR). Some authors also call this technique RTPCR, so care must be taken to distinguish between "real time" PCR and "reverse transcription" PCR.

Upon stimulation, cells will undergo a "signal transduction" process resulting in the transcription of mRNA which travels from the nucleus (where the DNA is) into the cytoplasm to be translated into proteins and enzymes. Quantification of amounts of a particular mRNA gives insight into a cell's natural function and reaction to stimuli such as drugs or signaling molecules from other cells and is of great importance in the field of

biology. Although there are various methods, in recent years RT-QPCR has emerged as the method of choice for this analysis[14].

1.3 Chapter Summary

Requiring simple, affordable machinery and components, real time PCR is easy to implement for extension of PCR that provides a new dimension to PCR analysis. By monitoring the amount of DNA present via fluorescence, quantification of the initial amount of DNA or RNA in the sample can be achieved.

2 Parylene Microfluidics

This chapter serves as a short introduction to microfluidics including some background, reasons for using microfluidics, and basic technologies. Parylene as a microfluidics material is discussed in the middle of the chapter and microfluidics as applied to real time PCR is discussed towards the end.

2.1 MEMS Background

The microelectronic industry has greatly matured since the discovery of the transistor effect in semiconductors in the 1940s. Whereas early computers filled entire rooms and were only accessible to a few users through terminals, today portable "smart" cell phones have far superior computational power packed into a hand-held device. These devices are small, light, and affordable.

Such a dramatic change in capabilities and portability in electrical and computational devices has inspired an analogous effort in the mechanical and biological realms using similar technology. Since MEMS was born from microelectronics, both fields share similarities in materials and patterning technology. Recently, however, with increasing interest in biological assays in MEMS, new materials and methods are being introduced that are more biocompatible.

2.2 General Microfluidics Technology

At the core of microfluidics technology is photolithography: using an energy beam to pattern thin photosensitive films (called photoresists). The energy beam can be composed of photons (light, UV), electrons, X-ray photons, or even ions. In this work

only UV photons are used. The thin films used depend on the energy source but their general principle is shown in Figure 2-1.

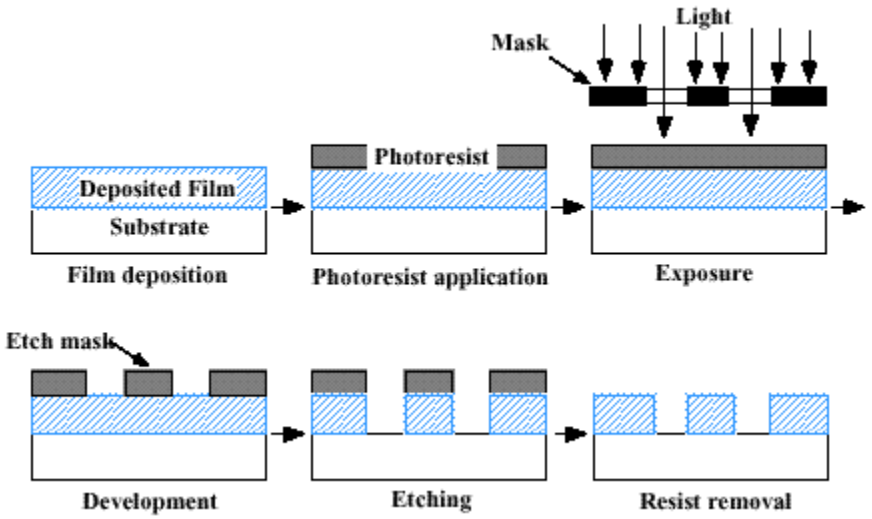

Figure 2-1: Basic schematic of photolithography [15]

- Film deposition: A thin film to be patterned is deposited onto a substrate. Because MEMS originated from microelectronics, silicon is still commonly used as a substrate. The thin film can be silicon oxide, silicon nitride, metal, poly silicon, or a polymer. Often it is the silicon itself that is to be patterned, in which case no thin film is deposited.
- Photoresist application: To pattern a thin film deposited on a substrate, a photosensitive photoresist layer is deposited. This is often performed by placing the substrate on a spinner, pouring the photoresist suspension onto a wafer then spinning between 1000–8000 rpm, depending on the desired thickness and viscosity of the suspension. The casting solvent is then removed by evaporation in an oven or hot plate.

- Exposure: A light source such as a mercury lamp is used to supply energy while a mask is used to supply the pattern. This mask itself is usually a glass plate with patterned chromium as the reflecting layer. The photoresist reacts to the light in a way that changes its solubility in a developer solution. One example of this process is the DQN family of photoresists. They are comprised of a photoactive diazoquinone ester (DQ) and a phenolic novolak resin (N). Upon exposure, the DQ undergoes a photochemical reaction that makes the DQN soluble in a basic developer solution while the unexposed regions remain insoluble[18]. Some types of resists also require a post-exposure bake to speed up reactions that initiated during exposure.
- Development: During this step, the wafer is exposed to a solution that selectively dissolves only the portions of the photoresist that has been exposed to UV. For "negative" photoresists, the portions that were *not* exposed are dissolved. The wafer is then rinsed and dried, resulting in a patterned photoresist layer. At this time, the resist is often "hard baked" or "post baked" by placing into an oven or hotplate to further drive away remaining development solution, casting solvent, or moisture, resulting in a hardened film with increased resistance to etching environments. A mild oxygen treatment referred to as "de-scumming" may also be executed here to etch away any photoresist residue that may not have been developed away.
- Etching: With the photoresist in place, the wafer can be placed into an etching environment such as a plasma or acidic metal etching solution. The photoresist

protects the layers that are underneath it from the etchant such that the thin film's pattern matches the resist pattern.

- Resist removal: After etching, the resist has served its purpose and can now be removed. A photoresist stripper solution can be purchased from the resist vendor. Some resists easily dissolve in common organic solvents such as acetone.

A key feature of the photolithography process is that features can be mass produced on wafers. As seen in Figure 2-2, the pattern from one mask can be projected onto a wafer repeatedly to make tens to hundreds of devices simultaneously. This projector can also reduce the size of mask features, for example, by a factor of 10. The optical limit for feature sizes is given by Rayleigh's criteria:

$$W_{\min} \approx \frac{k\lambda}{NA} \quad \text{Equation 2-1}$$

Where k is a constant related to the contrast of the photoresist (typically 0.75), NA is the numerical aperture of the projection system (about 0.6), and λ is the wavelength of light used (365 nm). In this example, the minimum feature size under the optical limit would be about 0.5 μm[16].

As a result of these basic fabrication features, MEMS devices are smaller, lighter, and possibly cheaper. In some cases performance is improved and potential integration of many functions onto one chip exists.

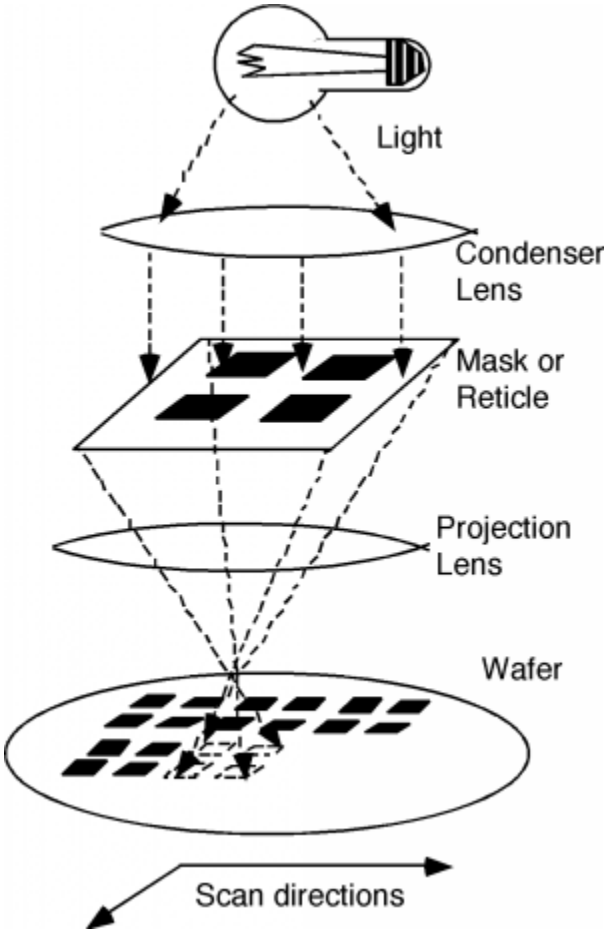

Figure 2-2: Photolithography using a stepper[17]

2.3 MEMS Technologies for PCR Microdevices

The general outline of photolithography given above is now extended to include MEMS techniques that are of particular interest in making PCR microdevices.

2.3.1 Bulk Micromachining

Bulk micromachining refers to the fabrication schemes that form a fluidic channel by etching into the substrate (glass or silicon) then bonding to a cover unit (also glass or silicon).

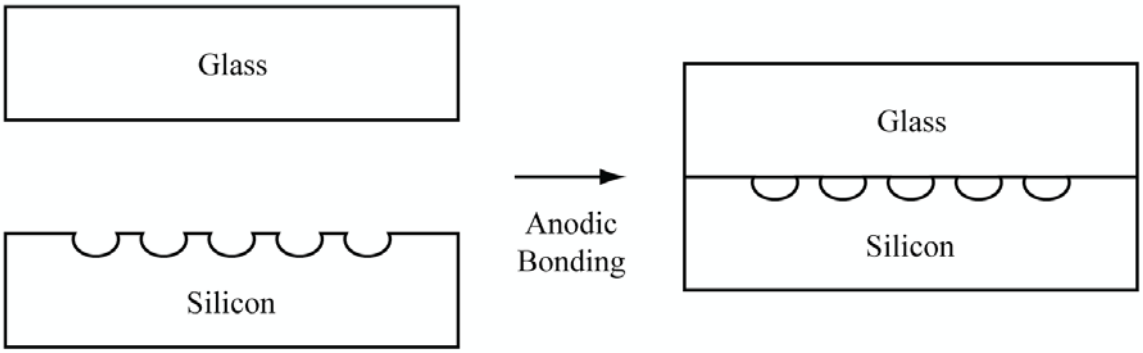

Figure 2-3: Example of bulk micromachining

Silicon is often used as a substrate because of the wide variety of etching methods already developed for it and the potential of starting fabrication with a pre-fabricated CMOS chip. Both isotropic and anisotropic wet and dry etching technologies are available (see Table 2-1).

Table 2-1: Methods for etching silicon

	Wet Etching	Dry Etching
Isotropic	HNA	XeF_2
Anisotropic	KOH	RIE, DRIE

HNA etching is an isotropic mixture of hydrofluoric acid, nitric acid, and acetic acid to form a solution that oxidizes silicon (caused by the nitric acid), then etches the oxide (caused by the hydrofluoric acid), subsequently oxidizing the freshly exposed silicon (caused by the nitric acid). Acetic acid is used as a diluent instead of water because it prevents dissociation of the nitric acid since oxidation requires undissociated NHO_3[18]. The overall reaction is:

$$Si + HNO_3 + 6HF \rightarrow H_2SiF_6 + HNO_2 + H_2O + H_2 \quad \text{Reaction 2-1}$$

KOH etching utilizes potassium hydroxide which anisotropically etches the {111} planes of silicon 30–100x slower than the {100} planes. These solutions are usually kept at high pH values (>12) and high temperatures (70^{o}C) as they are considerably slower than the isotropic etching due to the slow chemistry at the surface. One proposed overall reaction mechanism is:

$$Si + 2OH^- + 2H_2O \rightarrow SiO_2(OH)_2^{2-} + 2H_2 \quad \text{Reaction 2-2}$$

In addition to KOH, other oxides used are sodium hydroxide (NaOH), tetremethyl ammonium hydroxide (TMAH), ammonium hydroxide (NH_4OH), and many more.
For dry isotropic etching, XeF_2 gas is used. The overall reaction is:

$$2\ XeF_2 + Si \rightarrow 2Xe + SiF_4 \quad \text{Reaction 2-3}$$

This reaction does not require ion bombardment, heat, or other external energy sources. Since it is dry and chemical in nature, many masking materials can be used including aluminum, silicon dioxide, silicon nitride, photoresist, and parylene. These properties make it useful in post-processing CMOS integrated circuits[19]. Etch rates are in the 1 μm/min order of magnitude with actual rate highly dependent on silicon load and feature sizes.

Slight anisotropic etching (2:1 aspect ratio) can be achieved using a plasma based on SF_6 (sulfer hexafluoride) and will etch silicon to form the gaseous product SiF_4 which diffuses back into the plasma, creating a new surface to be etched. In the reactive ion etching (RIE) configuration, a parallel plate chamber is formed, producing a biasing electric field that drives ions towards the substrate. Since the pressure is in the 300 mTorr range (compared to 2.5 Torr for XeF_2), the mean free path is low enough for slightly directional (in the z direction) etching with a smaller component of lateral etching caused by interactions between etching molecules.

If true anisotropic etching is required, deep reactive ion etching (DRIE) can be used. In this modification of the RIE configuration, a SF_6 plasma is still used to etch silicon but the plasma is either alternated with a C_4F_8 passivation layer for the side walls (Bosch process) or the substrate is chilled to -110^oC (cryogenic process) to minimize chemical etching rates while preserving the ion bombardment mechanism still present in the upward facing surfaces.

Another advantage of the ICP configuration is the separation of the plasma power source and the substrate bias voltage power source. This allows independent control of plasma density and kinetic energy at which ions bombard the substrate. High densities mean the plasma is more chemically reactive while lower kinetic energy means nonspecific mechanical etching (erosion) of mask materials is reduced[20]. This means higher specificity which allows for thinner masking materials, which then allows better in-plane patterning of mask materials since aspect ratios are reduced.

To transform the silicon trenches into channels, the fourth wall must be introduced. This usually occurs by bonding the silicon to either another silicon or glass wafer. A common technique is anodic bonding, where the silicon is placed in contact with a special high-sodium glass at 200–500^{0}C and a high DC voltage (~kV) across the bond. This combination allows the sodium ions in the glass to migrate away from the interface causing a negative charge on the glass side and a positive charge on the silicon side. Electrostatic force then holds the two pieces in place to create a water-tight seal.

Early pioneers using this technology to create PCR devices include Peter Wilding et al. In these early chips, the silicon was etched about 40--80 μm deep and anodically bonded to Pyrex glass to create reaction chambers between 5–10 μL. An external Peltier heater and cooler was used for thermal cycling[21,22]. M.A. Burns et al. published an early integrated DNA analysis system with PCR chamber, elctrophoresis, and optical detector by etching glass slides and bonding them to the electrical and optical components on the silicon[23]. The glass sealing also allows optical access to the solution while thermal cycling for usage in real time PCR. The glass and silicon surface of these devices, however, inhibit the PCR reaction by adsorbing components such as Taq polymerase[24] to an extent that surface treatments such as the addition of BSA must always be used. Furthermore this scheme uses two rigid materials, complicating the integration of moving parts such as valves and pumps.

2.3.2 Soft Lithography

Soft lithography generally refers to the use of elastomers such as polydimethylsiloxane (PDMS) in conjunction with molds to form channels. First, a master mold is formed by bulk methods such as DRIE of silicon or surface methods such

as SU-8 photoresist on top of silicon. A fluid mix of pre-polymer is then poured onto the master and allowed to cure at 80–100 ^{0}C. The PDMS can then be peeled from the master mold, forming a negative replica. Similar to bulk micromachining, a second surface is required to complete the channel. Common glass slides work well as they bond well with PDMS. Surface treatment such as oxygen plasma surface cleaning or application of a thin adhesion layer of PDMS on the glass slide is often used to enhance bonding.

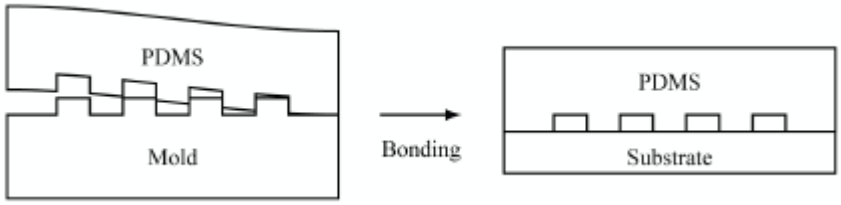

Figure 2-4: PDMS micromolding

The main advantage of soft lithography is its ease of use. Formation of the master mold is the only step that requires a clean room environment. Further processing can be performed in a standard laboratory environment with relatively few pieces of equipment. Furthermore, PDMS is cheap and easily obtained. Inlet and outlet fluidic connections become simple: a needle-poked hole is formed which acts as both a gasket and stabilizer for the capillary tubes. Flexibility allows structures such as pumps and valves to be integrated with channels. This simplicity has allowed a burst of attention and innovation to this microfluidics paradigm. Components such as pumps, valves, and mixers have been fabricated for applications in biochemistry and cell culture[25]. Liu et al[26] demonstrated a novel rotary device in which a plug of PCR solution was passed through a circular channel containing 3 heated regions at 94 °C, 55 °C, and 72 °C. The heaters were fabricated using metal lift-off on the supporting glass slide with tungsten as the

heating component with aluminum leads. This design allowed usage of only 12 nL of solution. The fluid was pushed by peristaltic style pumps fabricated on a separate PDMS layer (control layer) on top of a layer of PDMS with the fluidic channels (fluidic layer). This control scheme provides the actuation for valves, pumps, and fluidic metering for large scale integration. The same group later developed the technology to enable real time PCR on the picoliter scale[27]. A much simpler design for a PDMS QPCR device which does not require any photolithography was presented by Q. Xiang, et al.[28]. Holes of various sizes (1–7 mm) were punched into an unpatterned sheet of PDMS, while another PDMS sheet with a larger (5 mm) hole was placed on top. The bottom holes contained the QCR fluid while the top sheet contained the mineral oil placed on top of the QPCR solution to prevent evaporation. Using a fluorescent microscope and a CCD camera, QPCR reactions were performed.

The advantages of using PDMS are its ease of use and flexibility. Disadvantages of using PDMS arrive from its porosity and surface properties. Evaporation of liquids is common as solvent vapors penetrate the material. Surface treatments are necessary to prevent bio-fouling and protein adsorption. The PDMS-glass interface is not capable of supporting high pressures (over 30 psi). Furthermore, integration into a standard MEMS process or pre-fabricated CMOS chip is limited to placing a finished PDMS piece on top of the chip.

2.3.3 Surface Micromachining

Surface micromachining involves building structures onto the surface of the substrate. Channel formation in this case does not require a second bonding step with

another wafer. Instead the structural material such as polysilicon is deposited on top of a sacrificial layer such as silicon oxide. See Figure 2-5.

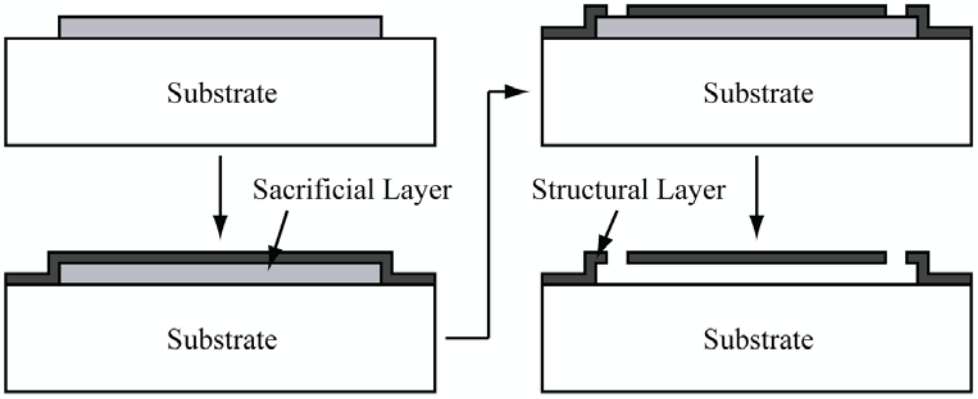

Figure 2-5: Surface micromachining

In this way all four walls of the channel are already present and the inside is hallowed by dissolution of the sacrificial layer. If the finished device uses only surface methods, the substrate may be a cheaper material such as polycarbonate. If polysilicon is used as a structural layer, biocompatibility will be poor, requiring surface treatments. Flexibility and ability to integrate movable parts will also be difficult. An alternative set of materials are parylene for the structural material and photoresist as the sacrificial layer[29]. This scheme will be explored in detail in the next chapter.

2.4 Parylene MEMS Technology

2.4.1 Why Use Parylene?

There are many reasons to use parylene to make microfluidics devices. A brief list of advantages will be given here followed by more detailed discussion in the sub-sections. Parylene is a biocompatible material as shown by its USP Class VI classification, which means the FDA has previously approved its usage in long term human implants. This

elite classification translates well into the biochemical arena as it has been shown as a good material for *in vitro* experimentation as well. Parylene is chemically inert, able to withstand various solvents ranging from organic to acidic. This is convenient for testing purposes as well as during device fabrication where organic solvents are used, for example, to dissolve photoresist. Parylene is optically transparent, allowing direct measurement of fluorescence signals — a requirement for real time PCR. It is flexible (Young's Modulus 4Gpa) rather than brittle, allowing formation of a more robust thin free standing structure/sheet. This also allows for micro-actuation for use in devices such as on-chip valves and pumps. Since parylene is electrically insulative, metal wires which serve as heaters and temperature sensors can be placed directly on top of it, making thermal management more efficient and temperature measurement more accurate. Parylene also has low permeability to gases which prevents evaporative loss of the pcr mixture during thermal cycling. Finally, parylene is compatible with various MEMS processing techniques, which means the usual well established techniques such as metal deposition and photolithography can be used in conjunction with parylene on the wafers.

Parylene is not a new material. It has been used in electronics industry as protective and insulation coatings for circuit boards, wiring assemblies, and as dielectrics for capacitors because of its resistance to moisture penetration and ability to coat devices conformally. It has also been used in the biomedical field as microencapsulation for controlled drug release devices and medical instruments[30] because of its inert properties when interfaced with human tissues. It is thus a natural extension to use parylene in MEMS and in particular, bio-MEMS applications.

2.4.2 Parylene Chemical Structure

The proper chemical name for parylene is poly(para-xylylene). Many variants exist with varying substitutions on the benzene ring, three of which are down in Figure 2-6:

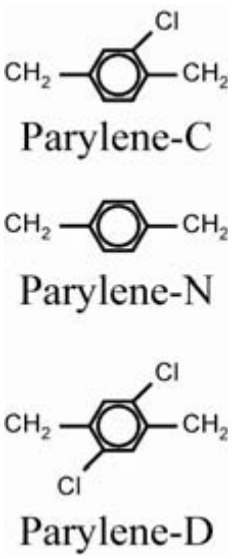

Figure 2-6: Chemical Structure of Parylene

Variants that have halogens placed in the aliphatic carbons are also available. These simple chemical changes result in differences in chemical and physical properties as well as deposition kinetics. In this work, the word parylene will imply Parylene-C unless otherwise stated.

2.4.3 Physical Properties

Below is a list of properties for Parylene-C

Table 2-2: Physical values of parylene[31] (Unless otherwise stated, values are from ref 17)

Property	Value	Comparison
Tensile strength, Mpa	69	
Yield strength, MPa[32]	59	
Elongation at break, %	200	
Young's Modulus GPa[33]	2.8	0.027 times the value for silicon
Density, g/cm^3	1.289	
Index of refraction	1.639	
Melting temperature (°C)	290	
Thermal Conductivity (W/m.k)	0.082	3.2 times the value for air

Aside from these quantifiable properties, parylene has the distinguished advantage of being classified as Class VI by the United States Pharmacopeia (USP), a classification given to materials (and methods which are used to produce them) with superior biocompatibility suitable for long term implantation in humans. It is also transparent to light above 300 nm.

2.4.3.1 Parylene fluorescence

Unprocessed Parylene-C fluoresces weakly at 515–555 nm upon excitation with 465–495 nm light from a fluorescence microscope. Processing of Parylene-C using standard MEMS fabrication techniques such as plasma etching and electron-beam metal deposition are suspected to increase fluorescence, however further studies need to be done and conclusive evidence is not yet available. Parylene-HT has been shown to fluoresce less in this range[34].

2.4.4 Chemical Vapor Deposition Method

Parylene coats substrates at room temperature conformally because of its chemical vapor deposition process outlined in Figure 2-7.

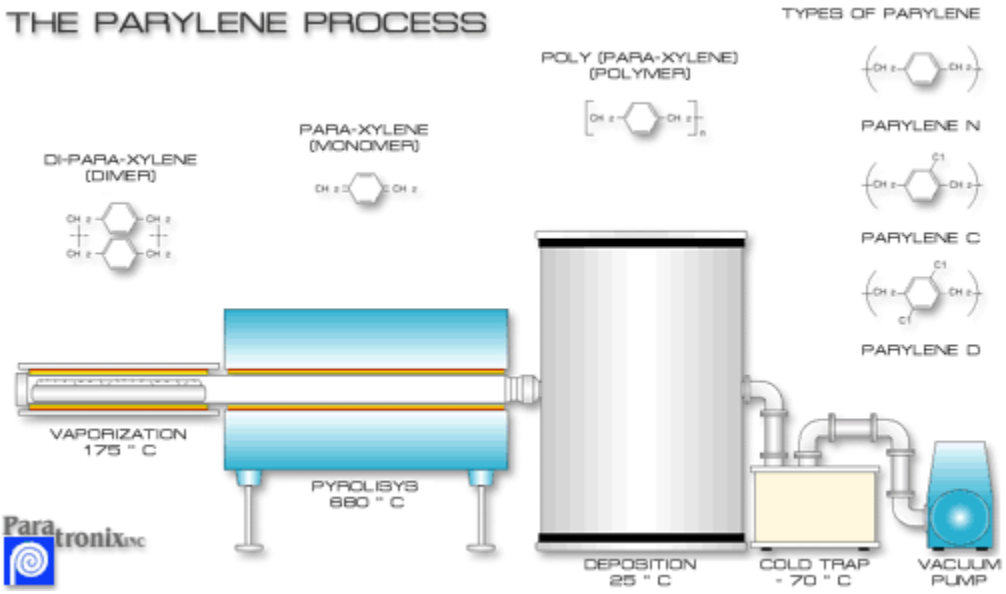

Figure 2-7: Schematic of parylene CVD deposition[35]

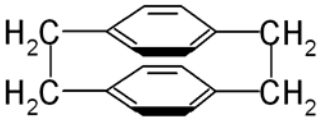

Figure 2-8: Chemical structure of di-p-xylylene, the dimer precursor to parylene N

- The desired parylene precursor (in the form of a dimer) is weighed and loaded into the vaporization chamber. There is a direct correlation between grams of dimer and microns of parylene deposited.
- The system is pumped down to a few millitorr base pressure.

- As the vaporization chamber gradually heats from room temperature to about 175 °C, molecules of dimer sublime and flow (due to the constant pumping by the vacuum pump) through the pyrolysis chamber which is at 680°C.
- In the pyrolysis chamber, the dimer is converted into reactive monomer units.
- These units flow into the room temperature deposition chamber, maintained at a steady 22 mTorr (by feedback from a pressure sensor) during deposition. For increased uniformity the monomers flow past a baffle and the substrates are placed in the center (both in the horizontal plane and in height) of a rotating stage.
- Monomers that do not bind flow past the deposition chamber where they adsorb to the walls of the cold trap. The standard temperature of the cold trap is -70 °C although a simpler option is to use a liquid nitrogen filled cylinder as a cold trap, resulting in a temperature approaching -196°C. This lower cold trap temperature has no effect on the deposition process.
- A vacuum pump continually runs during the process to power the flow of molecules.

This room temperature plasma-free deposition process allows the use of organic adhesion promoters such as silanes. One commonly used promoter is A-174 (gamma-methacryloxy propyltrimethoxysilane), which bonds to silicon oxide and presents an organic surface to promote adhesion of parylene.

2.4.5 Patterning

Parylene is chemically inert to most liquids at room temperature. Although dissolution in some aromatic solvents such as chloronaphthalene has been reported to occur at temperatures about 150^{o}C, this process is not compatible with many photo-resist-

based MEMS fabrication steps. The most effective method for etching it is using an oxygen plasma[36]. Typically etching rates range from 0–0.5 μm/min depending on plasma parameters such as oxygen flow rate, pressure, power, and configuration of the plasma chamber. For increased anisotropy, a Bosch-like process of C_4F_8 plasma alternated with an O_2 plasma can be used[37]. The mechanism for etching of parylene in an O_2 plasma is not well understood; however, based on studies using a remote microwave oxygen plasma, R.R.A. Callahan et al. proposed a mechanism involving hydrogen abstraction, oxgygen absorption, and ring opening resulting in formation of an aldehyde or carboxylic acid group.[38]

The most convenient masking materials for plasma-based etching are photoresist and metal. Photoresist has a 1:1 selectivity with parylene which is suitable for etching thin parylene films; however, since mass transfer effects are prevalent in the small feature sizes used in MEMS, a conservative guideline is to use a photoresist mask that is twice the thickness of the parylene etching required. For photoresist layers thicker than about 10 μm, photoresist cracking can become problematic due to the thermal stress resulting from the high temperatures used in a plasma system (despite water cooled wafer platters). Cracks originate at stress concentration sites such as small circular holes or sharp corners and propagate along the length of the wafer. Avoiding such features in design helps reduce this problem. Hard baking may also help, although at extreme temperatures (depending on the photoresist, in general above 140 °C) the photoresist becomes increasingly difficult to remove by simple room temperature dissolution in acetone. If tall features (~20 μm) already exist on the wafer, the flat-area photoresist thickness must not only be about twice as tall but care must be taken to ensure good step coverage. Out

of plane corners caused by such tall features are a site of stress concentration as well as nucleation sites for solvent bubble formation. Such bubbles can be reduced by optimizing the resist baking heat flow direction, temperatures, times, and ramp rates.

To address these limitations, a metal film can be used instead or in addition to a photoresist mask. A 2000 Å layer of metal such as Al, Cr, or Au is sufficient to etch more than 30 μm of parylene. Metal masks may not have the required step coverage, however, if the metal is deposited in a thermal evaporation chamber. It also requires an additional lithography step to pattern the metal. Evaporation of metal itself is a time consuming process due to the high levels of vacuum ($3x10^{-6}$ Torr) required.

2.4.5.1 Parylene Microfluidic Channels

One of the most fundamental components of microfluidics is the channel. Here two types of channels made from parylene are presented: surface micromachined channels and embedded channels.

Surface micromachined channels are built on top of the substrate surface using photoresist as a sacrificial layer[39]. The method is outlined in Figure 2-9 below:

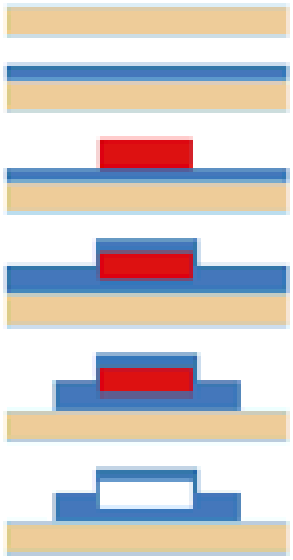

Figure 2-9: Surface micromachined parylene channel

An outline of the 6 steps shown above:

- The substrate's surface is properly cleaned and treated. An adhesion layer such as A-174 (gamma-methacryloxy propyltrimethoxysilane), the roughening of the lower level, or a molten layer of parylene may be used to improve adhesion.
- First layer of parylene is deposited, forming the bottom of the channel. This layer can be thin (~2 μm); however, should be sufficiently thick (~15 μm) if the underlying substrate will be eventually removed for a free standing channel.
- Sacrificial photoresist is deposited and patterned. This step is possible because adhesion between photoresist and parylene is good. For many cases, this resist must be baked at high enough temperatures and long enough times to evaporate any remaining casting solvent or water from development to prevent bubble formation in later steps.

- A second layer of parylene is deposited, forming the top of the channel. For improved adhesion, a thin portion of the first parylene layer can be etched away using an oxygen plasma. This serves two purposes: (1) it cleans the surface by etching organic contaminants (such as residual material from the photoresist processing) and lifting off inorganic contaminants in the top layer and (2) it leaves a rough surface with increased surface area for better adhesion. Following the plasma treatment, a 20 second dip in a 10% HF solution is performed to clean off any remaining contaminants and produce a more hydrophobic surface. Also before deposition, a masking material such as removable tape can be applied to the back side of the wafer to prevent parylene deposition there if necessary.
- Excessive area of both parylene layers are etched in oxygen plasma. Depending upon design, the excessive parylene may remain intact or be removed in later steps. If wafer dicing is performed on the front side of the wafer, removal of excess parylene is recommended as the water jet from the dicing saw can flow underneath this parylene and lift off the entire structure if adhesion is poor. With a trimmed channel, the water can be stopped by application of a dummy non-patterned layer of photoresist. Even if dicing is performed on the back side of the wafer, excess thick photoresist can impede smooth dice separation as the parylene layer needs to be manually ripped. This can leave jagged edges on the parylene edges

that can interfere with any chip housing. In general removal of excess parylene is recommended.

- For the inlet and outlet holes, a section of the second layer can be patterned and etched using an oxygen plasma. The sacrificial photoresist underneath acts as a safety buffer should over etching occur.
- The sacrificial photoresist is dissolved using an organic solvent such as acetone. For long channels (~1 cm) this step at room temperature can take weeks, as it is diffusion limited. If the photoresist has been excessively baked by a long (several days) and hot (140^{o}C or higher) hard bake, dissolution can take longer. More aggressive conditions such as higher temperature soaking and other solvents may speed up this step; however, this increases the likelihood that solvent can penetrate the parylene-parylene interface or parylene-substrate interface to delaminate the channel. For soak times in the time scale of months, solvent penetration through the parylene is a concern as solvent molecules can remain in the parylene interfaces.

A high performance liquid chromatography (HPLC) chip based on this scheme has been fabricated[40].

Alternatively, fluidic channels can also be made using embedded channel technology[41]

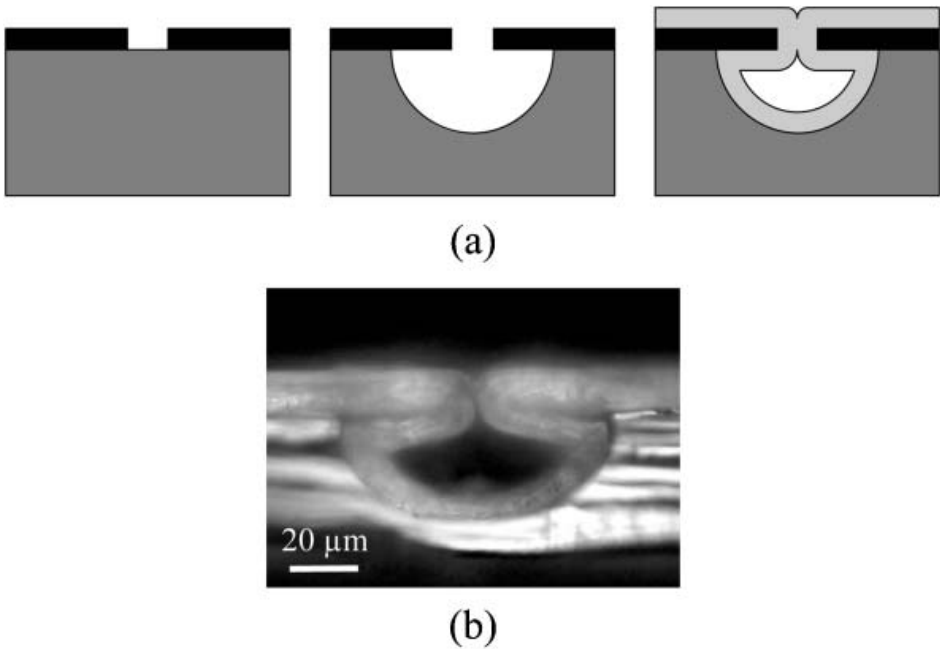

Figure 2-10: Embedded channel technology

An outline of the steps shown in Figure 2-10 is provided below:

- An overhang material (black) such as silicon oxide is deposited and patterned over a substrate (dark grey) such as silicon. This overhang material must be able to withstand the following substrate etching step and still be a free standing structure. This limits the extent to which the silicon can be undercut (the width of the channel). For microfluidics it is highly preferred that this material is transparent to allow optical monitoring of fluid in the channel.
- The silicon is then isotropically etched, causing an undercut that forms the overhang structure. A suitable method is silicon etching by XeF_2 gas, especially if wide channels are desired. If high-aspect-ratio channels are desired, a plasma can be used to etch the silicon if the overhang material is properly designed (e.g., thick enough even after non-specific etching by

the plasma). Wet etching techniques are generally not recommended as the surface tension from the drying process can pull the overhang structures down and break them. Thus, the bulk material should be one that can be etched by dry processes.

- A conformally coating layer (light grey) such as parylene is deposited and coats all surfaces creating a microfluidic channel that is embedded into the bulk substrate. Parylene is one of the only materials that can be deposited conformally and is also chemically inert and biocompatible for microfluidic applications. Theoretically the parylene thickness needs to be only half the width of the opening in the overhand structure. A conservative thickness would be equal to the width of the opening. The extra parylene ensures channel is completely sealed and the top surface is still flat enough for further processing.
- For the inlet and outlet holes, a cross section of the channel with a larger overhang structure opening will result in a partially open section of the channel. No sacrificial material is used here so excessively long channels can be fabricated as easily as shorter ones.

2.4.5.2 Parylene Microfluidic Components

Many microfuidic components have been fabricated using parylene technology including active valves, pumps, check valves, and nozzles[36]. This wide array of components demonstrates the versatility of parylene and shows the potential for integration of many components into one multifunctional device.

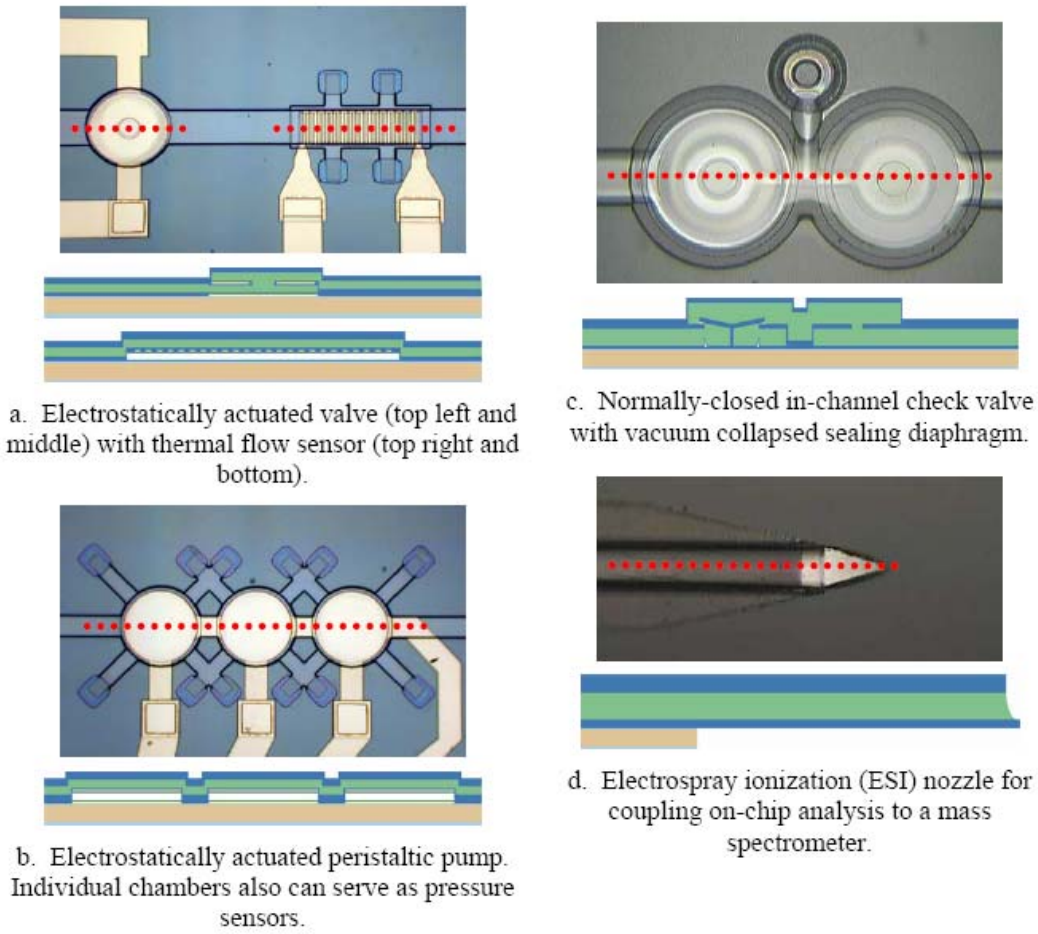

a. Electrostatically actuated valve (top left and middle) with thermal flow sensor (top right and bottom).

b. Electrostatically actuated peristaltic pump. Individual chambers also can serve as pressure sensors.

c. Normally-closed in-channel check valve with vacuum collapsed sealing diaphragm.

d. Electrospray ionization (ESI) nozzle for coupling on-chip analysis to a mass spectrometer.

Figure 2-11: Microfluidic components fabricated using parylene technology

One interesting component of interest to this thesis is the thermal isolation island. Such an island is a small (~mm) cut-out of silicon that is thermally isolated from the main chip yet mechanically connected to the chip by a gap composed of air and strips of parylene[42]. Since these "stitches" are made of parylene and can be as long as 100 μm, they make good thermal insulators.

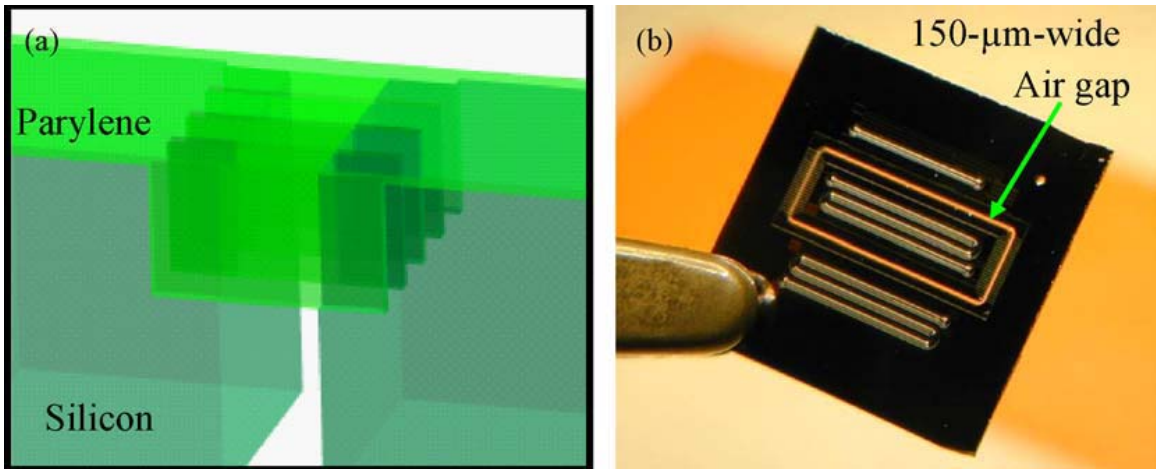

Figure 2-12: Thermal isolation by parylene "stitches"

2.4.5.3 Integration

A key advantage in using the parylene microfluidics platform is the promise of system integration resulting in a sophisticated chip capable of many functions. Such a system has been realized[43] in a fully integrated HPLC system comprised of the column, mixer, electrolysis pumps, composition sensor, mixer, filter, and electrospray nozzle. This promising example proves the feasibility of a fully integrated RTPCR chip with possibly integrated solution storage units, mixers, pumps, valves, and even gel electrophoresis chamber.

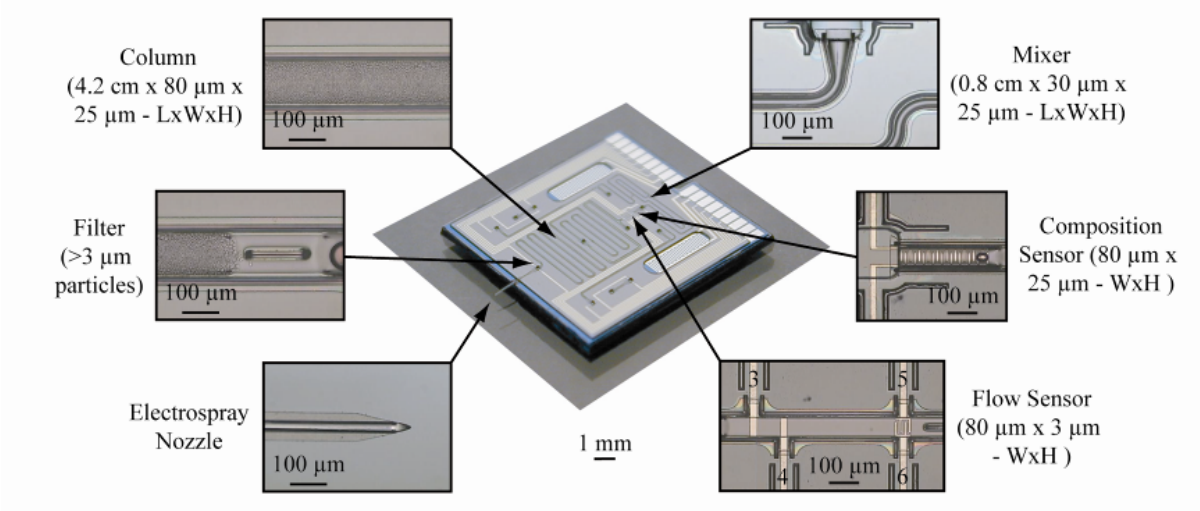

Figure 2-13: Integrated HPLC system

2.4.6 Biocompatibility of Parylene as a Real Time PCR Material

2.4.6.1 Parylene-C Coated Reaction Tubes with Low Volume Solutions

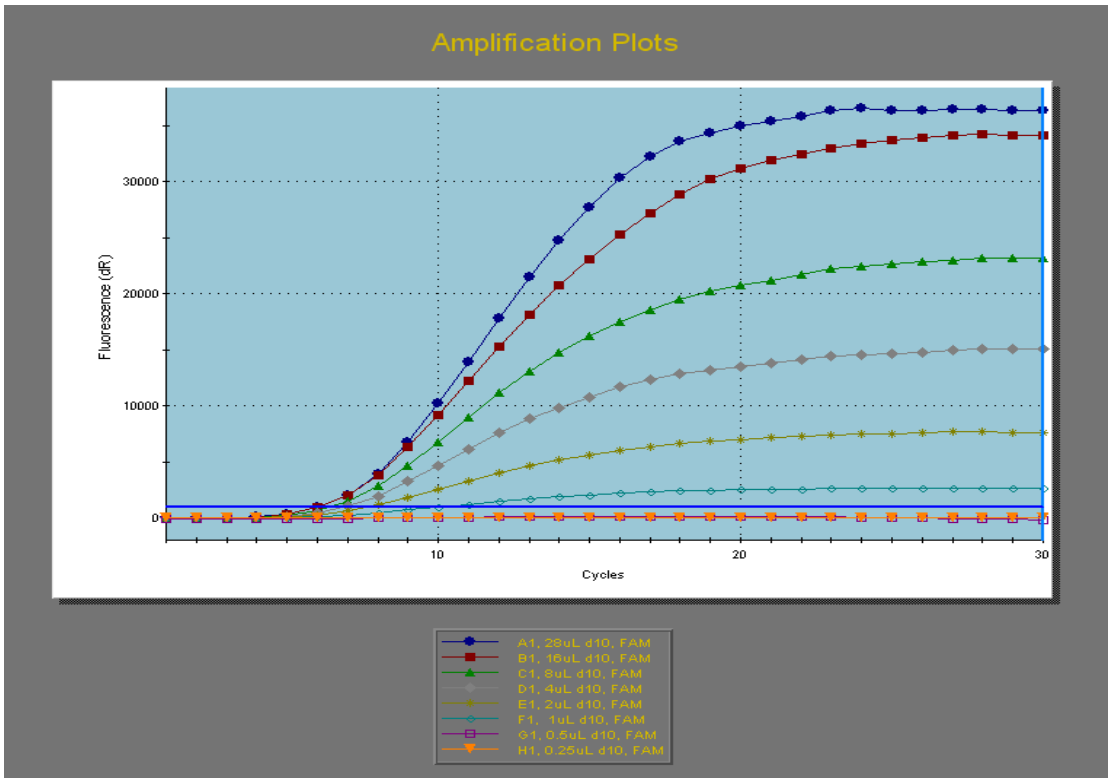

Figure 2-14: QPCR on low volumes in parylene coated tubes

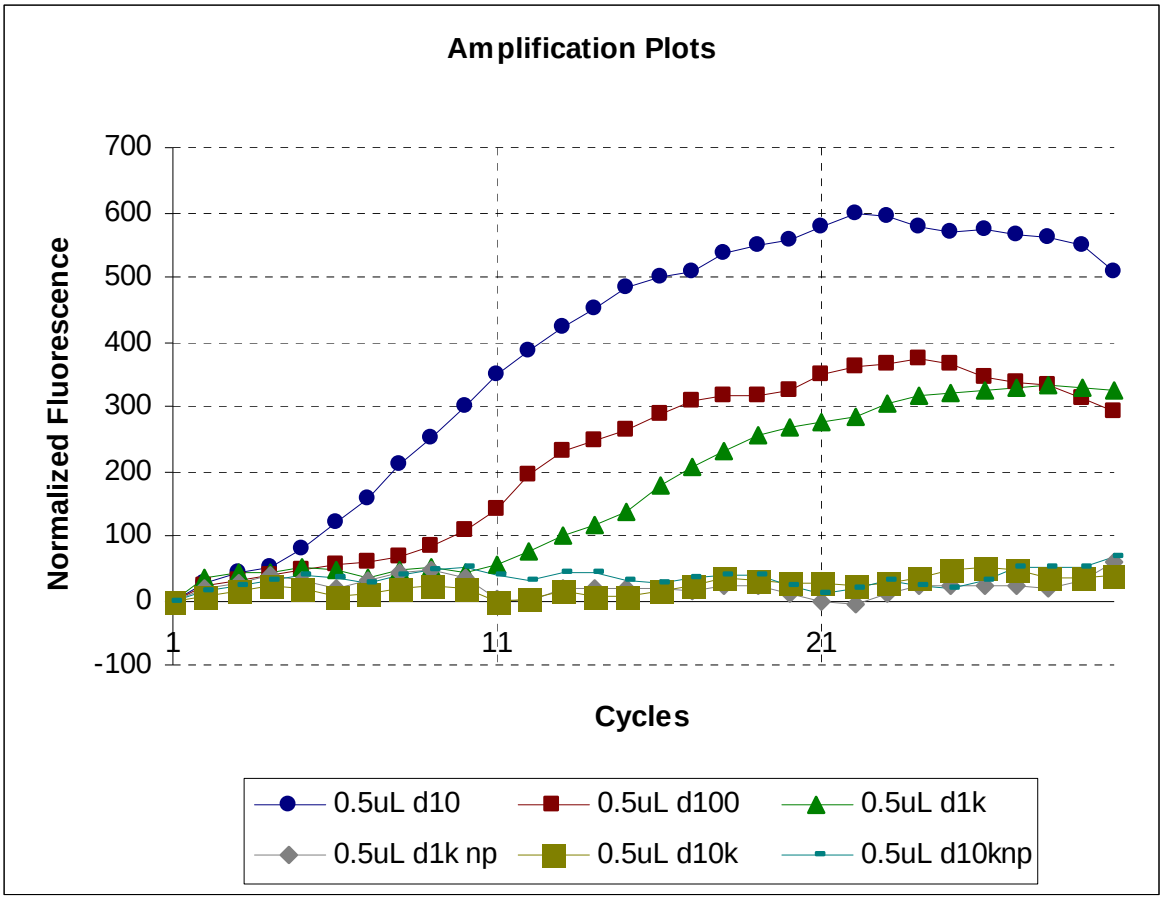

Figure 2-15: Amplification of 0.5 µl QPCR solution

As show in Figure 2-14 and Figure 2-15, using a conventional QPCR machine and parylene coated tubes, amplification can occur in reaction volumes from 28 µL down to 0.5 µL. There does not seem to be any adverse effects due to low volumes except increased noise from the optical measurement system. For very low (<1 µl) reactions, consistency is decreased. In the above figure, D10 refers to a reaction with 1.63E9 molecules of DNA, d100 = 1.63E8, and d1k = 1.63E7. The d10k sample was 1.63E6; however, it was indistinguishable from the no-primers controls.

2.4.6.2 Biochemical Compatibility of parylene with QPCR

To study the effects of Parylene-C on the PCR reaction from a biomaterials standpoint, the reaction tubes were coated with parylene and additional parylene sheets were included at different surface-area-to-volume ratios. To fit inside the tubes, these sheets were crunched with tweezers until their entire area was submerged in the PCR solution. Measured in inverse millimeters, the ratios were 0, 15/mm, and 60/mm. The parylene coated reaction tube itself contributes about 1.5/mm to the surface area/vol ratio. The ratios of the QPCR chips in this work are about 50/mm.

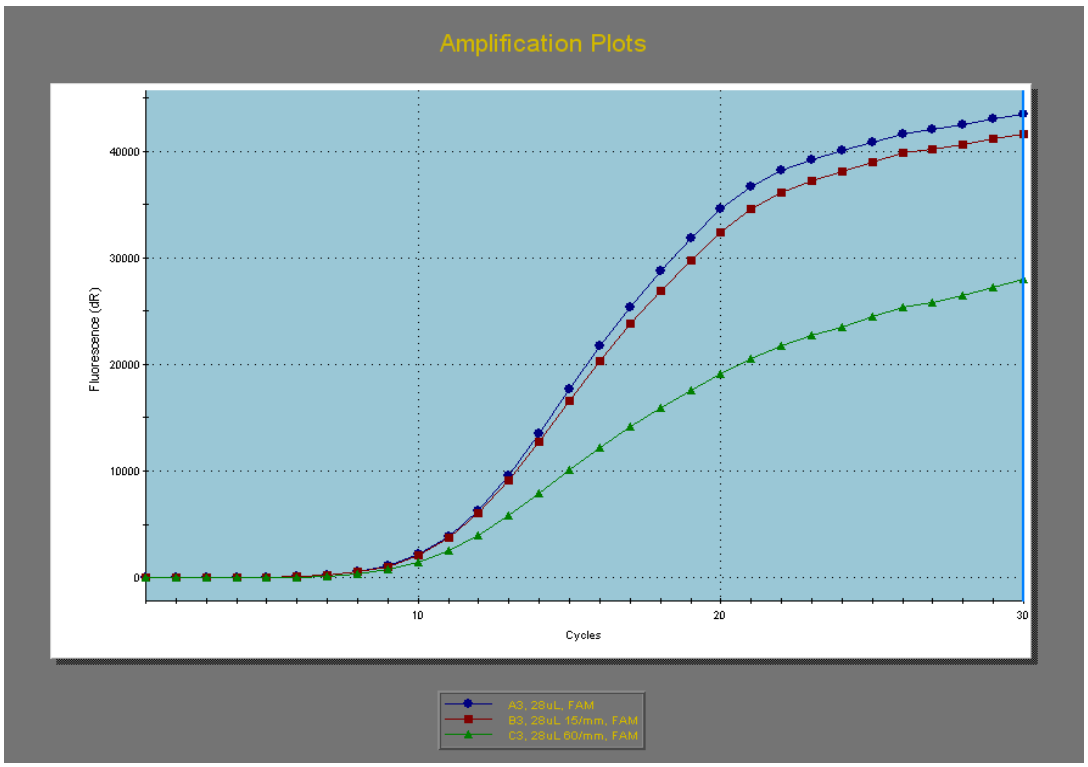

Figure 2-16: QPCR with various S.A./volume ratios of Parylene-C

Figure 2-16 shows that a ratio of 15/mm did not have any effect on the biochemistry nor the fluorescent readings of QPCR. At 60/mm, what appears to be inhibition did occur relative to the other two samples.

As shown in Figure 2-15 , a 10-fold serial dilution showed that a minimum of 1.63E7 DNA template molecules in 0.5 µl showed amplification in this setup. This suggests on-chip QPCR would be possible for these low volumes. The combination of the parylene surface and low volume effects is shown in Figure 2-17. For this 0.5 µl sample cycled in the conventional machine, a surface-area-to-volume ratio of 60/mm is noticeably attenuated whereas a ratio of 80/mm is indistinguishable from the no-primers control. Thus, a parylene based chip should not have a ratio greater than 60/mm.

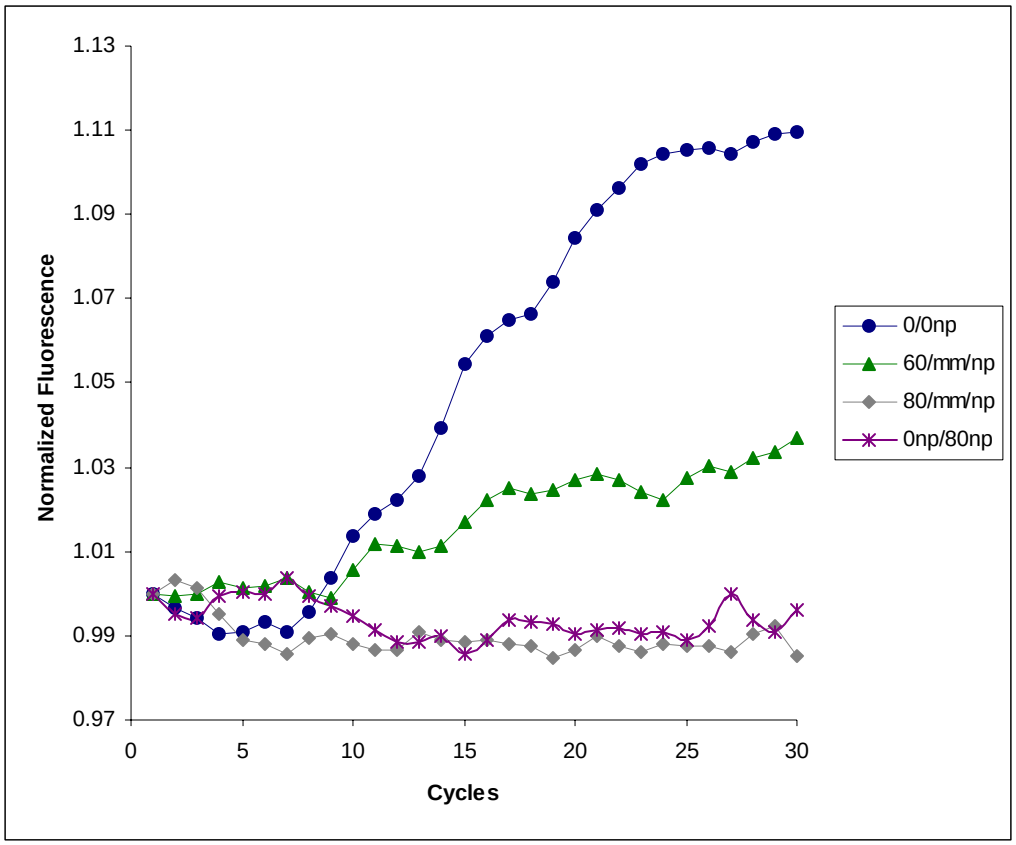

Figure 2-17: High SA/vol ratios of Parylene on a 0.5uL RTPCR sample

In an attempt to quantitate the extent to which parylene (or any material in general) inhibits RTPCR, comparisons were made between samples with parylene added to those with small volume. It was observed that adding parylene sheets into the reaction tube had an effect similar to that of using small volumes. Thus, by adding sheets of parylene the sample acts as if its volume was decreased. This "lost" volume was then plotted against the surface area added to yield Figure 2-18. Fitting a straight line resulted in a reasonable linear fit and a slope of 0.0084 mm or 8.4 μm. This value represents an effective distance "h" from the surface of the parylene sheets within which PCR was inhibited. Thus, the minimum radius for parylene C microchannel to be a reaction vessel for RTPCR is 8.4

μm. It should be emphasized that this is an "effective" metric and no physical effect is claimed here.

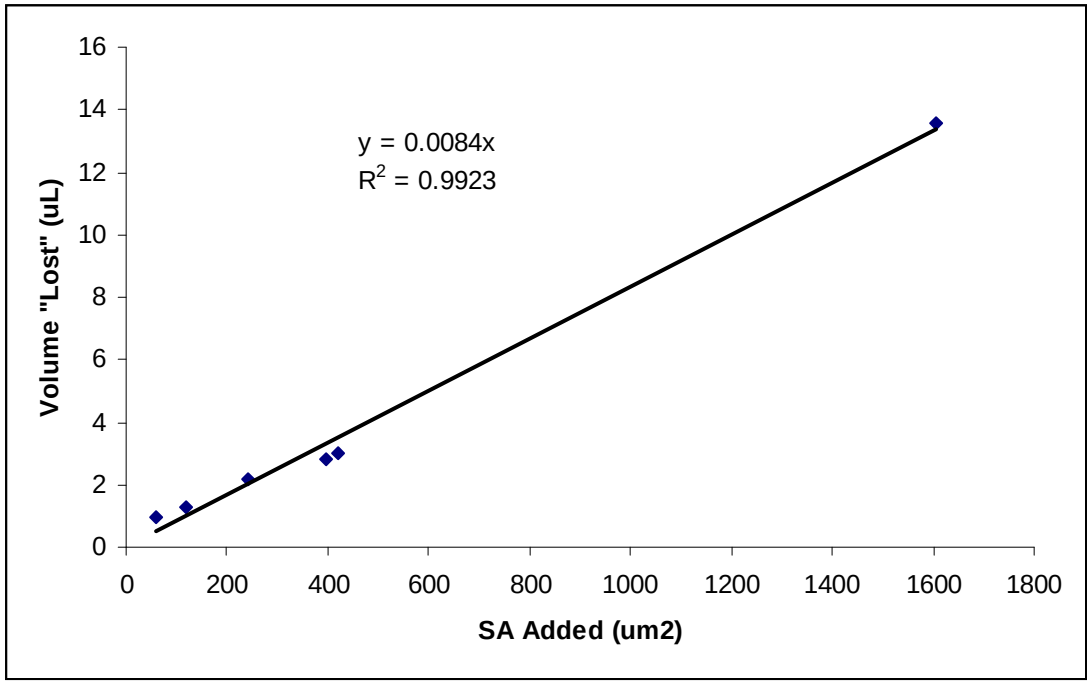

Figure 2-18: Concept of an effective distance "h" in which PCR is inhibited

2.4.6.3 QPCR with Other Materials

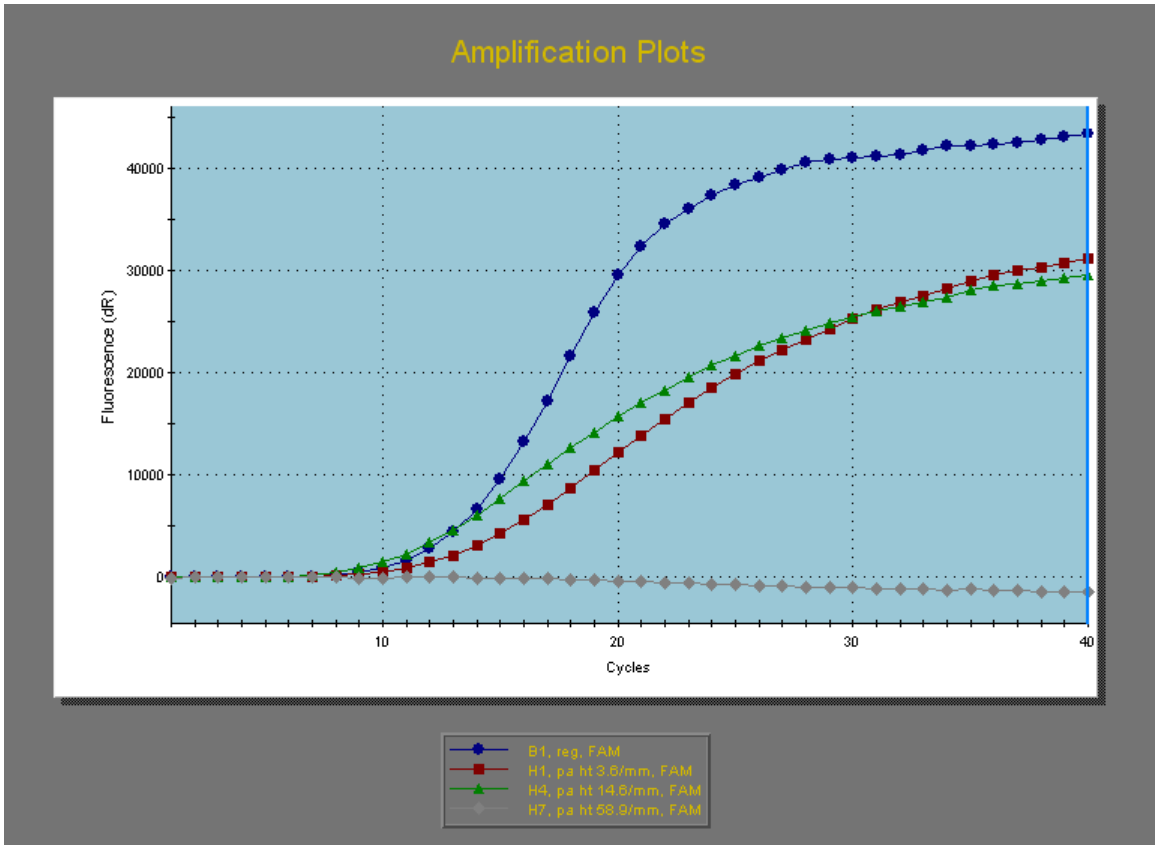

Figure 2-19: QPCR with various S.A./volume ratios of Parylene-HT

Parylene-HT has lower auto-fluorescence, thus provides lower background fluorescence for superior optical signal. Its interaction with the components of the QPCR solution, however, made it a less attractive material. As seen in Figure 2-19, even small S.A./Vol ratios of 3.6/mm and 14.6/mm of Parylene-HT had a noticeable adverse effect on QPCR. At 58.9/mm (similar to the chip's ratio), QPCR was totally inhibited. At has been shown that perfluoroalkoxy, a highly fluorinated hydrophobic material, can absorb DNA and SYBR Green[44]. The similarly highly fluorinated Parylene-HT might inhibit QPCR by a similar mechanism, as they both have a contact angle of about 105°[45]. Adsorption of Taq

Polymerase is also a possibility. Thus, from a biomaterials standpoint untreated and unprocessed Parylene-HT would not be a good choice for a QPCR material.

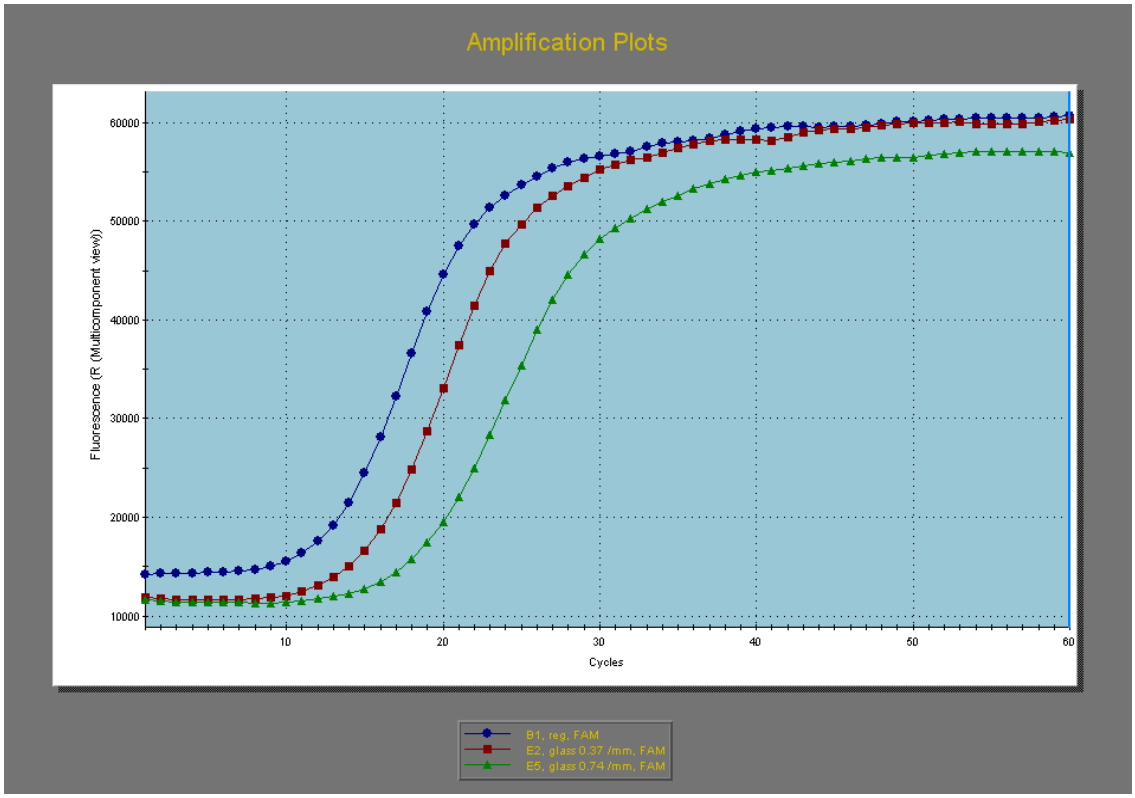

Figure 2-20: QPCR with glass added into reaction tubes

Glass was tested for QPCR inhibition (Figure 2-20). Compared to the curve with various amounts of parylene, the glass curves have noticeable shifts to the right. These shifts resemble the phenomenon observed when less templates are added into a QPCR reaction. Thus, it appears that glass is causing the adsorption of template DNA molecules onto its surface. This is consistent with the fact that glass is used to bind and purify DNA in chromatography format (although those occur in different salt and pH values).

Thus, it seems materials that are too hydrophilic, such as glass (contact angle 15°), or too hydrophobic, such as parylene-HT (contact angle 105°), inhibit PCR whereas

the slightly hydrophilic Parylene-C and polypropylene have the least inhibitory effect. Based on current literature, it is postulated that hydrophilic materials cause the adsorption of DNA and Taq polymerase[24] whereas hydrophobic materials cause adsorption of Taq polymerase and SYBR Green[44]. Although these hypotheses are offered by the author based on these simple experiments, definitive rules and literature are lacking in this area of materials interaction with QPCR.

2.5 Chapter Summary

Parylene MEMS technology has been shown to enable fully integrated microfluidic devices because of the superior properties of the material and its method of deposition. This technology has matured enough for the fabrication of advanced HPLC devices. Based on initial studies of low volume QPCR in a parylene environment, building and designing a parylene-based RTPCR device should be possible and is the first step towards a fully integrated bio analysis device capable of performing multiple bio assays.

3 RTPCR Microdevice, Air Gap Version

3.1 Fabrication

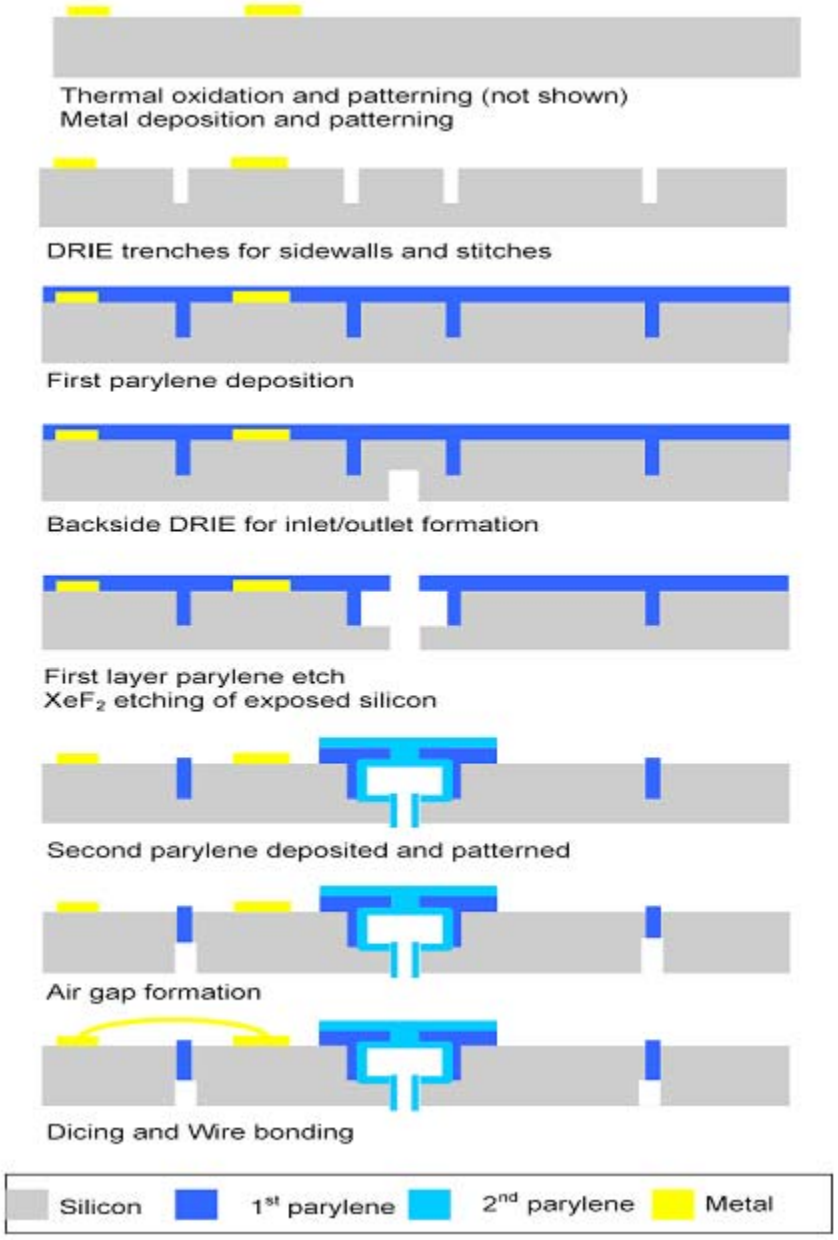

Figure 3-1: Overall process flow

The process flow diagram is provided in this section with explanations for each step. This is a detailed explanation describing how to build this device. Familiarity with semiconductor or MEMS processing procedures may be required to fully understand some steps. The overall process flow diagram is shown followed by illustrated step-by-step elaborations.

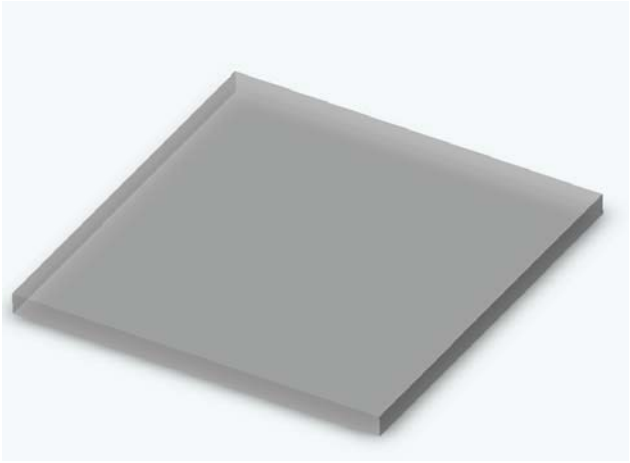

Figure 3-2: Silicon chip

All photoresist exposure was performed using a 10X reduction stepper at 436 nm (g-line) wavelength. The substrate is a 100 mm diameter silicon wafer, 500 μm thick, oriented in the 1-0-0 direction and polished on both sides.

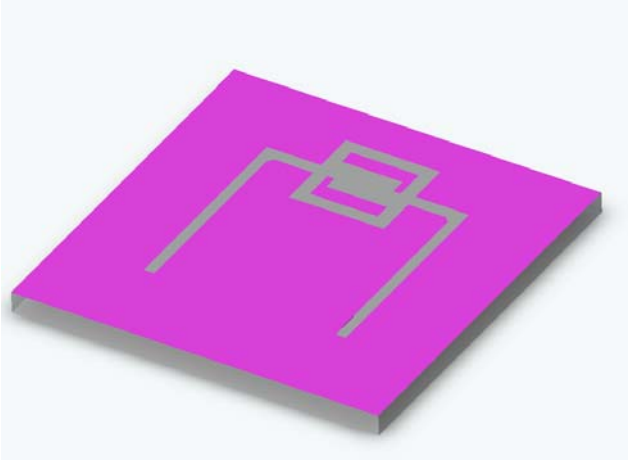

Figure 3-3: Patterned oxidation layer

Thermal oxidation and metal patterning. A 1 μm layer of thermal oxide was grown in a furnace at 1050^0C. The oxide layer was then patterned using 1 μm of AZ 1518 photoresist as the mask. It was etched for 8 minutes with buffered hydrofluoric acid. The buffered acid was used instead of diluted hydrofluoric acid for a more consistent etching rate. The oxide layer was preserved everywhere except the locations of the channels and air gap since their formation involves etching the bulk silicon. After etching the photoresist was stripped by submersing the wafer in an acetone bath followed by an isopropanol bath.

For metal patterning, a lift-off technique was used. A 0.5 μm layer of LOR 3B resist was spun onto the wafer then baked at 170^0C for 10 minutes on a hotplate.

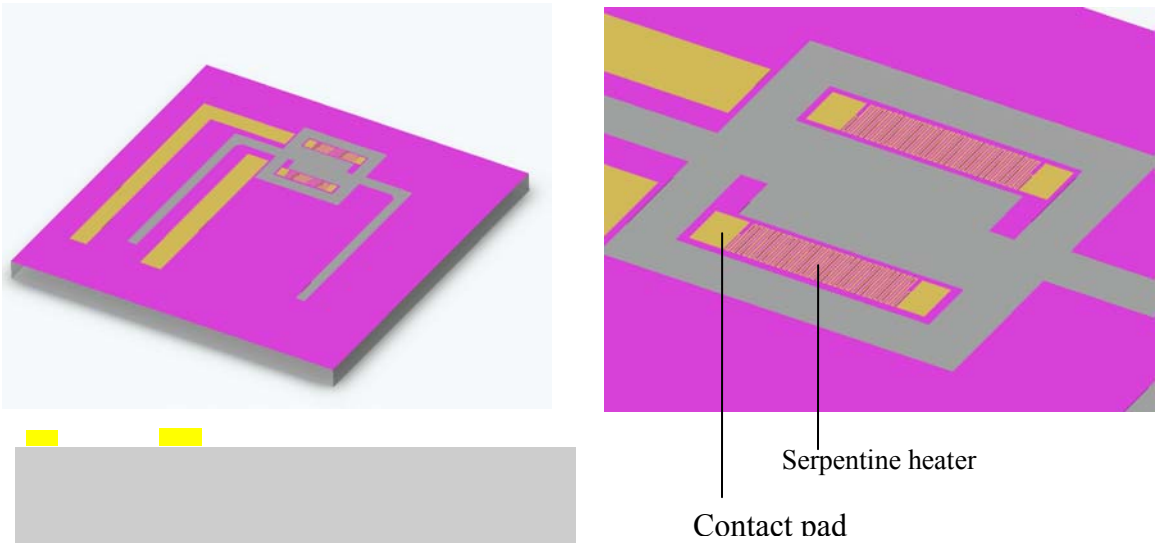

Figure 3-4: Metal deposition and patterning. Oxide layer (purple) underneath the metal (orange) acts as in electrical insulator.

A 1 μm layer of AZ 1518 photoresist was then spun onto the wafer on top of the LOR 3B. Both layers were then patterned by UV exposure and development in AZ 351 photoresist developer. LOB 3B is a lift-off resist based on polydimethylglutarimide (PMGI) that dissolves isotropically in AZ 351 photoresist developer solution, providing desired undercut when used underneath AZ 1518 for metal lift-off applications. The undercut ensures the metal film will be discontinuous at the features, thus lifting off cleanly. Without the LOR3B layer, the metal may provide good step coverage over the thin AZ 1518 resist, resulting in a continuous layer metal. After hard baking the wafer for 2 hours at 120^0C, metal was deposited using an electron beam thermal evaporator. A tri layer of 30 nm titanium, 200 nm platinum, and 200 nm gold was deposited. The lift-off resist layers were then dissolved in ST-22 photoresist stripper, a commercial product

based on N-methyl-2-pyrrolidone (NMP). This results in a patterned tri-metal layer. A serpentine design was used to obtain the desired 2 kOhm resistance in a small area. The gold is subsequently patterned using photoresist and gold etchant to remove gold everywhere except contact pads for improved adhesion between the metal and the gold wires used in wire bonding. The platinum layer serves as the heater and temperature sensor while the titanium is for better adhesion to silicon oxide.

DRIE trenches for sidewalls and stitches.

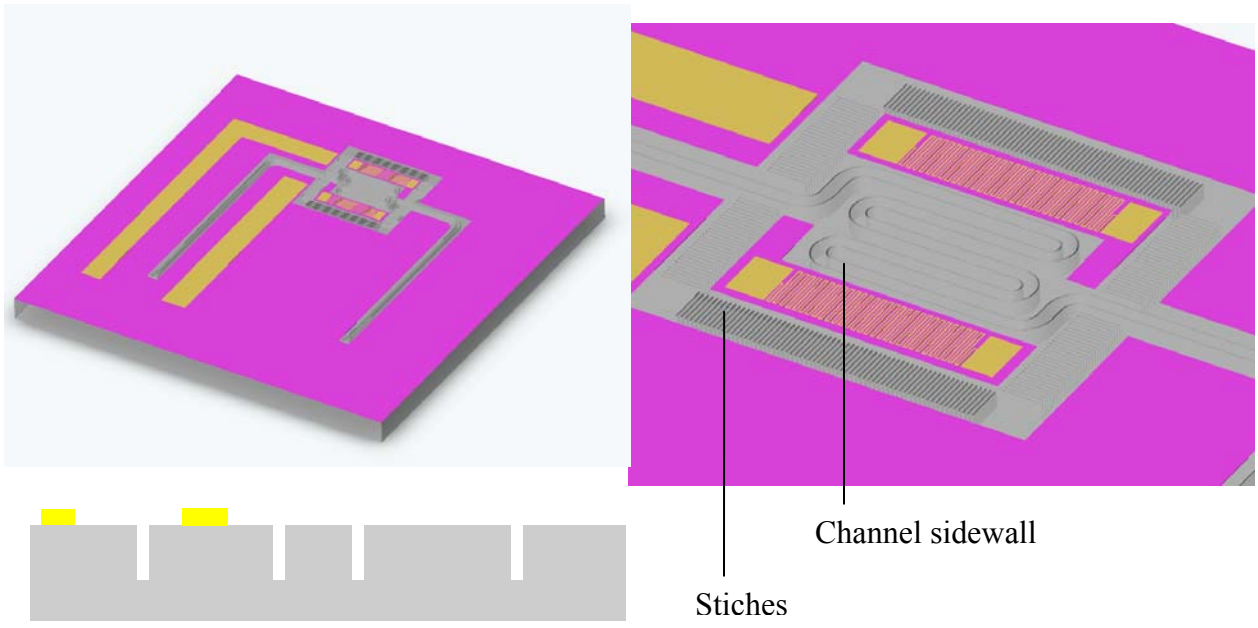

Figure 3-5: DRIE etching of the bulk silicon. The sides of the channels and the slots where parylene will fill and make stitches are etched.

The parylene stitches and channel sidewalls were defined simultaneously by etching the silicon wafer 100 μm deep using deep reactive ion etching. The sidewalls are defined by etching a 8 μm wide trench around the channel which in subsequent steps were completely filled with parylene and acts as an etch stop for isotropic XeF_2 etching. This

feature can be seen in Figure 3-5 as black line forming an outline of a channel. The channel itself is shaded gray indicating that it has not been etched yet. The stitches are formed by 8 µm wide trenches across the air gap. Upon filling with parylene, these trenches are 200 µm x 8 µm x 100 µm parylene slabs that connect the island to the main body. A thicker photoresist is used for DRIE: 15 µm of AZ 9260 which is patterned and developed in undiluted AZ developer. Following hard bake, this resist sustained 333 loops of the Bosch process. Photoresist etching for current conditions is 2 µm per 100 etching loops in the inductively coupled plasma (ICP) etcher used. Thus 6 µm minimum is required for 300 loops. 15 µm was chosen as a conservative thickness. After etching, the photoresist was stripped using ST-22. Acetone stripping may work, but residual fluorocarbons and excessive photoresist heating during the Bosch process make the photoresist more resistant to dissolution in acetone.

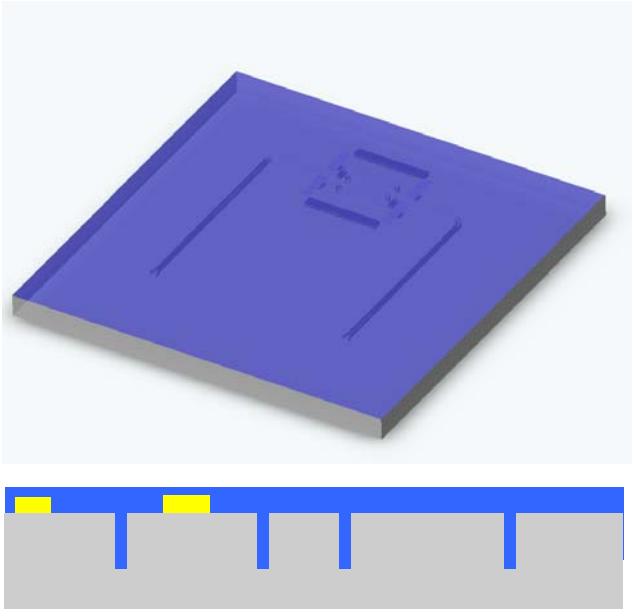

Figure 3-6: First parylene deposition

.

First parylene deposition

An adhesion layer of A-174 (gamma-methacryloxy propyltrimethoxysilane) was applied, followed by parylene deposition to fill the trenches, taking advantage of its conformal coating properties. The adhesion layer supplies a hydrophobic surface for improved adhesion between parylene and the substrate. These filled trenches function as either vertical etch stops for silicon etching or stitches that hold the air gap to the main chip body. A simple layer of tape was placed on the back side of the wafers to prevent parylene deposition there. The resulting top layer was flat enough (<2 μm features) for further processing steps such as application of photoresist by spinning.

Back side DRIE for inlet-outlet formation.

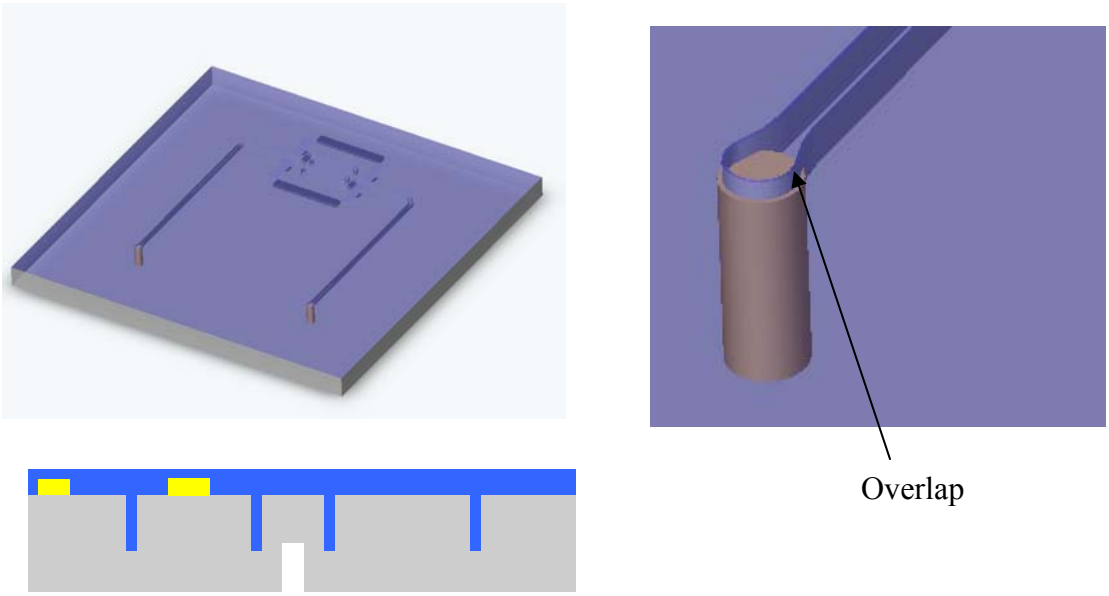

Figure 3-7: Inlet-outlet formation. Notice the back side etching (shaded in brown) overlaps the channel etching region, ensuring a continuous path when the channel is etched.

Taking advantage of dual side alignment marks, AZ 9260 photoresist was deposited and patterned on the back side of the wafer to serve as a mask for 800 loops of a modified Bosch process to form the inlet-outlet holes. The depths and diameter of these holes were designed such that when the channels are formed, there is a continuous path from the back of the chip to the channel.

First parylene patterning and XeF_2 etching of silicon.

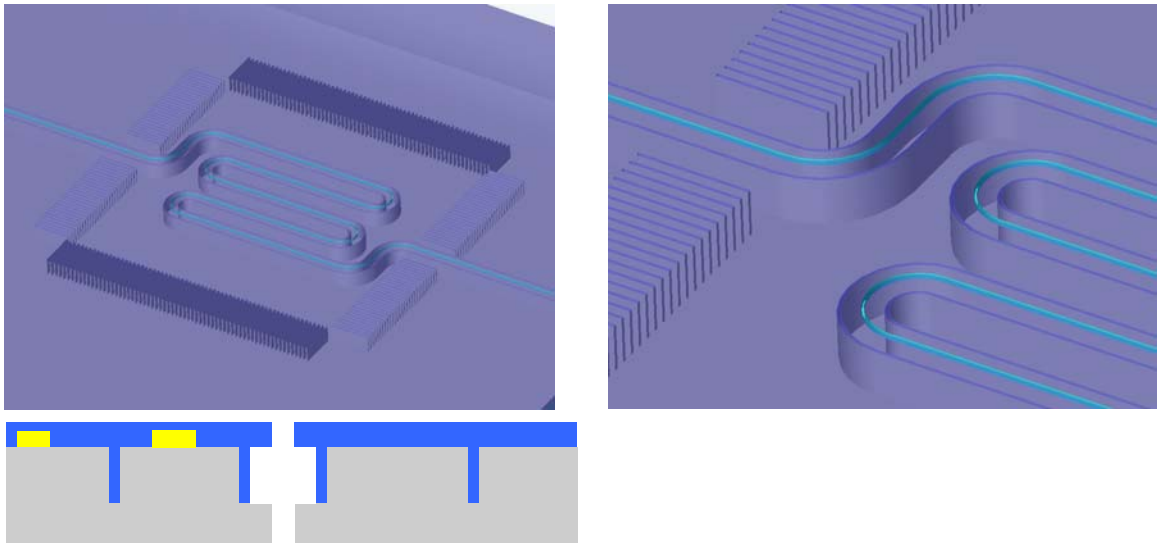

Figure 3-8: Etching of first parylene layer (light blue) and XeF_2 etching of underlying silicon

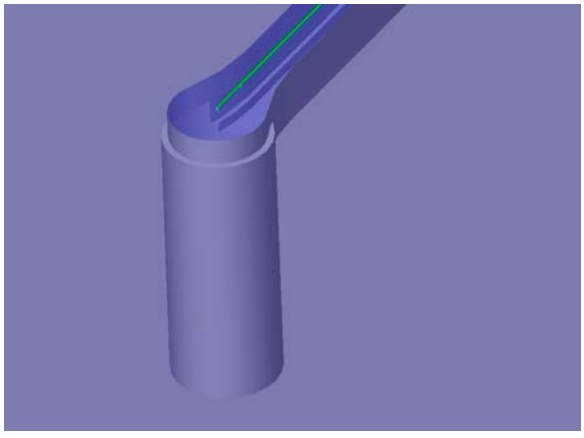

Figure 3-9: Inlet outlet hole

At this stage the parylene layer was etched in an oxygen plasma using an RF parallel plate reactive ion etcher (RIE). AZ 9260 was used as an etching mask for etching in 350 mTorr of oxygen plasma at 400 watts for about 8 minutes. The process was broken into 2–3 minute etching intervals to allow etching progress monitoring and wafer cooling. After complete etching, the photoresist mask was removed by dissolution in acetone then cleaned with isopropanol. The wafer was then exposed to a 200 W, 2 min, 200 mTorr O_2 plasma to remove remaining photoresist residue. The exposed silicon area was dipped into a 10% solution of hydrofluoric acid to remove native oxide and further clean the surface in preparation for XeF_2 gas etching. 20 loops of XeF_2 gas etching were performed, isotropically undercutting the parylene and creating an overhanging structure. Each loop consisted of exposure of the wafer to 2.5 mTorr of XeF_2 gas for 1 minute followed by evacuation and an additional 30 sec of exposure from a storage chamber. In the regions with the inlet-outlet holes, the XeF_2 was etched deep enough to form a continuous path with the previously etched inlet-outlet holes. This can be achieved by designing the process such that the sum of the heights etched by the back side DRIE and front side XeF_2 sum are greater than the thickness of the wafer.

Second layer parylene deposition and patterning.

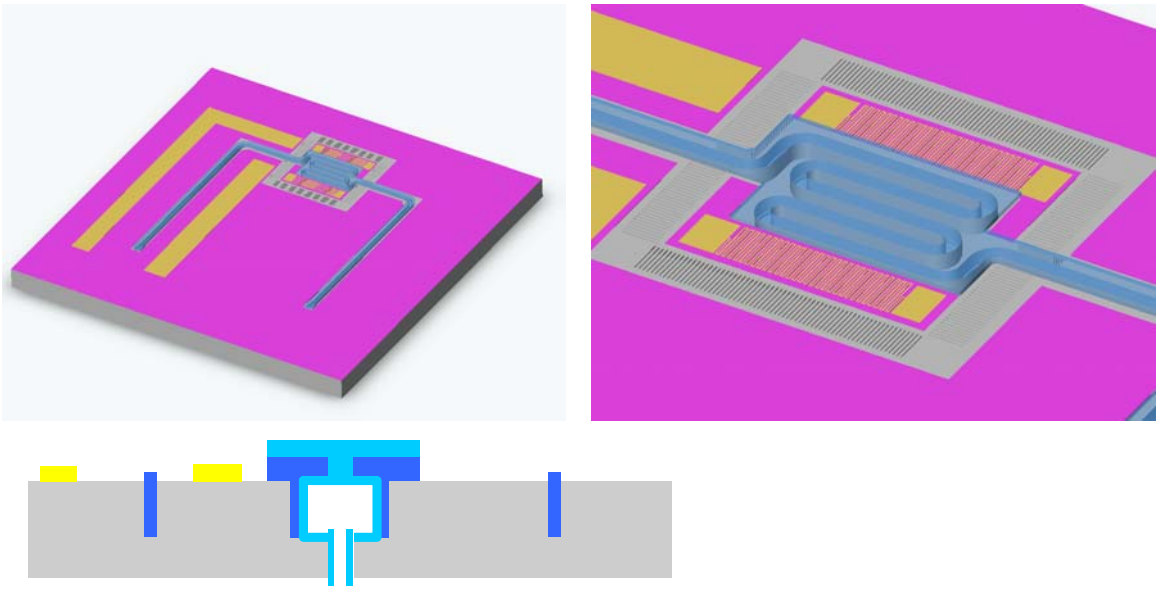

Figure 3-10: Second parylene patterning. Underlying oxide is once again the top layer.

A 16 μm parylene layer (second parylene) was then deposited. Since parylene coats substrates conformally, the second parylene seals off the gap in the overhanging parylene layer, thus creating a channel. Excess parylene on the wafer was then eliminated by etching in the RIE system, exposing the underlying oxide and gold contact pads (see Figure 3-10).

Air Gap Formation.

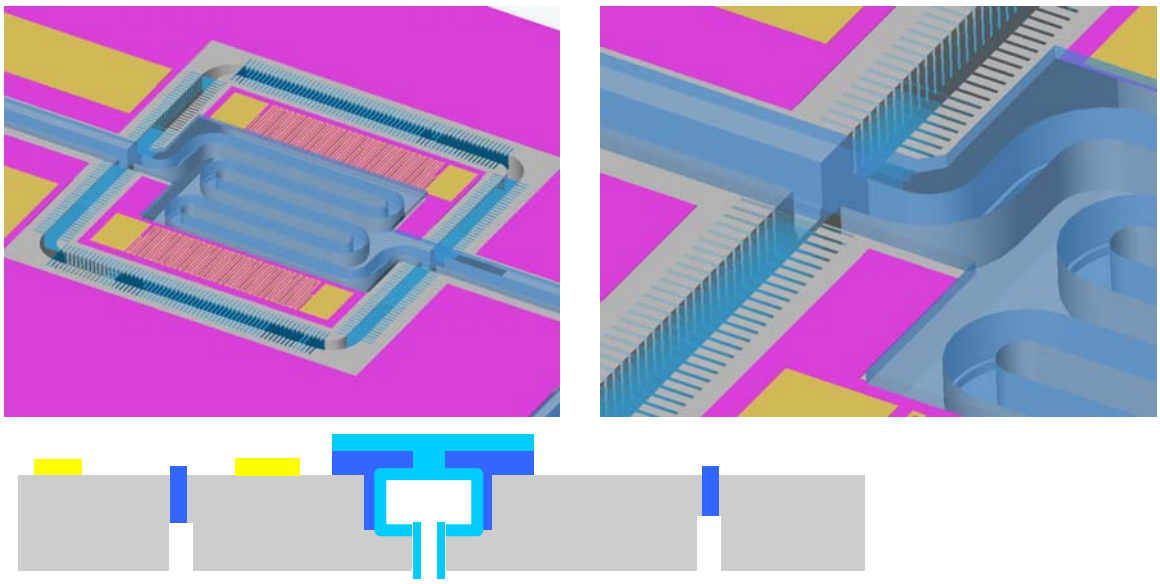

Figure 3-11: Air gap formation

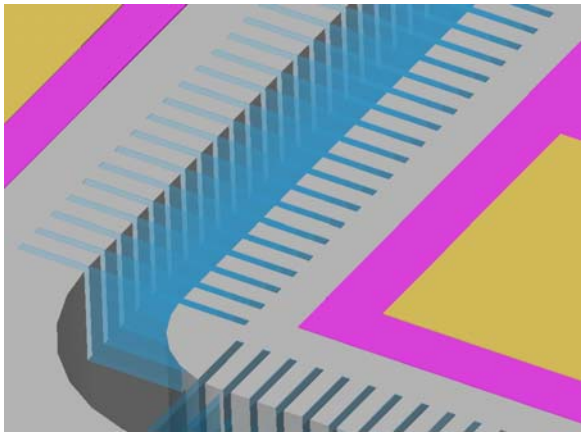

Figure 3-12: Zoom showing the parylene "stitches" used to connect the island to the main body

The air gap was formed by front and back side DRIE. Both sides use thick AZ 9260 photoresist as the masking material. The parylene stitches then became visible as a stack of parylene sheets bridging the gap between the air gap and main body (see Figure 3-13). At this point, light from the back side was able to shine through the air gap — a good test to check if the gap has been completely formed.

Dicing and wire bonding.

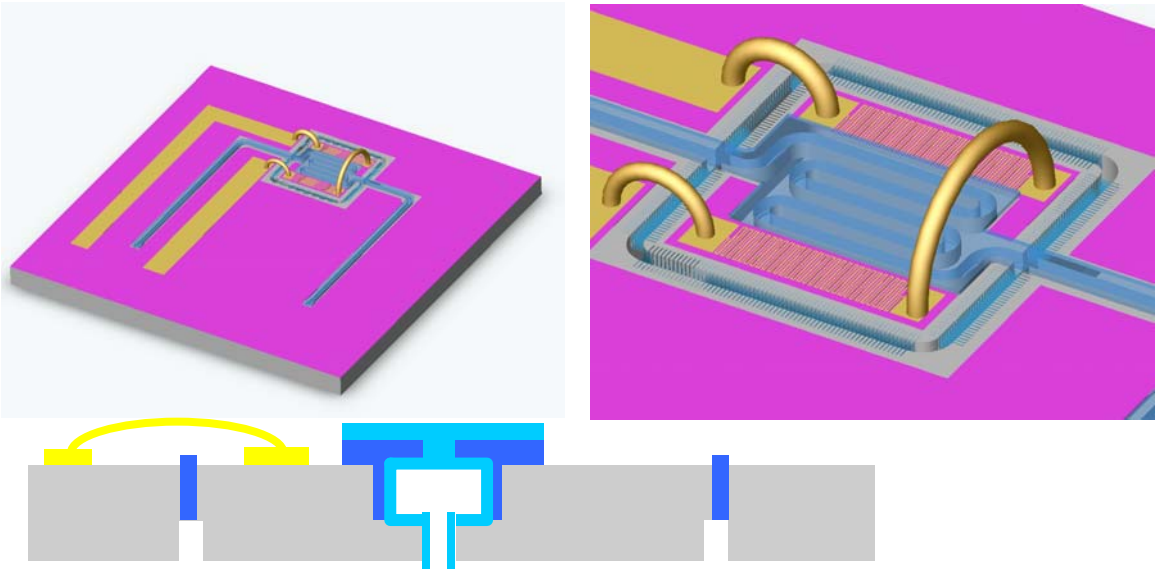

Figure 3-13: Wire bonding on the completed chip. The wire bonds provide electrical continuity across the parylene-stitched air gap

A dicing saw was used to cut the wafer into 1 cm x 1 cm dies. After device separation, a wedge wire bonder was used to electrically join the main chip body with the air gap. This provides a simple, elegant way to join the pads with the heaters on the island. Since both sections of the heaters were joined in series, they form one heater and can be controlled as one resistor.

3.2 Fluidic Channel Design

There are many design requirements for a quantitative PCR chamber. From a materials standpoint, the surface must be biocompatible so it does not interfere with the reaction. In particular, it must not cause adsorption and denaturalization of DNA molecules or Taq polymerase. The surface must also be transparent to allow optical fluorescence detection during thermal cycling. Transparency is also convenient for monitoring the fluid while inside the chamber. Similarly, the surface must not be excessively fluorescent itself; otherwise a high background emission may conceal the desired signal. The surface must also provide sufficient heat transfer. This property is a function of both material and design. By applying a thin layer, even low thermal conductivity materials can be used.

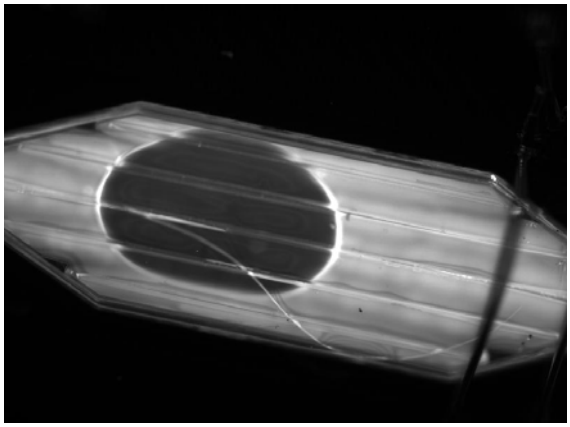

Figure 3-14: Bubble trapped in reaction chamber from early chip designs

From the design standpoint, it is also important that the channels limit the formation of bubbles and facilitate the removal of the formed bubbles. Variable cross sections make bubble flushing difficult as fluid simply flows around bubbles, even at

high fluid velocities (see Figure 3-15). The channels should also be sufficiently deep to allow enough optical cross section for measureable fluorescence. Quantifying this depth is difficult as many additional parameters such as focusing effects of the channel geometry, thickness of the top parylene layer, and intensity of the excitation light source contribute to the minimum depth required. Device volume is chosen to suit the application. Small volumes down to tens of nanoliters have been reported[46] which can be useful for highly parallel arrays of PCR reactions in small areas or when sample volume itself is small (e.g. DNA from a small number of cells). Smaller volumes also mean lower materials consumption, lower materials cost, and faster thermal cycling. Large volumes (on the order of tens of microliters), however, are still important even in chips. Detection of very dilute samples and off-chip gel electrophoresis are two examples where large volume is advantageous. In this case, the surface-area-to-volume ratio is reduced, which reduces material surface interference effects.

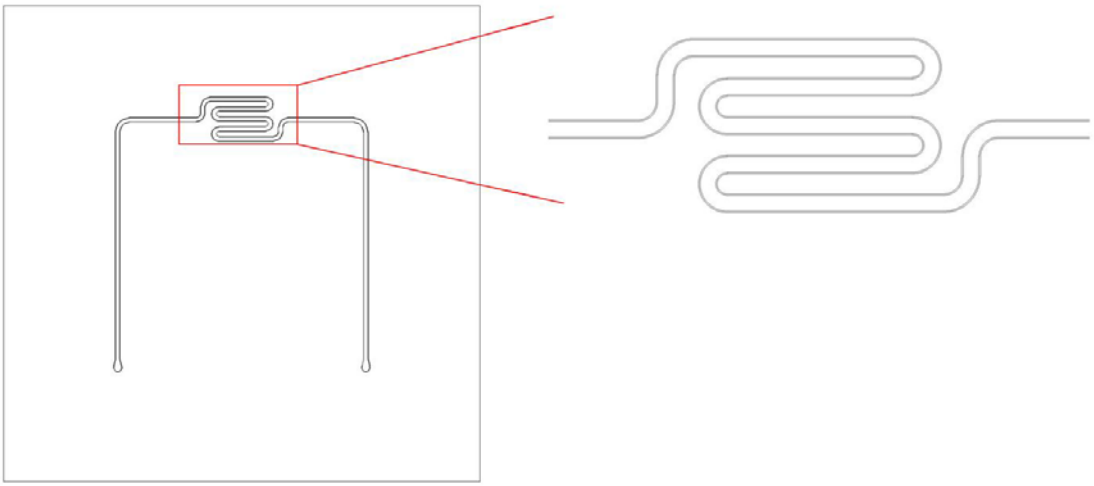

Figure 3-15: Channel layout

Figure 3-15 shows the channel layout for the QPCR device. Parylene is chosen as the surface material because it is known to be biocompatible and deposited using

methods that are compatible for current MEMS processes. It can also be deposited in thicknesses from 0.1–30 μm, which is thin enough to allow good heat transfer and limit effects of auto fluorescence. A serpentine design was used rather than a large chamber design to reduce bubble formation and facilitate bubble "flushing" should any trapped air appear during sample introduction. Designs with large chambers (changes in channel cross-sectional area) allow bubbles to become trapped in the chamber as fluid flows around the bubble. The channels are 110 μm deep, 60 μm wide, and about 8 mm long, making the total sample volume ~50 nL.

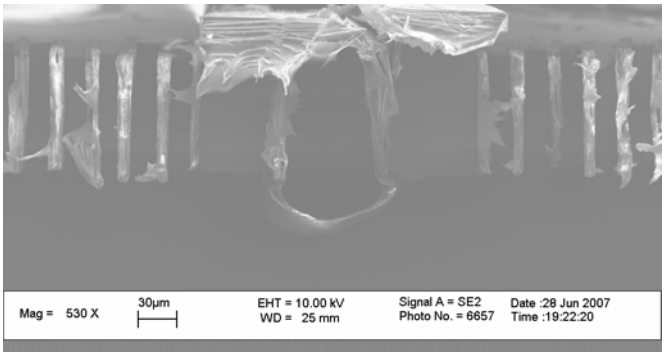

Figure 3-16: Channel cross section

3.3 Device Thermal Engineering

3.3.1 Heat Transfer Background

The three heat transfer mechanisms are conduction, convection, and radiation. Radiation is not relevant for this thesis and will not be discussed.

3.3.1.1 Conduction

Conduction occurs through movement of molecules and their electrons on the molecular scale. Conductive heat transfer is described by Fourier's law:

$$\vec{\phi} = -k\nabla T \text{ , Equation 3-1}$$

Where φ is the heat flux, k is the material thermal conductivity, and T is temperature. If the material is anisotropic, k becomes a tensor. In isotropy, it is a scalar. This equation is useful in thermal engineering, as a low k material is an insulator, preventing heat from flowing despite a large temperature gradient, while a high k material is thermally conductive, allowing heating to easily flow, thus creating a more homogenous temperature distribution. Thermal conductivities of materials important to this thesis are given in Table 3-1

. It should be noted that the thermal conductivity of parylene is only 3.15 times that of air and $6x10^{-4}$ times that of silicon making it a relatively insulative material for a parylene-based chip system. Silicon, on the other hand, maintains a homogenous temperature distribution in this work.

Table 3-1: Thermal conductivity of selected materials

Material	k (W/m-K)
Water	0.6
Si	130
Parylene	0.082
Still Air	0.026

3.3.1.2 Convective heat transfer

Convective heat transfer (or convection) is a mechanism of heat transfer by which heat is moved by the bulk motion of fluids. It is broken down into two categories: natural

heat convection and forced convection. In many cases both these affects are present. In natural convection, bulk fluid movement occurs due to density differences caused by temperature differences within a fluid. In forced convection, an external force such as a fan supplies the bulk fluid motion. Analytical solutions to such fluid flow (with the exception of a few simple cases) are extremely difficult; thus, engineers routinely rely on correlations to quantify the extent of heat transfer using the heat transfer coefficient:

$$\Delta Q = hA\Delta T \quad \text{Equation 3-2}$$

where

ΔQ = rate of heat flow

h = heat transfer coefficient

A = heat transfer area

ΔT = temperature difference between the solid surface and the bulk fluid

Thus, in convective heat transfer, much of the analysis involves choosing an accurate value for h. General correlations are available in the form of nondimensional numbers.

For example, if we wish to calculate the heat transfer coefficient for the 2 mm x 2 mm thermally isolated island on the chip, we can refer to correlations under similar conditions. To use these correlations we must determine the Rayleigh and Nusselt nondimensional numbers:

Rayleigh number

$$Ra_L = \frac{g\beta}{\nu\alpha}(T_s - T_\infty)L^3 \quad \text{, Equation 3-3}$$

The Nusselt number.

$$Nu_L = \frac{hL}{k} \quad \text{, Equation 3-4}$$

We know that the island cycles temperatures between 95^0C and 55^0C in air at a temperature of 23^0C. For this situation, definitions and values for the parameters for the nondimensional numbers are given below:

Table 3-2: Values for calculation of Rayleigh number for air

Variable Symbol	Definition	Value
g	gravitational acceleration	9.8 m/s^2
β	thermal expansion coefficient	3.1x10^{-3} /^{0}C
ν	kinematic viscosity	1.8x10^{-5} m^2/s
α	thermal diffusivity	2.7x10^{-5} m^2/s
T_s	temperature at the solid surface	75 ^{0}C = (95+55)/2
T_∞	room temperature of air	23 ^{0}C
$L_{top/bottom}$	ratio of solid's surface area to perimeter (top/bottom)	5x10^{-4} m
L_{sides}	ratio of solid's surface area to perimeter (sides)	2x10^{-4} m
k	Thermal conductivity of air	27.8x10^{-3} W/m^{0}C

From , Equation 3-3, the Rayleigh number is: Ra = 0.41 for the top and sides and Ra = 0.026 for the sides. Using empirical correlations such as those found in the CRC Handbook of Mechanical Engineering[47], this Ra correlates to various Nusselt numbers depending on the surface orientation:

Table 3-3: Nusselt numbers. All correlations from CRC Handbook[47]

Surface	Nu	h
Top surface (2mm x 2mm)	1.23	68.3 W/m^{2}C
Bottom surface (2mm x 2mm)	1.15	64.1 W/m^{2}C
Side surfaces (0.5 mm x 2mm) x 4	0.842	117 W/m^{2}C

By scaling each heat transfer coefficient with its area, an overall coefficient can be found:

$h_{overall} = 83$ W/m^{2}C.

3.3.1.3 Analogues to Electrical Engineering

An alternative way to thermally analyze a system is using an electrical engineering analogy to construct "thermal circuits." This is particularly useful in simplifying time varying temperature changes. Below is an RC circuit:

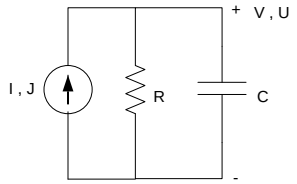

Figure 3-17: EE analogue for thermal characterization

where

V = voltage difference (U = temperature difference)
V_0 = voltage difference at time = 0
I = current source (J = heat source)
R = electrical (thermal) resistance
C = electrical (thermal) capacitance

The equation describing this RC circuit under constant current is:

$$V(t) = V_0 e^{-t/RC} + IR(1 - e^{-t/RC}) \quad \text{Equation 3-5}$$
$$\tau = RC$$

Please see the appendix for detailed derivation.

This model can be used to characterize a system such as a thermally homogenous solid with an internal heat source surrounded by air. In the analogous thermal circuit, the current source is the heat source, the voltage differences are the temperature difference between the solid and room temperature, the resistance becomes the thermal resistance from the solid to the air (by convection), and the capacitance is the heat capacitance of the solid. Hence, the solution to the thermal circuit is:

$$U(t) = U_0 e^{-t/RC} + JR(1 - e^{-t/RC})$$
$$U = T - T_\infty \qquad \text{Equation 3-6}$$
$$\tau = RC$$

Connecting the thermal circuit with physical values,

$$R = \frac{1}{hA} \qquad \text{Equation 3-7}$$
$$C = \rho C_p V$$

where

h = heat transfer coefficient
A = heat transfer area
ρ = density of the solid
C_p = heat capacity
V = volume of the solid

3.3.2 Device Thermal Design

A metal trace comprised of 2000 Å thick platinum over a 300 Å thick titanium adhesion layer was used as both a temperature sensor and heater. The room temperature

resistance of the stack was dominated by the thicker platinum portion and about 2.3 kOhms. Characterization of both temperature sensor and heater functions is given in this section.

For fast chip performance temperature cycling must occur quickly. To achieve this end, the chip was designed with a thermally isolated silicon island so that only the area of the chip containing the fluidic channels was heated. Originally designed for use in temperature control for high performance liquid chromatography chips[48], the technology works nicely for this RTPCR chip as well.

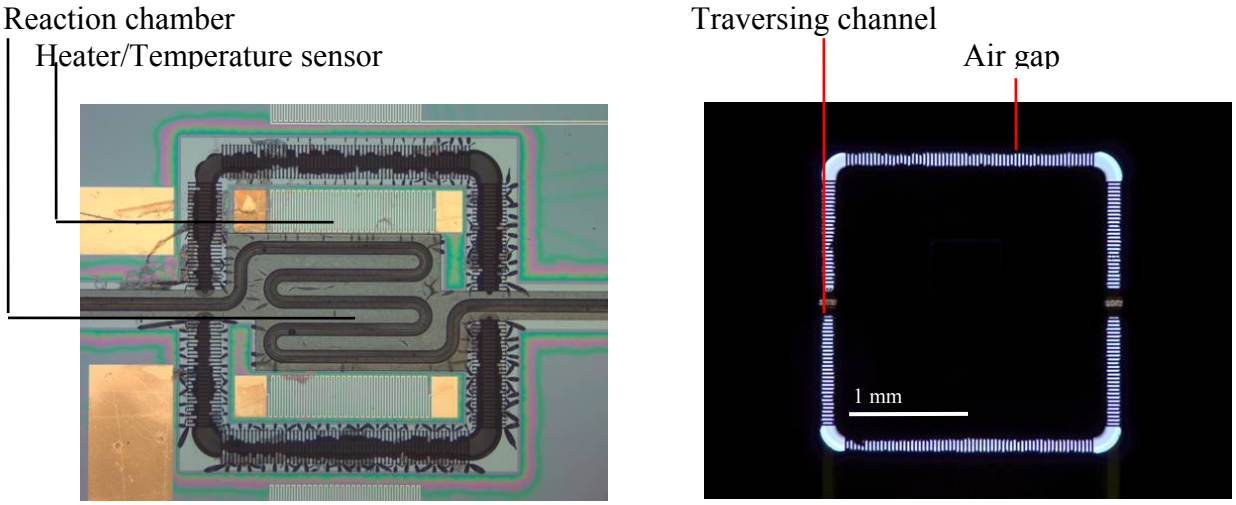

Figure 3-18: Thermally isolated island

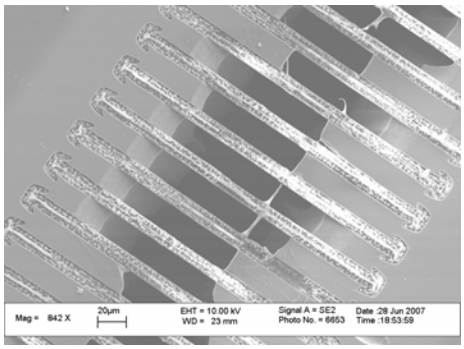

Figure 3-19: Parylene stiches

The thermal model described in Figure 3-17 would characterize the temperature on the thermally isolated island. This island, however, can still exhibit a non-zero "leak" of heat. To account for that leak into the chip body, the model can be extended by adding another resistor and capacitor in parallel (representing the body of the chip) and a resistor that represents the resistance to leaking heat through the parylene stitches and air gap (Figure 3-20).

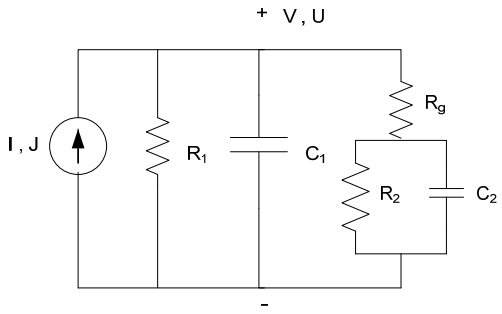

Figure 3-20: Extended RC Model

Where
R_1 = Thermal resistance from island to the environment
C_1 = Heat capacity of the island
R_2 = Thermal resistance from chip body to environment
C_2 = Heat capacity of chip body
R_g = Thermal resistance from island to chip body

An analytical solution for temperature as a function of time exists; however, it is a long expression that does not offer any insight into the system. Instead, the solutions will be plotted in the thermal characterization sections for various special cases.

3.3.2.1 Temperature Sensor

A resistance temperature detector (RTD) configuration was used because of its simplicity. Such a sensor takes advantage of the relationship between temperature and resistance of a metal given by the Callendar-Van Dusen equation:

$$R(T) = R_0(1 + AT + BT^2) \quad \text{Equation 3-8}$$

Where R is the resistance at temperature T (in Celsius), R_0 is the resistance at 0^0C, and A and B are coefficients that are characteristic of the material. For the temperature range of interest for PCR, 0^0C–100^0C, the coefficient B becomes negligible. Furthermore, instead of creating a 0^0C environment for measuring R_0, it is common practice to replace the Callendar-Van Dusen equation with an equation of the form:

$$\frac{R(T)}{R(T_0)} = 1 + \alpha(T - T_0) \quad \text{Equation 3-9}$$

where T_0 is a reference temperature (not necessarily 0^0C) and α is the temperature coefficient of electrical resistance. Linear regression of a set of resistances at different temperatures will yield suitable value for α. From Equation 3-9 it can be seen that resolution of such a device improves by increasing the product of α and R_0.

For the RTPCR chip, the following R versus T behavior was observed:

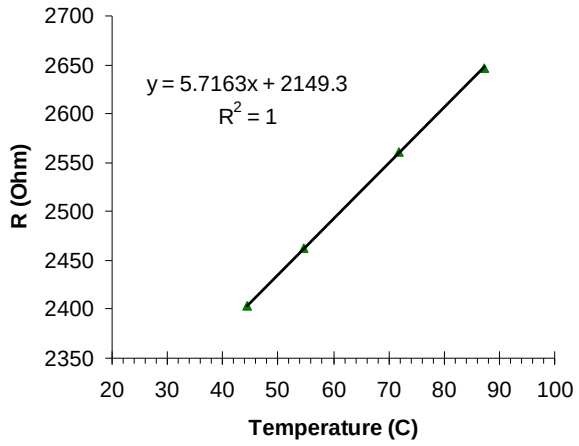

Figure 3-21 Temperature sensor calibration

The calibration curve shows the expected linear relationship between R and T, with an α value of $2.3x10^{-3}/^{0}C$. This value is lower than the literature value of α for platinum ($3.7x10^{-3}/^{o}C$), perhaps due to differences in atomic or crystalline configuration of the thinner thermally evaporated platinum used in this work. Previous group members have reported a 200A Ti/W adhesion layer with 1000 A platinum with a TCR value of $1.0\ x10^{-3}/^{0}C$ ([49]) and a 300 A titanium / 2000 A platinum hybrid layer with a TCR value of $2.1x10^{-3}/^{0}C$ ([50]). Thus, the values reported in this thesis are consistent with those of previous group members. Resolution of $0.1^{0}C$ difference can be sensed by a measurable 0.571 Ohm change in resistance. Resistance in lead wires is less than 1 Ohm. The largest source of inaccuracy is likely the calibration standard. A thermocouple coupled to a signal processor that converts degrees to voltage was used without checking its certificate of calibration, thus this inaccuracy is likely to be above the precision of the system.

3.3.2.2 Heater

The thin film metal trace heater based on joule heating provides a sufficient and simple heat source. The power dissipated by such a metal line is given by Joule's First Law:

$$P = VI = \frac{V^2}{R} = I^2 R \quad \text{Equation 3-10}$$

In designing such a heater, it is important to choose a resistance value such that the available power sources can supply the required voltages and current. Below are the relevant parameters for the heater:

Table 3-4: Power specifications for the air gap version

Maximum Power Required	300 mW
Heater resistance	2300 ohms
Maximum voltage required for 300 mW	30 Volts
Maximum current required for 300 mW	10 mA

These values are within the capabilities of the available power supply.

3.3.2.3 Equipment Setup

The off-chip hardware and control software complete the temperature control system.

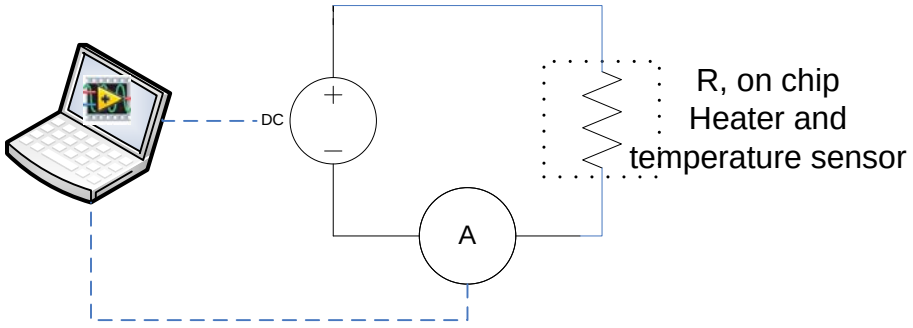

Figure 3-22: Temperature control hardware arrangement

The temperature control hardware consisted of the chip, power source, multimeter (set to ammeter mode), and computer. The hardware was connecting via GPIB connections and controlled using LabView.

3.3.3 Thermal Performance Results

Thermal performance can be characterized by establishing the parameters in the model described by Figure 3-20. These can be isolated by studying special limiting cases as described below.

3.3.3.1 Steady State Temperature — Thermal Resistances

In order to determine the rate of heat transfer to the surrounding air and through the air gap, steady state power experiments were performed.

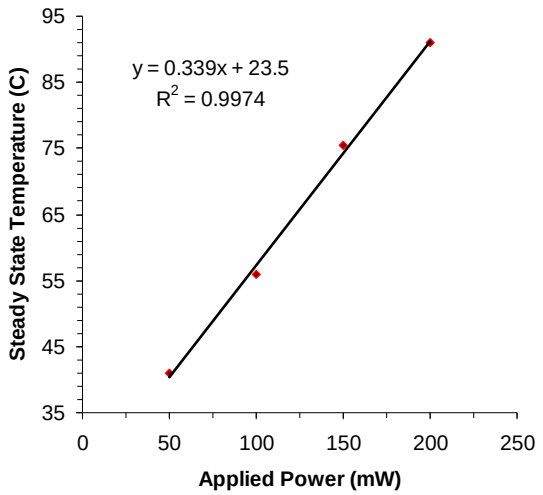

Figure 3-23: Steady state temperature

From Figure 3-20, at infinite time the capacitors become open circuit elements leaving an effective resistance of:

$$R_{ss} = R_1 \| (R_2 + R_g) = \frac{R_1 (R_2 + R_g)}{R_1 + R_2 + R_g} \quad \text{Equation 3-11}$$

Here R_{ss} is simply the slope of Figure 3-23. Furthermore, R_1 and R_2 are scaled by area since they share the same mechanism of heat transfer:

$$R_2 = R_1 (\frac{A_1}{A_2}) \quad \text{Equation 3-12}$$

Where A_1 and A_2 are the heat transfer areas of the island and body, respectively. Thus, by calculated R_1 using heat transfer correlations, R_g can be determined using R_{ss}. Caution should be used when using the empirical heat transfer correlations, however, as they are mainly determined for macro-scale (millimeter or larger) features and may not

be as accurate at these small length scales where viscous forces are much higher relative to buoyancy forces[51]. Values used in the model are shown in Table 3-5.

3.3.3.2 Heating Rates

Analysis of time dynamics of temperature were performed using data from heating and cooling experiments. For heating, the island is heated from room temperature by applying heat as a step function.

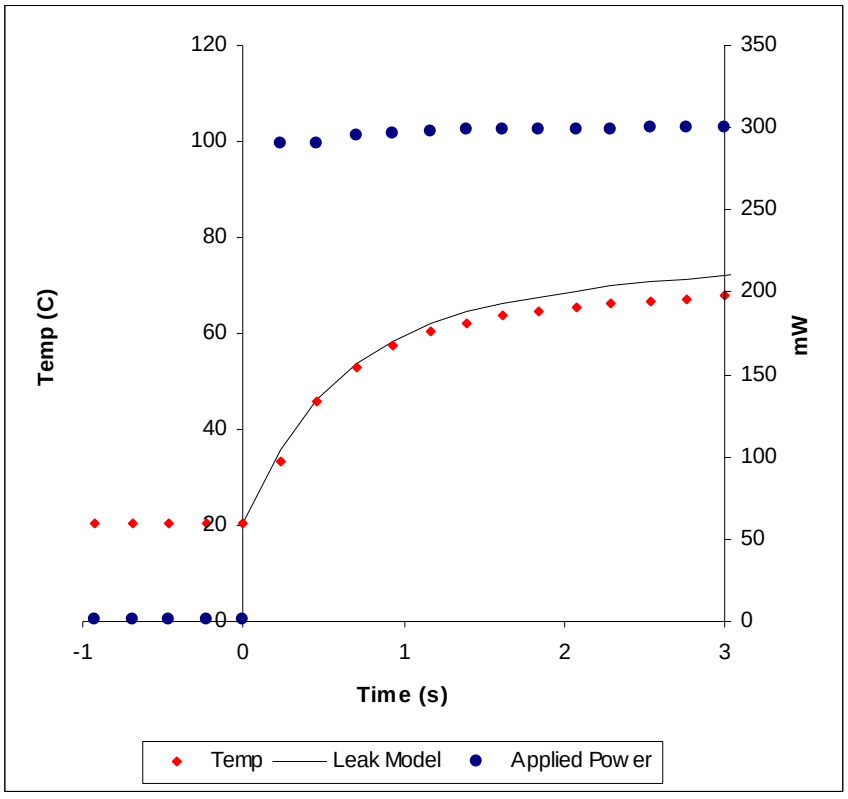

Figure 3-24: Heating with step function applied power

Here, the important parameters are the thermal capacitances (i.e., heat capacity) of the island and the body. These were calculated using known values for specific heat and multiplying by the appropriate mass. Values are shown below:

Table 3-5: Parameters used for thermal model

Description	Param	Value	Units
R from island to room	R_1	1.51	C/mW
R from body to room	R_2	0.131	C/mW
R from island to body	R_g	0.175	C/mW
Heat capacity of island	C_1	3.73	mJ/C
Heat capacity of body	C_2	78.7	mJ/C

3.3.3.3 Cooling Rates

Analysis of temperature drop with zero applied power shows the island can drop from the denaturing temperature (95°C) to the annealing temperature (55°C) in about 1.5 seconds.

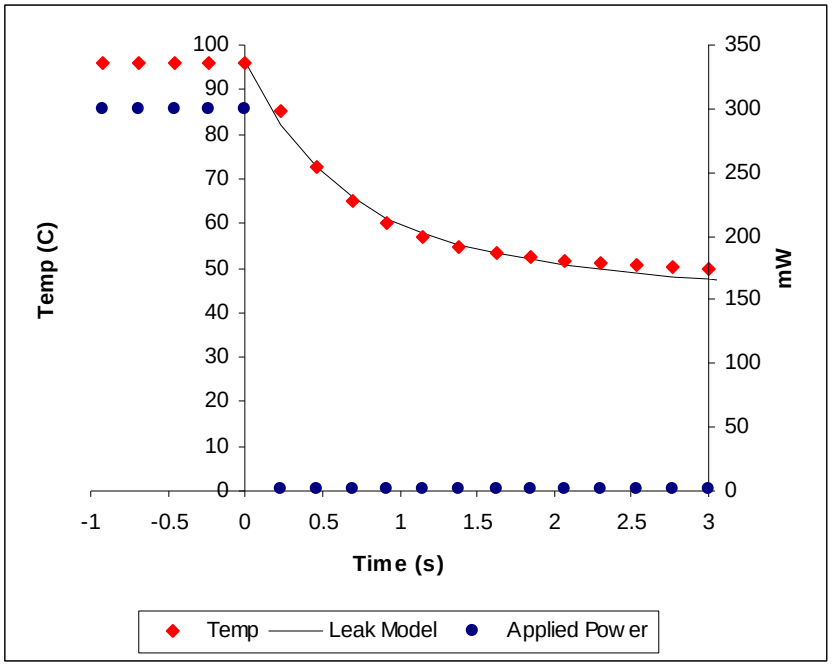

Figure 3-25: Temperature cooling dynamic with zero applied power

The same parameters were used as in the heating model. The only "fitted" parameter here was the initial body temperature, which was given a value of 56 °C. It should be noted that the time varying portion of the model begins to lose accuracy at time greater than a few seconds, possibly due to non-linearity in the actual system, thermal leakage to

the body housing, and non-uniform temperature distributions. Nevertheless, these experiments and model describe the time and temperature regions that are most important to an RTPCR chip.

3.4 Interface with Housing

To interface the chip to the macro world, a custom built housing was designed using solid works and fabricated in house using a computer numerical controlled (CNC) milling machine.

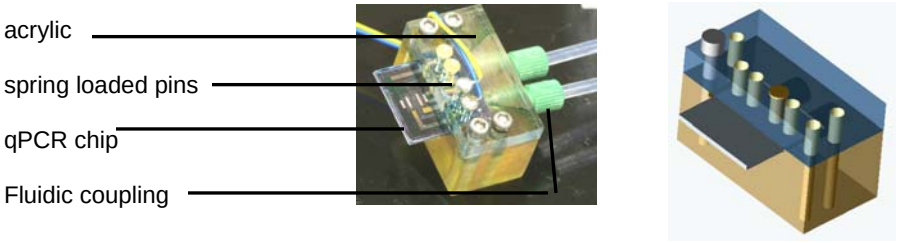

Figure 3-26: Chip housing assembly

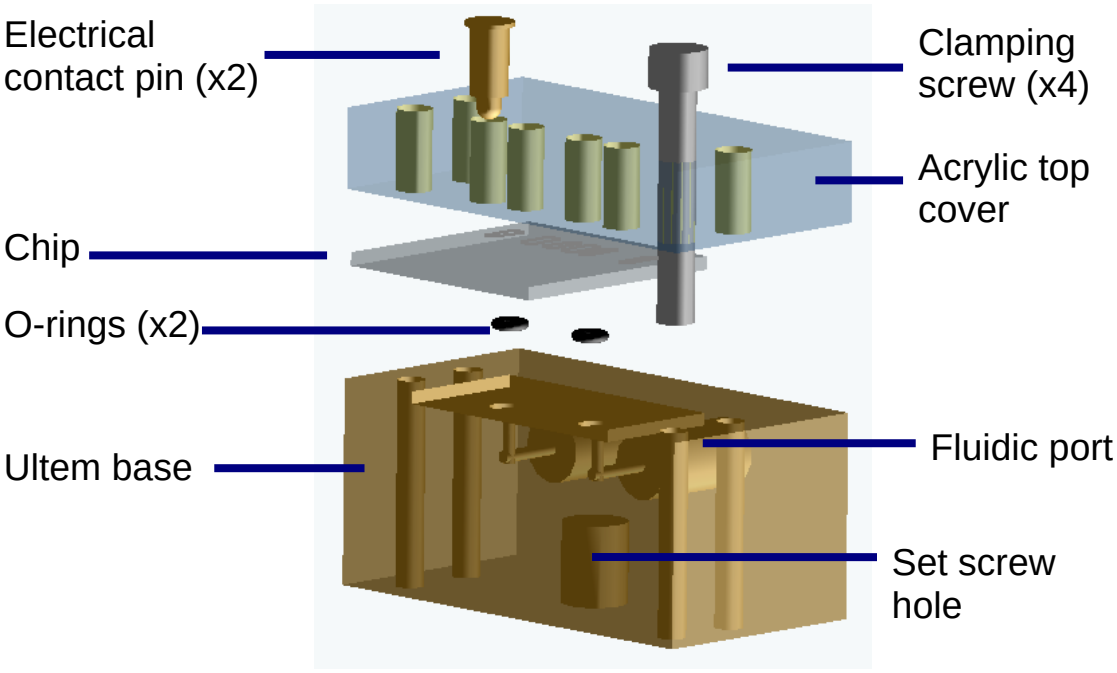

Figure 3-27: Chip housing components

The base was machined from Ultem (polyetherimide), a material that can be supplied as USP Class VI compliant (implying good biocompatibility). It contains two grooves for positioning the O-rings, a set screw hole to receive the set screw, four through holes to receive the clamping screws, and 2 fluidic ports machined to accept a 6–40 fluidic coupling nut. A achieve a smooth flat surface, the fluidic port was drilled using a 7/64 inch end mill instead of a drill bit. The acrylic top cover contained four holes for the clamping screws and four holes for electrical contact pins (although only two were used).

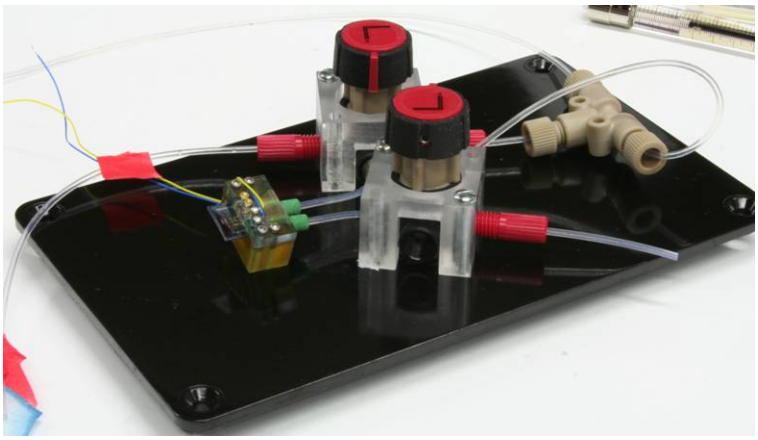

Figure 3-28: Chip housing with external valves

3.5 Device Performance

3.5.1 Real Time Polymerase Chain Reaction Components

The components of the PCR reaction will be detailed including the substrate: the M13 virus.

3.5.1.1 PCR Solution

The protocol for preparation of the PCR solution is given below. Details about each component are discussed in Chapter 1.

- Start with 22 µl PCR Mix (Platinum PCR Supermix from Invitrogen)
    - Mix contains: 22 U/ml DNA polymerase, 22 mM Tris-HCl (pH 8.4), 55 mM KCl, 1.65 mM $MgCl_2$, 220 µM (dGTP,dATP,dTTP,dCTP), and "stabilizers"
- Add 2.4µl DMSO (2.2%)
    - DMSO disrupts base pairing to reduce results of secondary DNA structure of the targets and reduce non-specific primer-dimer formation[52]
- Add 0.6µl of 40X SYBR Green I

- Fluorescent dye (for more details see Chapter 1)

- Add 1 µl of each primers (right then left)
  - Final concentration is 0.01 nmoles of each primer.
- Add 1µl virus sample or its pure DNA
  - See below for more details

3.5.1.2 The Sample: M13 Virus

The sample used in this study is the M13 bacteriophage, a model DNA virus. The template was thus its 6.4 kilobases long circular single stranded DNA genome. The phage is about 900 nm long and 9 nm diameter with a cylindrical shape[53]

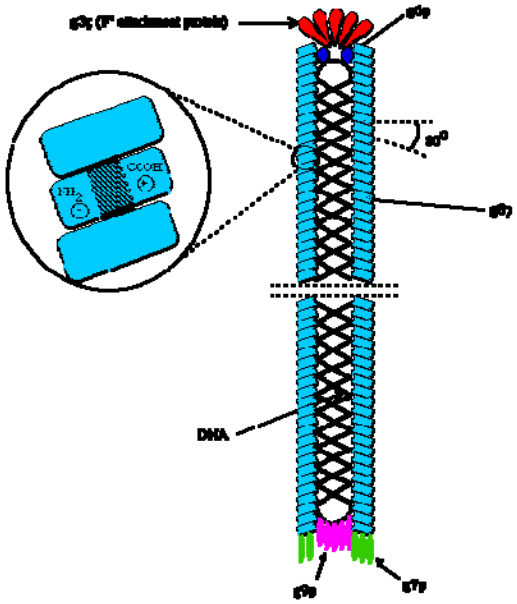

Figure 3-29: Structure of the M13 virus

It is categorized as an Ff phage because it requires the *E. coli* F pilus for infection. The bulk of the capsid is composed of about 2800 copies of a 50 amino acid polypeptide protein derived from gene 8 (g8p). This protein has an alpha helix structure with three domains. The hydrophilic amino end is negatively charged, comprised mostly of acidic

amino acids, and forms the outer surface of the virus. The inner surface is positively charged so that it is stable next to the negatively charged DNA genome. This charge is a result of basic residues near the carboxyl terminal. The middle region is hydrophobic, which allows interactions with other g8p proteins to form a stable membrane structure. These hydrophobic interactions are key to the use of the M13 virus as a model virus for PCR. At 95^0C, the thermal energy is high enough to disrupt these interactions, causing lysis of the virus and allowing its DNA genome to participate in the PCR reaction.

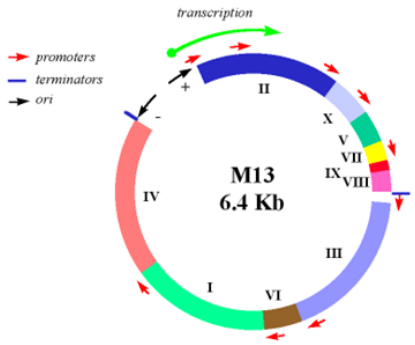

Figure 3-30: Genome of the M13 virus

The capsid has an interesting "plasticity." If the genome is artificially made to be longer by insertion of DNA into the non-essential intergenic regions of the genome, the resulting capsid is automatically assembled longer to accommodate this longer genome. This is possible because of the modular design: the virus simply includes more g8p proteins into the capsid. This property makes the M13 virus a good cloning vector. Foreign DNA can be inserted into the M13 genome then transfected into a suspension of *E. coli*. If sequencing of the genome (with foreign DNA) is desired, the viral particles can be isolated from the *E. coli* cells by centrifuging the solution and keeping only the supernatant. Various mutations of the M13 virus have been produced, each containing useful DNA sequences built into the genome[54]. Thus usage of this virus allows others to

clone pieces of DNA into its genome to be amplified by PCR. The target length for this study is about 180 bp.

3.5.2 Thermal Cycling Protocol (94, 72, 55; 30 s each)

Although not optimized, the following temperature protocol was used:

- 95°C for 15 seconds
- 55°C for 15 seconds
- 72°C for 15 seconds

Each temperature transition used 5 seconds. Further reduction in temperature soaking times can be made experimentally, especially denaturation time. A reduction in transition times can be made by optimizing different PID control constants.

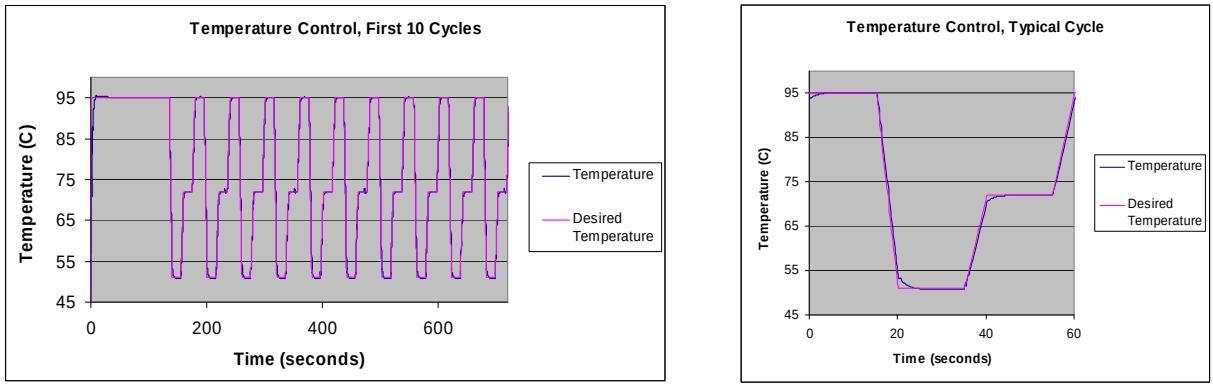

Figure 3-31: Temperature recipes

As seen in Figure 3-31, the temperature control was quite good as there was good agreement between desired and actual temperatures.

3.5.3 Optical Detection Protocol

3.5.3.1 Background

Optical measurements were performed using a fluorescence microscope and the SYBR Green fluorescent dye. With this dye, fluorescence increases as the amount of double stranded DNA increases.

3.5.3.2 Equipment

Fluorescence measurements were made using a microscope, CCD camera, and image analysis software. The microscope was a Nikon Eclipse E800 fluorescence microscope with a mercury arc lamp (USH-102DH) and Nikon B-2E/C filter block (see Figure 3-32). The excitation filter allows wavelengths of 465–495 nm to pass to the sample while the emission filter allowed wavelengths 515–555 nm to pass from the sample to the camera. A long pass dichromatic mirror with cut-off wavelength 505 nm was used to control light paths.

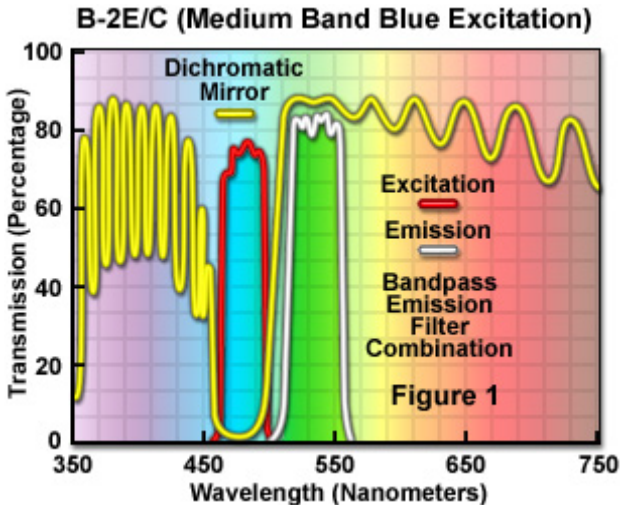

Figure 3-32: Filter block for SYBR Green I detection

The CCD camera was an RT KE from Spot Diagnostic. This is a one-CCD based camera with an LCD-based optical filter that cycles between red, blue, and green for color images. Thus each image is the composite of 3 separate images taken in succession. For optical measurement purposes, only one LCD mode was used (monochromatic mode) and all signal processing (noise reduction, auto contrast, etc.) was turned off. Manual settings ensured consistent shutter speeds.

The image analysis software was the free software Image J from the NIH[55]. Measurements were made in units of intensity related to the 16 bit images. Lowest intensity was given a value of 1 whereas the saturation intensities had value 65536 (2^16). Due to fluctuations in the mercury arc lamp intensity, normalization was performed for every image.

3.5.3.3 Normalization

Fluorescence emission intensity (I) is related to the excitation intensity (X) and quantum yield φ by:

$$I = \phi X \quad \text{Equation 3-13}$$

When SYBR Green binds to DNA, it is φ (of the DNA in solution) that changes. Thus in quantitative PCR we are actually interested changes in φ with respect to time, which we try to extract by measuring I at a region of interest (region A in Figure 3-33).

$$I_t^A = \phi_t^A X_t^A$$
$$I_0^A = \phi_0^A X_0^A \qquad \text{Equation 3-14}$$
$$\frac{\varphi_t^A}{\phi_0^A} = \frac{I_t^A}{I_0^A}\left(\frac{X_0^A}{X_t^A}\right)$$

where

I_t = Fluorescence intensity at time = t
I_0 = Fluorescence intensity at time = 0 (first cycle of PCR)
X_t = Excitation intensity at time = t
X_0 = Excitation intensity at time = 0
φ_t = quantum yield at time = t
φ_0 = quantum yield at time = 0

The problem is that X is also changing with time due to the nature of the halogen light source and thus must also be measured. Fortunately, one only needs the relative change in time of excitation intensity X_0/X_t, not its absolute value. One convenient way is get this information is to analyze an area of the image where quantum yield is constant (region B in Figure 3-33).

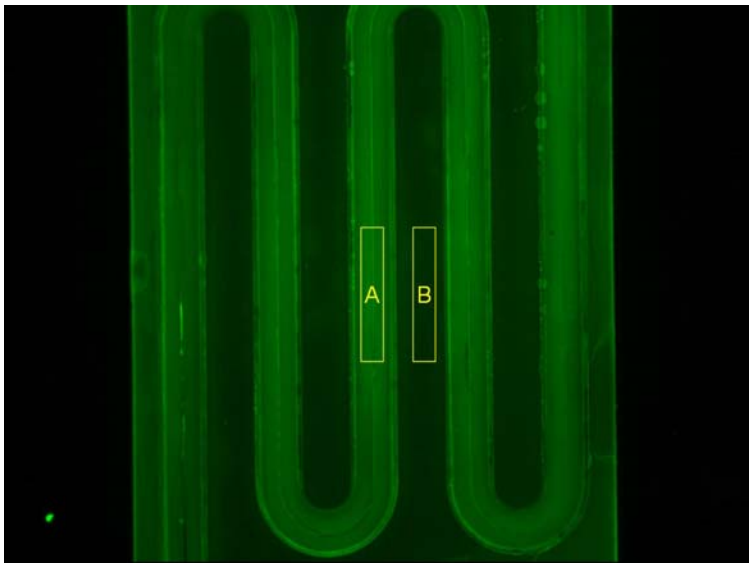

Figure 3-33: SYBR Green fluorescence in microchannel

In region B Equation 3-13 still applies and since φ is constant, relative I can be obtained by directly looking at relative X:

$$I_t^B = \phi X_t^B$$
$$I_0^B = \phi X_0^B \quad \text{Equation 3-15}$$
$$\frac{I_t^B}{I_0^B} = \frac{X_t^B}{X_0^B}$$

where
I_t = Fluorescence intensity at time = t
I_0 = Fluorescence intensity at time = 0 (first cycle of PCR)
X_t = Excitation intensity at time = t
X_0 = Excitation intensity at time = 0
$\varphi = \varphi_t = \varphi_0$ = constant quantum yield

Now if regions A and B are spatially close enough and the intensity distribution of light is fairly uniform we can assume $X^A=X^B$. This assumption links our equation together to obtain:

$$\frac{\varphi_t^A}{\phi_0^A} = \frac{I_t^A}{I_0^A}\left(\frac{I_0^B}{I_t^B}\right) \quad \text{Equation 3-16}$$

3.5.4 Results

A raw sample of M13 virus from ATCC was detected using the qPCR device.

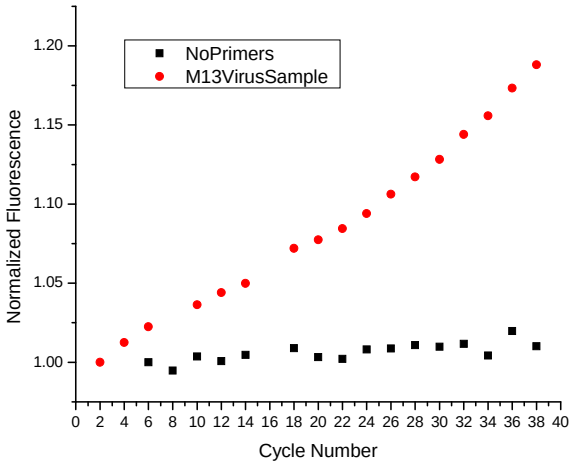

Figure 3-34: Detection of M13 virus. Data normalization described above

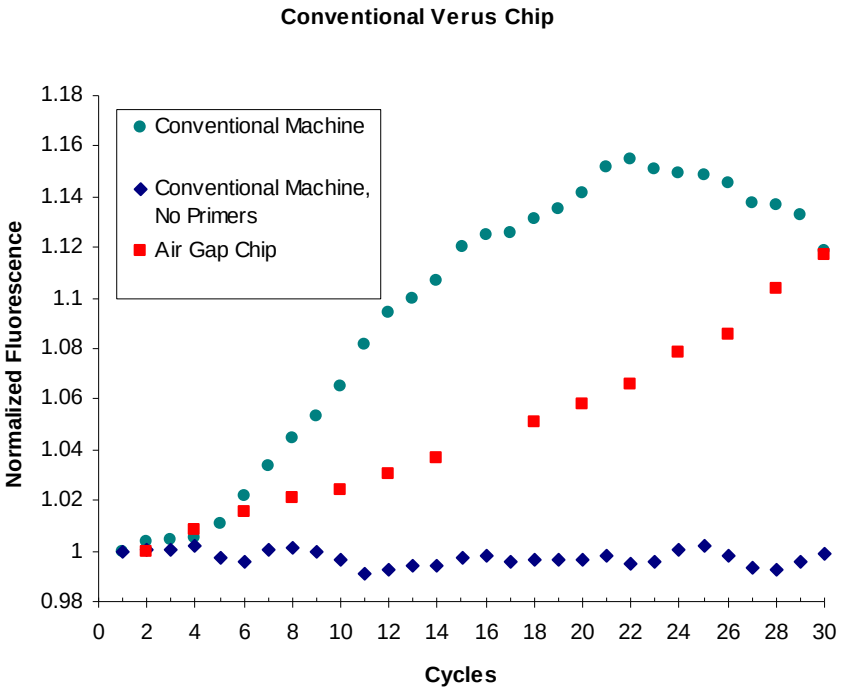

Figure 3-35: Air gap chip versus conventional QPCR machine

The no-primers control and M13 virus sample are distinguishable. Although the data shows proof of concept, some imperfections exist. The amplification curve appears linear and not exponential. This might be caused by incomplete reactions in each step. Although parylene is known to be an inert surface, extensive studies on the effect of parylene on micro-PCR reactions have not been done. Poor primer binding or sluggish extension steps can result from altered salt concentrations or reactants becoming denatured from interactions with the parylene chamber walls. Figure 3-35 shows a comparison of the air gap QPCR chip versus a conventional thermal cycler. The chip performs fairly although exponential amplification is muted.

3.6 Chapter Summary

The first version of the device was designed, fabricated, and tested. Further improvements can be made by simplifying the fabrication process, removing the passive silicon on the thermal island, and varying the biochemical parameters during the PCR step.

4 RTPCR Microdevice, Free Standing Version

4.1 Fabrication

Here an improved version of the RTPCR chip is presented, featuring a free standing chamber with the heater/temperature sensor placed on top. This new design allows for even more efficient heat transfer by eliminating the passive silicon underneath the channel. The overall fabrication steps are presented in Figure 4-1. Details of each step are presented in the text body.

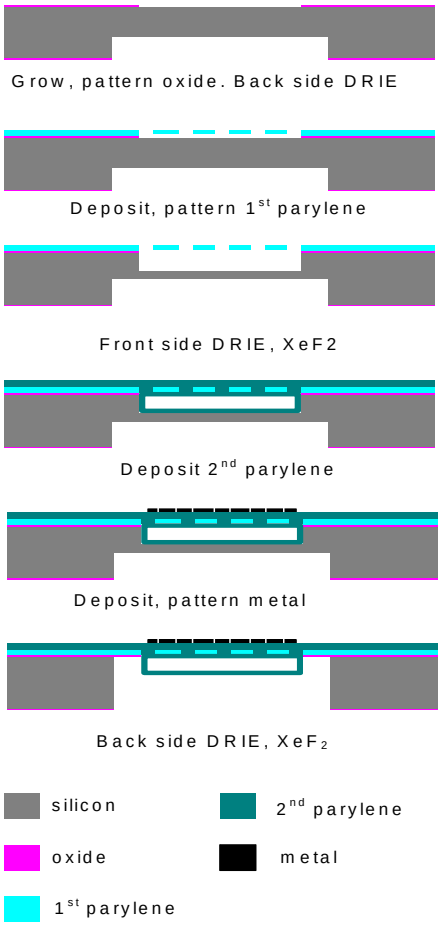

Figure 4-1: Overall device fabrication steps

The starting substrate is a 100 mm diameter, 500 μm thick, one-side-polished silicon wafer. For diagrammatic purposes, only one 1 cm x 1 cm chip is used to represent the entire wafer.

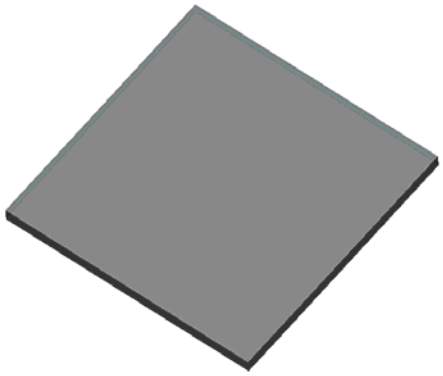

Figure 4-2: Bare silicon chip

Following piranha cleaning (submersion in a 120^0C bath of H_2SO_4 and H_2O_2), a 1 μm thermal oxide layer is grown onto the wafer using an oxidation furnace at 1050^0C.

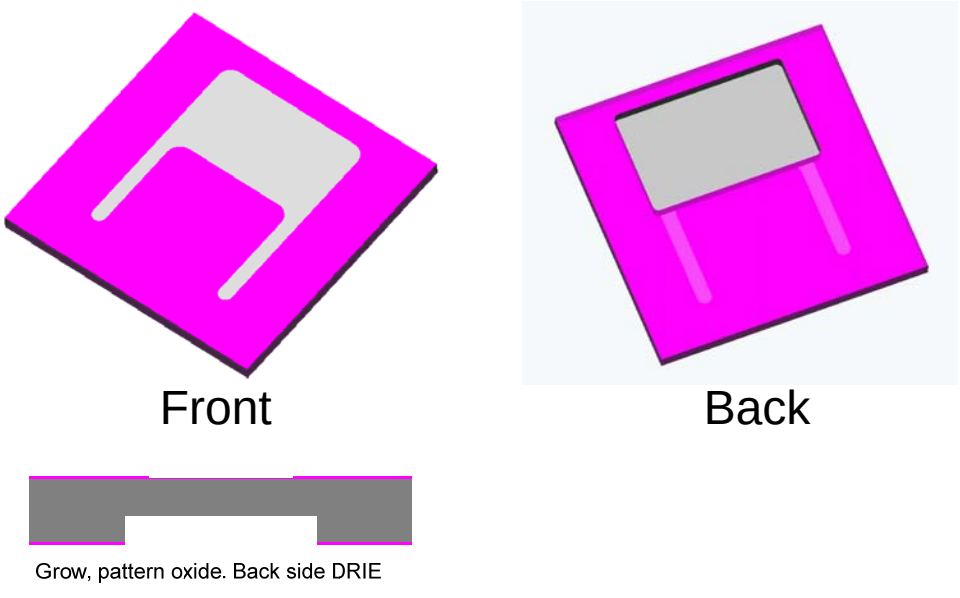

Figure 4-3: Oxide layers. Notice the back side shows silicon etched by the DRIE. Back side also shows the "legs" of the front side oxide pattern for clarity. Actual silicon is not transparent.

The oxide layer is then patterned using 1 μm of AZ 1518 photoresist as mask for 8 minutes of etching in buffered hydrofluoric acid. The buffered acid is used instead of diluted hydrofluoric acid for a more consistent etching rate. The oxide layer is preserved everywhere except the channels and back side window (Figure 4-3). Initial back side etching of about 350 um of silicon is performed at this step to reduce the amount of silicon etching required towards the end of the process. After etching, the photoresist is stripped using acetone followed by isopropanol.

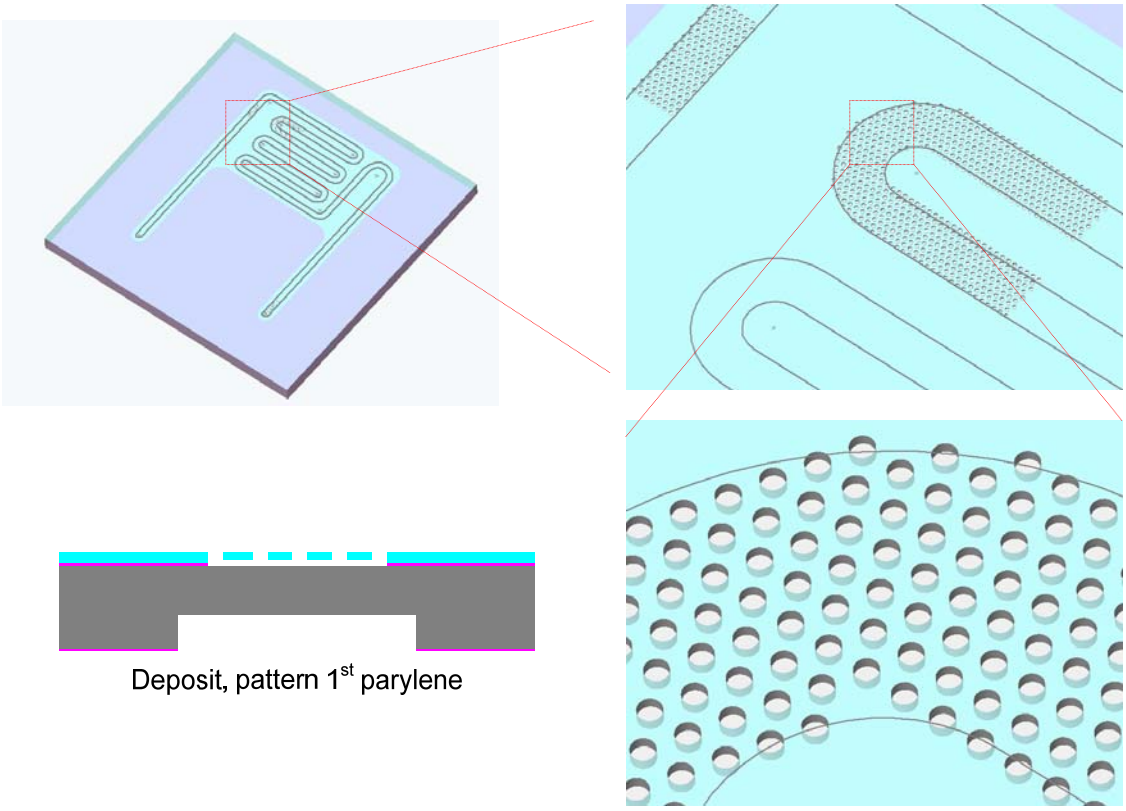

Figure 4-4: First parylene layer with representative holes. The holes are actually present throughout the outlined channel region.

An adhesion layer of A-174 (gamma-methacryloxy propyltrimethoxysilane) was applied, then 12 μm of parylene is deposited onto the wafer. The adhesion layer provides a

hydrophobic surface for improved adhesion between parylene and the substrate. A simple layer of tape is placed on the back side of the wafer to prevent parylene deposition there. After deposition, 10 µm holes are etched into the parylene layer using a photoresist mask and reactive ion etching (RIE) with an oxygen plasma at 350 mTorr and 65 W applied power for 25 minutes. These holes allow the silicon underneath to be later etched away, forming the channel. Their arrangement (and thus, channel layout) can be seen in Figure 4-4.

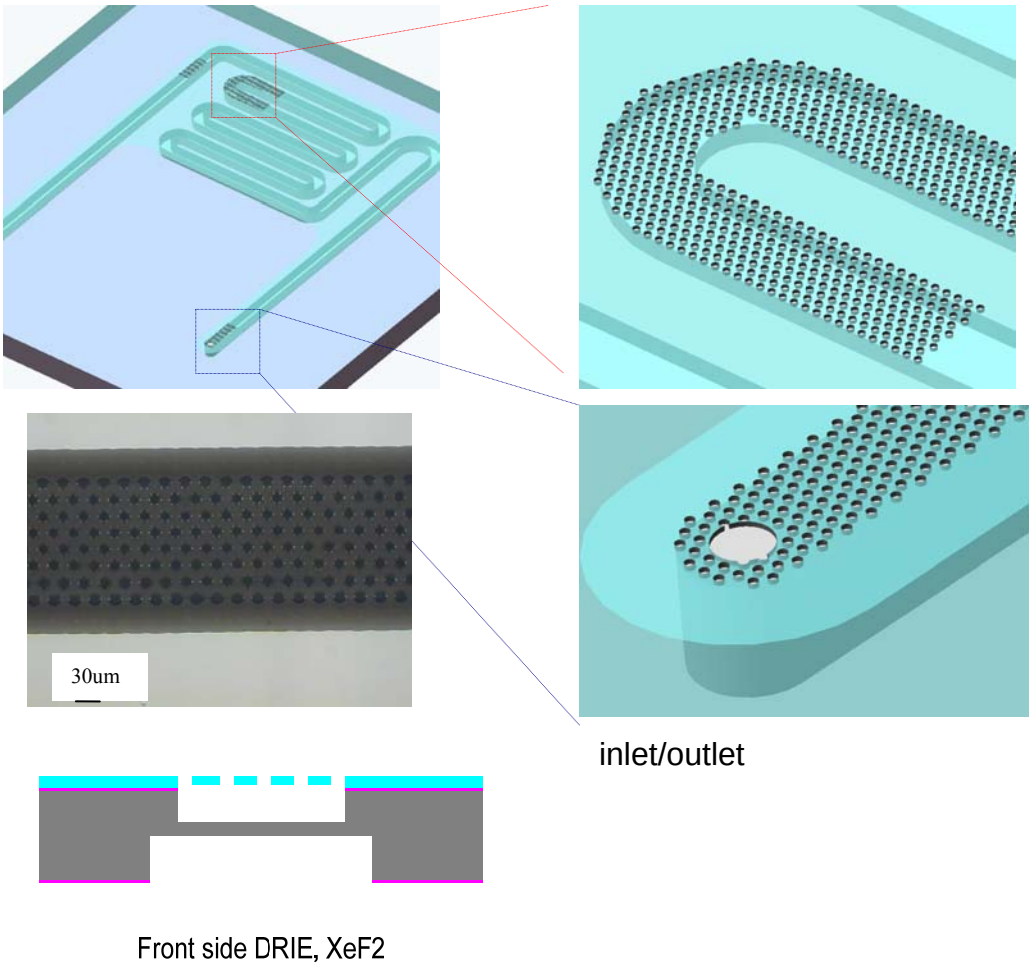

Figure 4-5: Channels etched into silicon. Bottom right is i/o hole.

Using the parylene layer as a mask, silicon is etched about 80 µm deep using a modified DRIE process followed by isotropic XeF_2 etching. These steps allow the formation of the channel (Figure 4-5). The inlet and outlet holes (bottom right in Figure 4-5) are larger diameter holes that cannot be filled with parylene in the next step and thus allow for fluidic access to the channels.

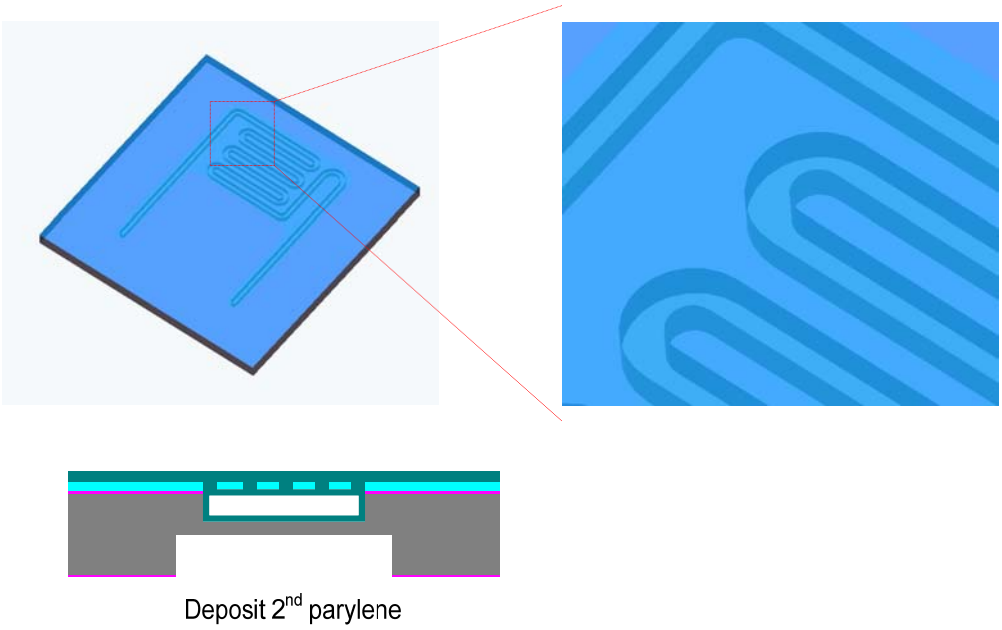

Figure 4-6: Second parylene layer deposited

A second parylene layer (20 µm) is then deposited (Figure 4-6). This layer covers the silicon sidewalls with parylene and also fills the holes, completing the channel.

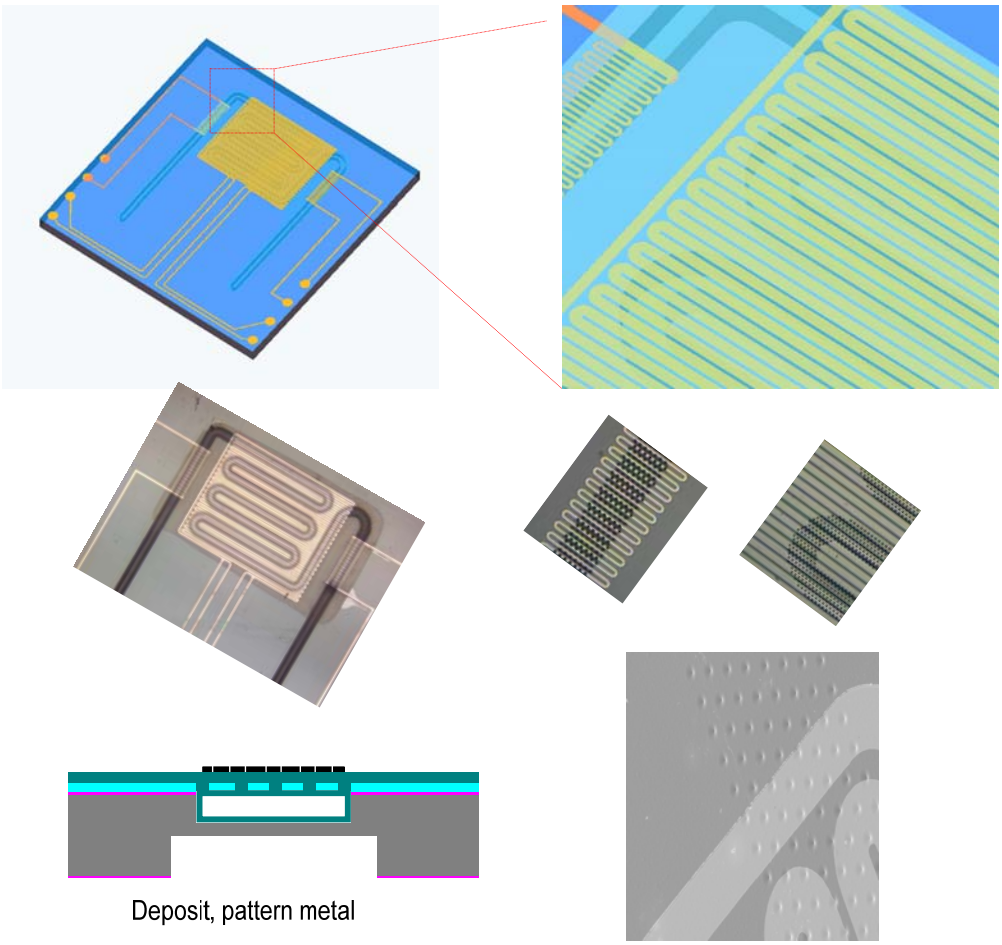

Figure 4-7: Platinum pattern

A 2000 Å platinum layer is then deposited on the second parylene. It is patterned using the metal lift-off method. No adhesion layer is necessary because parylene and platinum have good adhesion to each other. The engineering reasons behind the metal layout are discussed in the section about thermal engineering below. Despite the 1–2 μm dimples on the surface due to the filled holes, the metal is still a continuous film (Figure 4-7).

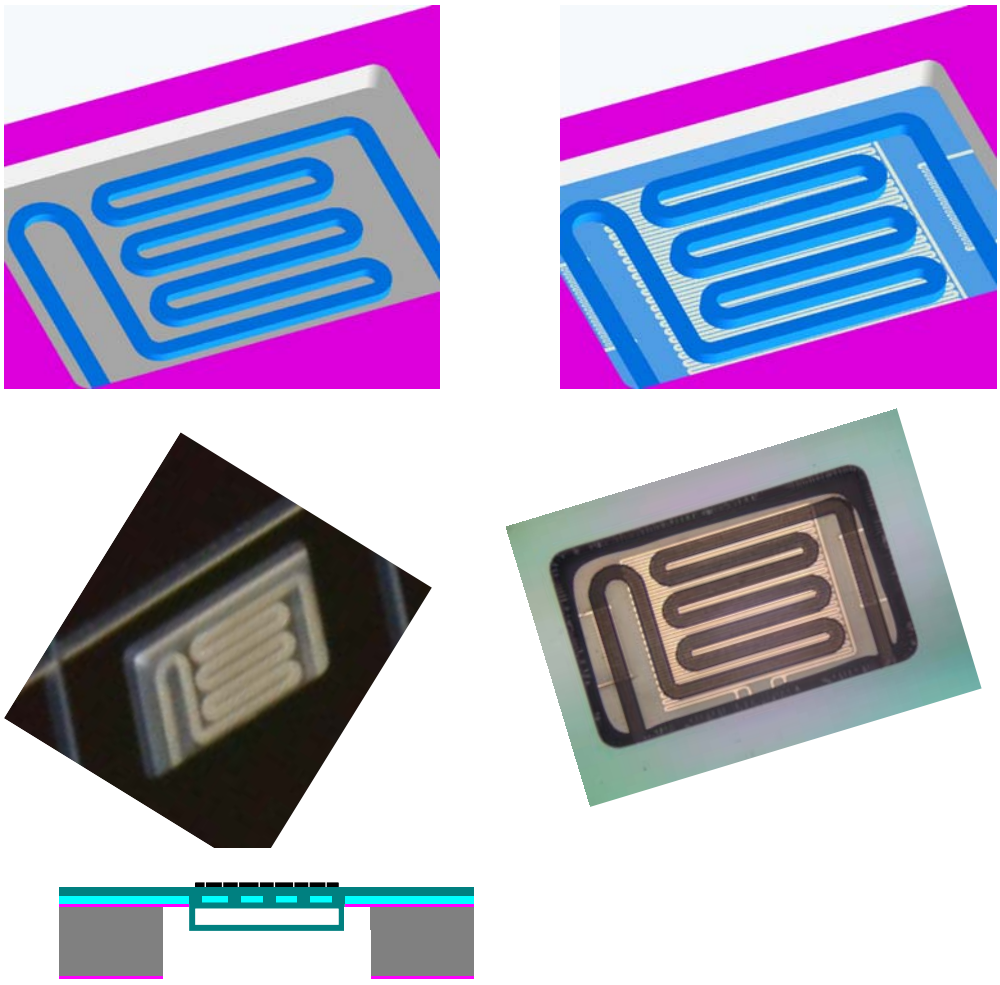

Figure 4-8: Back side finishing. View from back side. Left: After DRIE. Right: After XeF_2

After metallization, the back side of the wafer is etched using DRIE with the oxide layer as a mask. This etches the silicon down to the lower surface of the channels (Figure 4-8 upper left). Further plasma etching at this point can damage the parylene channels. To etch the remaining silicon, XeF_2 is used. The gas based chemical reacting mechanism has excellent selectivity to silicon and leaves the parylene intact. Following this step, all the silicon in the back side window is removed, making the platinum layer on the front side of the device visible from the back (Figure 4-8, right side).

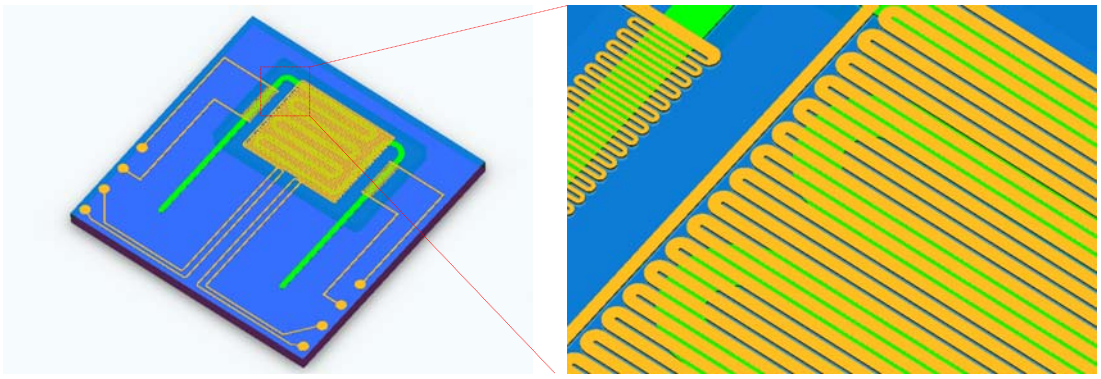

Front

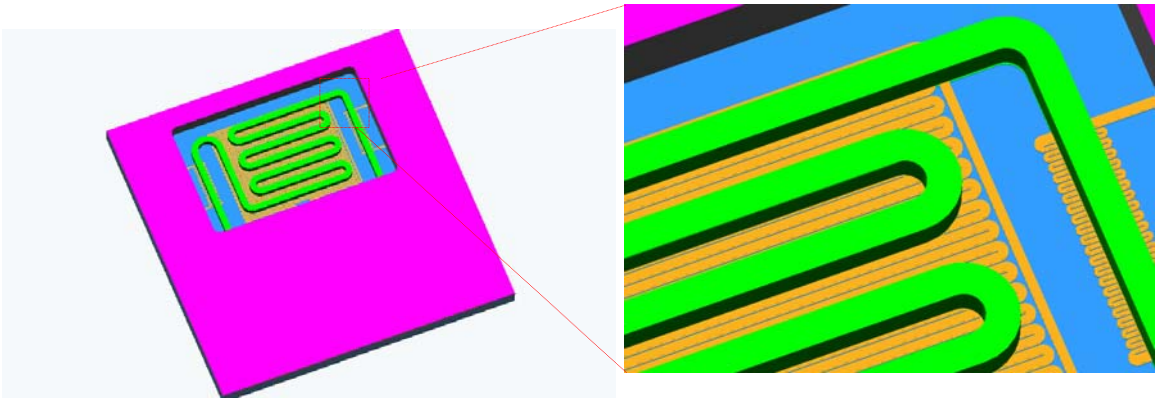

Back

Figure 4-9: Finished chip front and back

The finished chip is shown schematically in Figure 4-9. Here the channels are shown in green (as they appear during testing with green fluorescent dyes). Optical measurements are performed on the back side of the device so that the platinum layer serves as a reflector (along with its normal roles as heater and temperature sensor) for increased optical efficiency.

4.2 Fluidic Channel Design

Requirements for a PCR chamber were discussed in the previous chapter. Like the previous version of the device, this design features a constant cross-section channel for easy removal of bubbles (by flushing with high velocity liquid) should they appear. The effective radius of the channel is 75 μm with a total length such that the total volume of liquid contained within the amplification region is about 550 nL.

4.3 Device Thermal Engineering

4.3.1 Heat Transfer Background

Please refer to the previous chapter for a theoretical introduction to the heat transfer principles used in this work.

4.3.2 Device Thermal Design

Since the theoretical framework for thermal design was provided in the previous chapter, only quick explanations pertaining to differences between this version and the previous are discussed here. Unlike the previous version, which had a silicon support piece, this version has free standing channels with no support. This minimizes excess mass, which reduces heat capacity, which in turn reduces the characteristic time constant τ, allowing faster heating and cooling rates. Once again, platinum was used as the heater and temperature sensor. This time, however, no metal adhesion layer was necessary as platinum was deposited directly onto the parylene channels (see Figure 4-10) and the materials have good adhesion to each other.

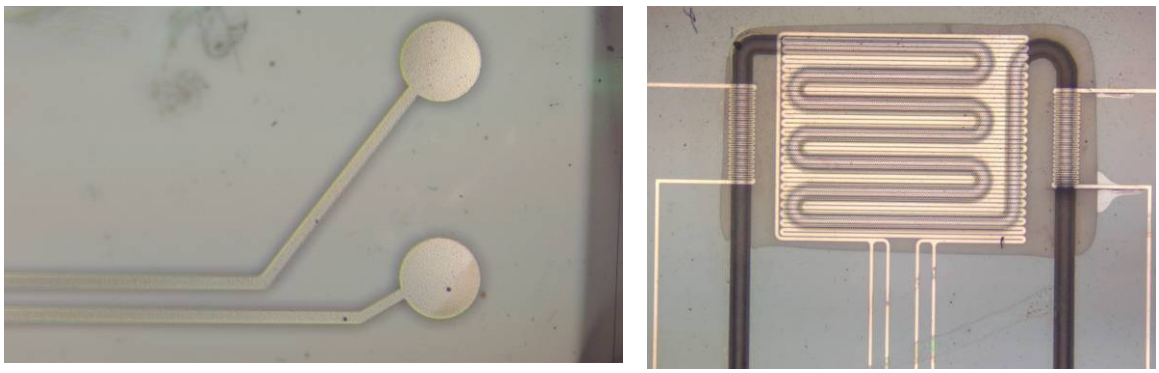

Figure 4-10: Platinum traces directly on parylene. Left: contact pads. Right: heaters

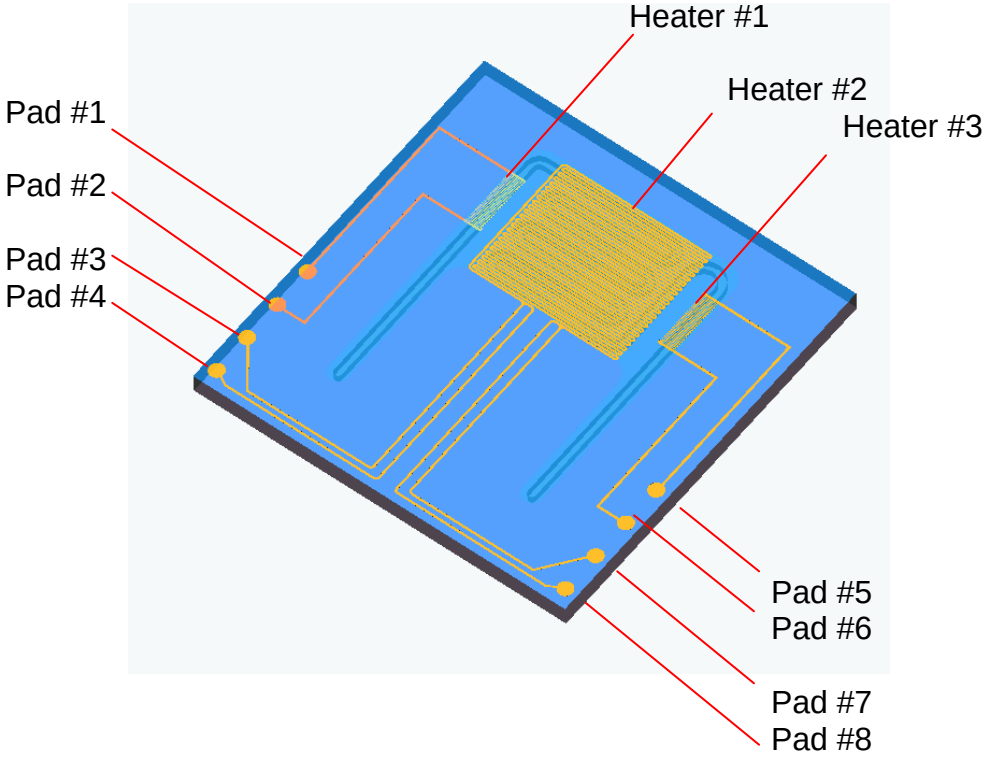

Figure 4-11: Metal layout

The metal layout is diagrammed in Figure 4-11. There are three heaters, labeled #1, #2, and #3. Heater #2 is the main heater and the one used for all the experiments here. Heaters #1 and #3 were placed for possible use in future experiments including measuring the temperature at those distant positions. It should be clear from Figure 4-11 that pads #1, #2, #5, and #6 serve heaters #1 and #3. Pads #3 and #4 (and also pads #7 and #8) connect near the bottom of heater #2. The original intent was for them to be used in a four-wire resistance measurement configuration; however, they were eventually shorted after processing to allow larger bonding pads for interfacing with the chip housing. More on this will be discussed in the section dealing with chip housing.

4.3.2.1 Temperature Sensor

The 2000 Å platinum trace resulted in a resistance of about 2.9 kOhms at room temperature. The temperature calibration curve showed a highly linear relationship (see Figure 4-12). The TCR (temperature coefficient of resistance) value was about 2.0×10^{-3} $/^{0}C$, which is consistent with the previous version.

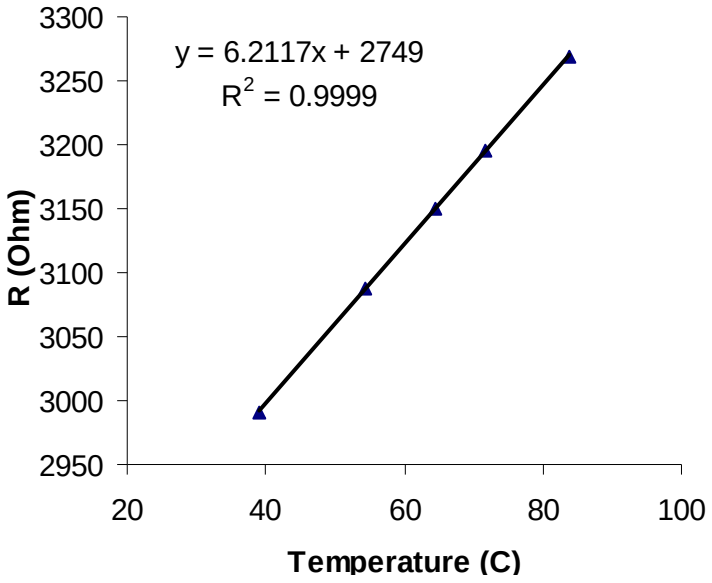

Figure 4-12: Temperature sensor calibration

4.3.2.2 Heater

The thin film metal trace heater based on joule heating provides a sufficient and simple heat source. The power dissipated by such a metal line is given by Joule's First Law:

$$P = VI = \frac{V^2}{R} = I^2 R \quad \text{Equation 4-1}$$

In designing such a heater, it is important to choose a resistance value such that the available power sources can supply the required voltages and current. Below are the relevant parameters for the heater:

Table 4-1: Parameters for heater

Maximum Power Required	100 mW
Heater resistance	2900 ohms
Maximum voltage required for 100 mW	20 Volts
Maximum current required for 100 mW	5 mA

These values are within the capabilities of the available power supply

4.3.2.3 Equipment Setup

This device uses the same setup as the previous version, so please refer to the previous chapter for details.

4.3.3 Thermal Performance Results

The simple RC circuit analogue (described in the previous chapter) is used to describe the thermal results:

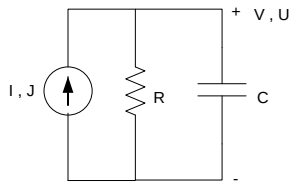

Figure 4-13: Simple circuit analogy

$$U(t) = U_0 e^{-t/RC} + JR(1 - e^{-t/RC}) \quad \text{Equation 4-2}$$

$$R = \frac{1}{hA} \qquad \text{Equation 4-3}$$
$$C = \rho C_p V$$

where

h = heat transfer coefficient
A = heat transfer area
ρ = density of the solid
C_p = heat capacity
V = volume of the solid

Chip characterization can be performed by analyzing some special cases. At steady state, t→∞, Equation 4-2 reduces to:

$$U(t = \infty) = JR \quad \text{Equation 4-4}$$

Data from this case can be analyzed to obtain the thermal resistance R. Another interesting case occurs when applied power is zero J=0, which reduces the equation to:

$$U(t) = U_0 e^{-t/RC} \quad \text{Equation 4-5}$$

With this equation one can deduce the thermal capacitance C, by analyzing the rate of cooling. Both these analyses will be discussed below.

4.3.3.1 Steady State Temperature Resistance

The resistance to heat transfer into the environment in this case is the slope of the line in Figure 4-14. R = 1/(hA) = 0.923 ^{0}C/mW. Thus for an area of 25 mm^2 (12.5 mm^2 on each side), the overall (including top and bottom) heat transfer coefficient h = 43.5 W/m^2/^{0}C.

This is in good agreements with the calculated heat transfer coefficient of h = 46 $W/m^2/^0C$ based on empirical correlations[56].

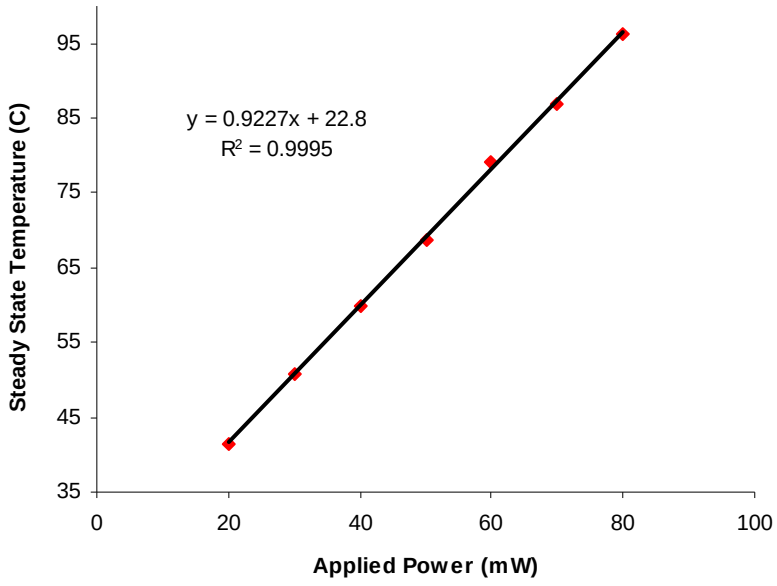

Figure 4-14: Thermal resistance to heat transfer into environment

4.3.3.2 Thermal Capacitance

To determine the thermal capacitance, heating and cooling experiments were performed. For the cooling experiments, the zero applied power model was used:

$$U(t) = U_0 e^{-t/RC} \quad \text{Equation 4-6}$$

Using this model, a thermal time constant τ=RC was fitted to the data in Figure 4-15. The fitted model below uses τ = 3 seconds, corresponding to a thermal capacitance C = 3.25 mJ/C. Using published data on specific heat capacities of water and parylene, the calculated thermal capacitance was 3.03 mJ/C, which is fairly consistent with the experimental results.

These same parameters also fit the heating experiments well (Figure 4-16), maintaining a consistent model for both cooling and heating data. In this case, the zero initial temperature difference case of Equation 4-2 was used:

$$U(t) = JR(1 - e^{-t/RC}) \quad \text{Equation 4-7}$$

4.4 Interface with Housing

To interface with the new chip design, modifications were made to the housing unit. Using the same CNC machining techniques and materials described in the previous chapter, a housing unit was designed and fabricated with back side fluidic inlet/outlet ports along with back side electrical contact pins (Figure 4-17). To prevent the pins from penetrating the thin platinum and parylene layers, a layer of conductive epoxy (epoxy made conductive by incorporating silver particles into the matrix) was placed over the contact pads. This had the unfortunate consequence of shorting the narrowly pitched pads that were originally designed to provide a 4-wire resistance measurement configuration. Good electrical function was still achieved, however, using a 2-wire configuration.

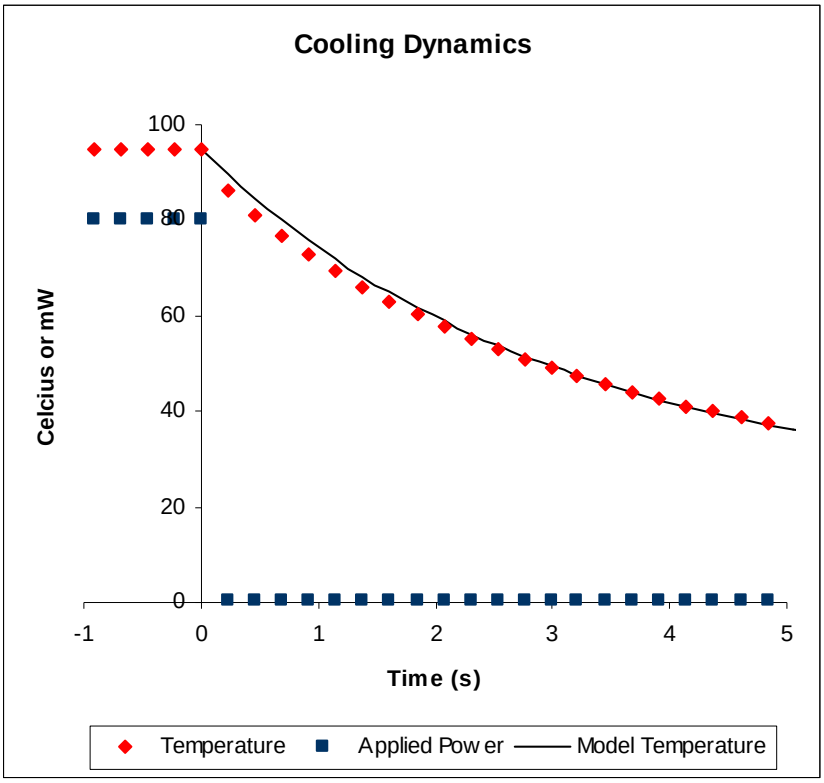

Figure 4-15: Cooling experiments used to determine thermal time constant and capacitance

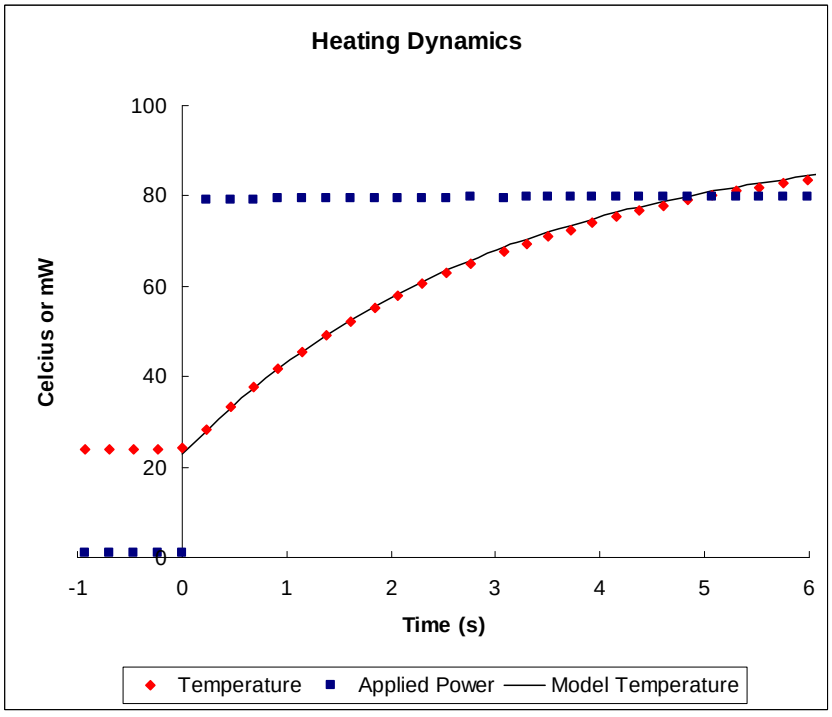

Figure 4-16: Heating experiments

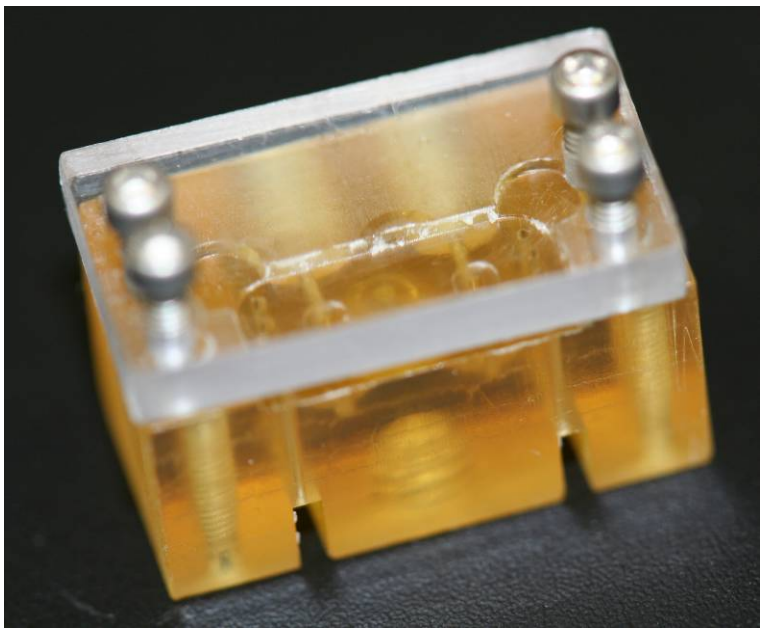

Figure 4-17: Chip housing assembly. O-rings and pins not shown

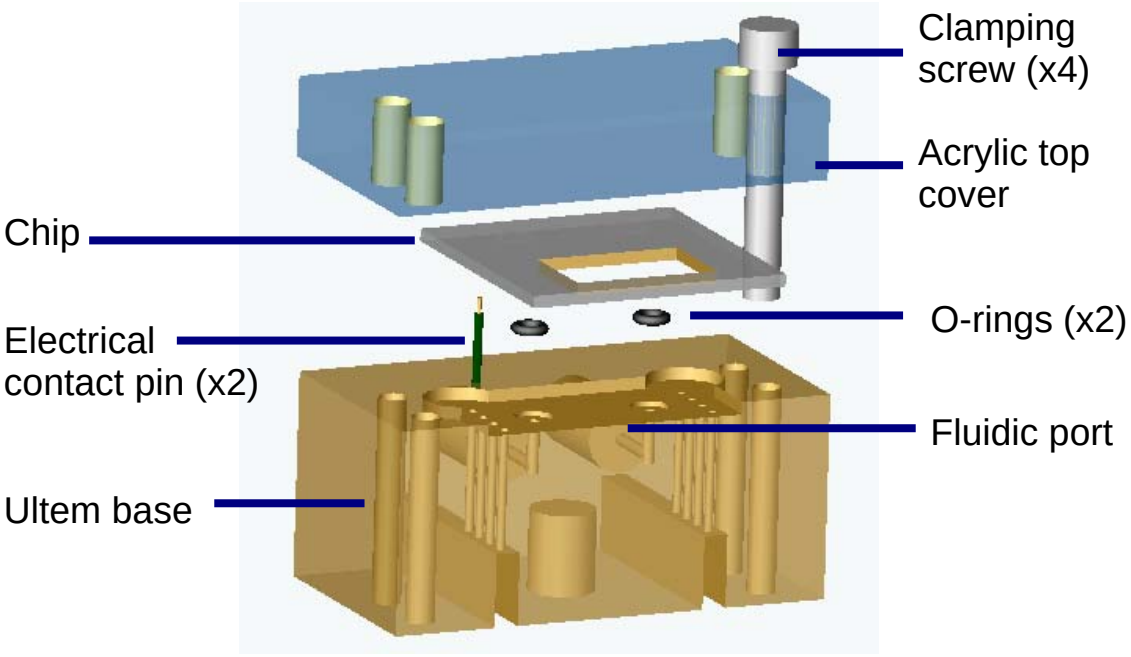

Figure 4-18: Chip housing components

4.5 Device Performance

4.5.1 Real Time Polymerase Chain Reaction Components

The same RTPCR mixture was used as in the previous version. Please see chapter 3 for more details.

4.5.2 Thermal Cycling Protocol

The same thermal recipe was used as in the previous version. Please see chapter 3 for more details.

4.5.3 Optical Detection Protocol

The same optical protocol was used except a 4X objective (instead of 10X) was used, at a shutter speed of 350 ms. The same normalization scheme was also used. Please see Chapter 3 for details.

4.5.4 Results and Discussion

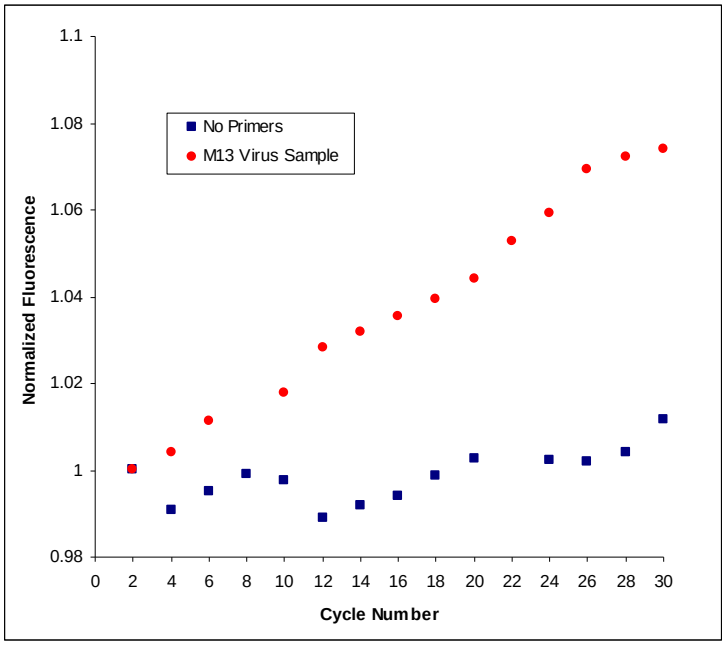

Figure 4-19: Detection of M13 virus on chip

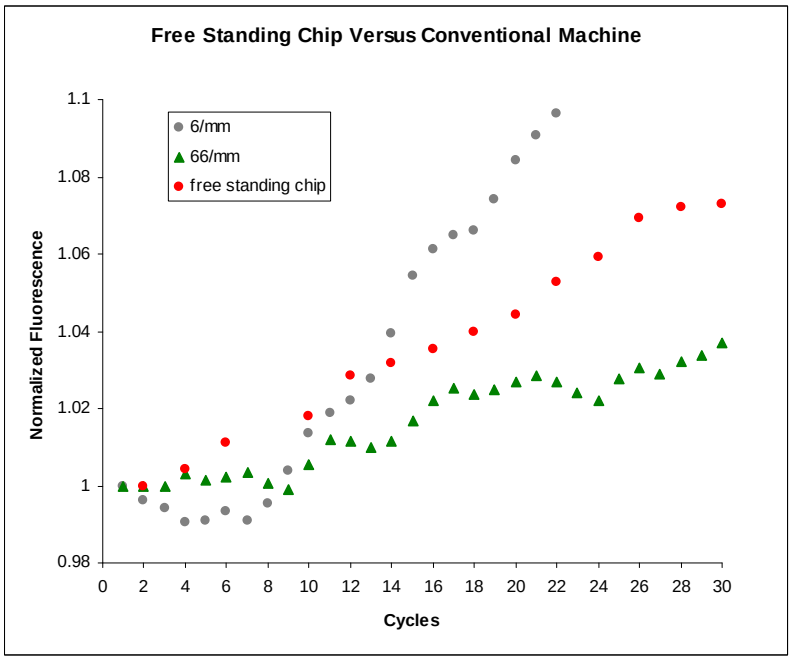

Figure 4-20 Comparison of chip versus conventional machine. Sample volumes and surface-area-to-volume ratios of parylene were comparable.

The resulting amplification (Figure 4-19) is very similar to the previous version. The M13 virus sample shows an increasing fluorescence signal compared to the no-primers control. To compare the results to a conventional machine, total volume and surface area to volume ratio were considered. The chip had an estimated volume of 500 nL and SA/vol of 50/mm. Figure 4-20 shows the chip compared to cycling done with a conventional machine where the sample volume was 500 nL and SA/vol ratios of 6/mm and 66/mm were used. The 66/mm sa/vol sample was obtained by adding the appropriate surface area of parylene sheets into the reaction vessel. The chip performs fairly well in the comparison.

4.6 Chapter Summary

An improved design based on the previous version was fabricated and tested. Results were similar to the previous version but with improved thermal efficiency, a more elegant structure, and easier fabrication.

5 Conclusion

Recent advances in PCR have lead to real time PCR, where the reaction product is quantified during the reaction via fluorescent indicators. This allows quantification of starting material and faster reaction times since the reaction can be stopped once the amount of fluorescence reaches an acceptable level.

Recent advances in MEMS have lead to parylene-based bio-MEMS ranging from implantable microdevices to lab on a chip. Since this material is more bio-compatible while fitting in nicely with current microfabrication techniques, its usage is becoming more common.

By combining advances in both these fields, this thesis presented a real time PCR device based on parylene MEMS technology. Compared to current devices, the chip uses less fluidic reagents and less power while providing more efficient heating can cooling. Future work on this device should focus on improving the fluorescent signal by adjusting the biochemical parameters and focusing on optical engineering. In the longer term, highly parallel arrays of these devices should be fabricated to allow simultaneous reactions including a calibration set for quantifying the initial DNA amount in the sample.

References

[1] http://en.wikipedia.org/wiki/Nucleotide

[2] www.idtdna.com

[3] http://frodo.wi.mit.edu/primer3/input.htm

[4] M. McPherson and S. Moller. *PCR, Second Edition*. p. 5 (2006)

[5] F.C. Lawyer, S. Stoffel, R.K. Saiki, S.Y. Chang, P.A. Landre, R.D. Abramson, and D.H. Gelfand. *High-level expression, purification, and enzymatic characterization of full-length Thermus aquaticus DNA polymerase*. PCR Methods and Applications. 2: 275–287 (1993)

[6] *User's manual for Platinum PCR Supermix (part no. 11306.pps).* Invitrogen (Revised 01–July–2003)

[7] http://www.juliantrubin.com/encyclopedia/biochemistry/pcr.html

[8] Bio-Rad website: www.bio-rad.com

[9] *Product Manual for SYBR Green I. MP07567*. Invitrogen (Revised 16–March–2006)

[10] H. Zipper, et al. *Investigations on DNA intercalation and surface binding by SYBR Green I, its structure determination and methodological implications.* Nucleic Acids Research. 32:e103 (2004).

[11] Invitrogen company website: www.invitrogen.com

[12] Q.Y. Zeng, S.O. Westermark, A. Rasmuson-Lestander, and X.R. Wang. *Detection and quantification of Cladosporium in aerosols by real-time PCR.* Journal of Environmental Monitoring. 8:153–160 (2006)

[13] Same as ref 12

[14] B. Liss. *Improved quantitative real-time RT-PCR for expression profiling of individual cells*. Nucleic Acids Research 30:17, pp. e89 (2002)

[15] Image from Hitequest website: www.hitequest.com

[16] S.A. Campbell. *The Science and Engineering of Microelectronic Fabrication. Second Edition.* Oxford University Press, 167 (2001)

[17] Image from Connexions website: http://cnx.org/

[18] M. Madou. *Fundamentals of Microfabrication.* CRC Press (1997)

[19] G.T.A. Kovacs, N.I. Maluf, and K.E. Petersen. *Bulk Micromachining of Silicon*. Proceedings of the IEEE 86:8 (Aug 1998)

[20] G. Beheim. *Chapter 21: Deep Reactive Ion Etching for Bulk Micromachining of Silicon Carbide*. The MEMS Handbook (Chief Editor, M. Gad-el-Hak). CRC Press (2002)

[21] P. Wilding, M.A. Shoffner, and L.J. Kricka. *PCR in a Silicon Microstructure*. Clinical Chemistry. 40:1815–1818 (1994)

[22] J. Chen, M.A. Shoffner, G.E. Hvichia, L.J. Kricka, and P. Wilding. *Chip PCR. II. Investigation of different PCR amplification systems in microfabricated silicon-glass chips*. Nucleic Acids Research. 2:2 (1996)

[23] M.A. Burns, B.N. Johnson, S.N. Brahmasandra, K. Handique, J.R. Webster, M. Krishnan, T.S. Sammacro, P.M. Man, D. Jones, D. Heldsinger, C.H. Mastrangelo, and D.T. Burke. *An Integrated Nanoliter DNA Analysis Device*. Science 282:484–487 (1998)

[24] I. Erill, S. Campoy, N. Erill, J. Barbe, and J. Aguilo. *Biochemical Analysis and Optimization of Inhibition and Adsorption Phenomena in Glass-Silicon PCR-Chips*. Sensors and Actuators B 96:685–692 (2003)

[25] G.M. Whitesides, E Ostuni, S Takayama, X Jiang, and D.E. Ingber. *Soft Lithography in biology and biochemistry*. Annual Revue of Biomedical Engineering 3:335–373 (2001)

[26] J. Liu, M. Enzelberger, and S. Quake. *A Nanoliter Rotary Device for Polymerase Chain Reaction*. Electrophoresis 23:1531–1536 (2002)

[27] J.S. Marcus, W.F. Anderson, S.R. Quake. *Parallel Picoliter RT-PCR Assays Using Microfluidics*. Analytical Chemistry. 78:956–958 (2006)

[28] Q. Xiang, B. Xu, R. Fu, and D. Li. *Real Time PCR on Disposable PDMS Chip with a Miniatuizede Thermal Cycler.* Biomedical Microdevices 7:4,273–279 (2005)

[29] J. Shih. *PhD Thesis* (2008)

[30] J.C. Salamone. *Concise Polymeric Materials Encyclopedia*, pp. 1363–1365 (1999)

[31] V&P Scientific, Inc Website: www.vp-scientific.com

[32] C.Y. Shih, T.A. Harder, and Y.C. Tai. *Yield Strength of Thin-Film Parylene-C.* Microsystem Technologies 10:407–411 (2004)

[33] X.Q. Wang, Q.L. Lin, and Y.C. Tai. *A Parylene Micro Check Valve*. Proceeds from The Twelfth IEEE International Conference on MicroElectroMechanical Systems 1999 (MEMS 99), Orlando, Florida, pp.177–182 (1999)

[34] B. Lu, S. Zhang, and Y.C. Tai. *Parylene Background Fluorescence Study for BioMEMS Applications*. Proceedings of the 15th International Conferences on Solid-State Sensors and Actuators (Transducers 2009), Denver, Colorado (2009)

[35] Paratronix website: www.paratronix.com

[36] J. Shih, T.D. Lee, and Y.C. Tai. *Surface-Machined Parylene Microfluidics*. Lab on a Chip Technologies and Applications, Horizon Scientific Press, UK (2008)

[37] E. Meng and Y.C. Tai. *Parylene Etching Techniques for Microfluidics and BioMEMS*. Proceedings of the IEEE International Conference on Micro Electro Mechanical Systems (MEMS 2005), Miami, Florida. pp. 568–571 (2005)

[38] R.R.A. Callahan, G.B. Raupp, and S.P. Beaudoin. *Effects of gas pressure and substrate temperature on the etching of parylene-N using a remote microwave oxygen plasma*. Journal of Vacuum Science and Technology B. 19:725–731 (2001)

[39] K. Walsh, J. Norville, and Y.C. Tai *Photoresist as a sacrificial layer by dissolution in acetone*. Proceedings of the 14th IEEE International Conference on MicroElectroMechanical Systems (MEMS 2001), Interlaken, Switzerland, p. 114-117 (2001)

[40] J. Xie, J. Shih, Q. He, C.L. Pang, Y.C. Tai, Y. Miao, and T.D. Lee. *An integrated LC-ESI Chip with Electrochemical-based gradient generation*. Proceedings of the 17th IEEE International Conference on MicroElectroMechanical Systems (MEMS 2004). Maastricht, The Netherlands, 2004

[41] P.J Chen, C.Y. Shih, and Y.C. Tai. *Design, fabrication and characterization of monolithic emb.edded parylene microchannels in silicon substrate*. Lab Chip 6:803–810 (2006)

[42] C.Y. Shih, Y. Chan, and Y.C. Tai. *Parylene-strengthended thermal isolation technology for microfluidic system-on-chip applications* Sensors and Actuators A: Physical. 126:1, pp. 270–276 (2005)

[43] J. Shih, *PhD Thesis* (2008)

[44] A. Gonzalez, R. Grimes, E.J. Walsh, T. Dalton, and M. Davies. *Interaction of Quantitative PCR Components with Polymeric Surfaces*. Biomedical Microdevices 9:261-266 (2007)

[45] Y. Chen and Y. Momose. *Reaction of Argon Plasma-treated Teflon PFA with Aminopropyltriethoxysilane in its n-Hexane Solution*. Surface and Interface Analysis 27:1073–1083 (1999)

[46] C. Zhang and D. Xing. Survey and Summary. *Miniaturized PCR chips for nucleic acid amplification and analysis: latest advances and future trends*. Nucleic Acids Research 35:13, pp. 4223–4237 (2007)

[47] F. Kreith (Editor in Chief). *The CRC Handbook of Mechanical Engineering.* Section 4-16 (1998)

[48] C.Y. Shih, Y. Chen, J. Xie, Q. He, and Y.C. Tai. *On-Chip Temperature Gradient Liquid Chromotography*. Technical Digest of the 18th IEEE International Conference on MicroElectroMechanical Systems (MEMS 2005), Miami, Florida, pp. 539–542 (2005)

[49] E. Meng. *MEMS Technology and devices for micro fluid dosing system*. PhD Thesis, p. 123 (2003)

[50] C.Y. Shih, *Temperature-Controlled Microchip Liquid Chromatogrphy System.* PhD Thesis, p. 86 (2006)

[51] J.S. Kim, B.K. Park, and J.S. Lee. *Natural Convection Heat Transfer Around Microfin Array*. Experimental Heat Transfer 21:55–72 (2008)

[52] S. Frackman, G. Kobs, D. Simpson, and D. Storts. *Betaine and DMSO: Enhancing Agents for PCR*. Promega Notes 65, p.27 (1998)

[53] http://www.microbiologybytes.com/virology/Phages.html

[54] D. Greenstein and R. Brent. *Vectors Derived from Filamentous Phages*. Current Protocols in Molecular Biology 1.14.1–1.14.5 (1990)

[55] W.S. Rasband. *ImageJ*. U.S. National Institutes of Health, Bethesda, Maryland http://rsb.info.nih.gov/ij/ (1997-2007)

[56] F. Kreith (Editor in Chief). *The CRC Handbook of Mechincal Engineering*. Section 4-16 (1998)